A Kinetic and Mechanistic Study of Dinuclear Platinum(II) Complexes with bis-(4'-terpyridyl)-α,ω-alkyldiol Ligands

By

Varvara I. Nikolayenko

BSc (Honours) (University Of Kwazulu Natal)

Master of Science

January 2012

UNIVERSITY OF KWAZULU-NATAL

School of Chemistry

Pietermaritzburg

FACULTY OF SCIENCE AND AGRICULTURE

Abstract

A series of novel *Bis* 2,2′:6′,2″-terpyridinyl ligands, linked through a flexible alkyl chain situated at the 4′ position, were synthesised and characterised by microanalysis, FTIR, NMR, UV-Visible spectroscopy, and MS-ToF. Single crystals of all the ligands were obtained, of which one has been published, one has been submitted for publication and one is in preparation for publication. These ligands were then coordinated to platinum(II) and characterised, including ^{195}Pt NMR spectroscopy. A detailed kinetic study involving the substituting the chloride co-ligand with the following nucleophiles thiourea, 1,3-dimethyl-thiourea and 1,1,3,3-tetramethyl-thiourea was conducted using stopped-flow techniques. An associative reaction mechanism was suggested for the pendant ligand substitution and the following trend in reactivity was observed: **L2-Pt**$^{\alpha}$ > **L3-Pt**$^{\beta}$ > **L1-Pt**$^{\chi}$. UV-Visible absorption spectra were recorded on sequentially diluted solutions of the ligands (in chloroform), and the platinum complexes (in water). These spectra obeyed the Beer-Lambert law. The values of the molar absorption coefficients at the wavelengths of maximum absorption for the ligands followed the trend **L1** < **L2** < **L3**, whilst for the complexes the trend was **L1-Pt** < **L3-Pt** < **L2-Pt**. It has been concluded that at low concentrations **L2-Pt** and **L3-Pt** undergo *intra*molecular folding. Variable temperature and variable concentration NMR spectroscopic studies were performed on all three complexes. At higher complex concentrations *inter*molecular self-association takes place for **L2-Pt** and **L3-Pt** but not for **L1-Pt**. The reactivity of the complexes is predominately determined by their structural conformations in solution. At low concentrations the **L1-Pt** complex remains in its linear conformational state, whilst the **L2-Pt** and **L3-Pt** complexes undergo *intra*molecular folding with the formation of an axial Pt—Pt bonded and π—π stacked dinuclear platinum terpyridine centre. The latter is believed to be more active in the substitution reaction than the original mononuclear centre. The reasons for the folding and self-association in the **L2-Pt** and **L3-Pt** systems are related to the steric crowding and stress in the spacer region of the folded or self-associated complexes.

$^{\alpha}$ 4",4"'-[butane-1,4-diyl*bis*(oxy)]-2',2":6",2"'-terpyridine-platinum(II)chloride
$^{\beta}$ 4",4"'-[hexane-1,6-diyl*bis*(oxy)]-2',2":6",2"'-terpyridine-platinum(II)chloride
$^{\chi}$ 4",4"'-[ethane-1,2-diyl*bis*(oxy)]-2',2":6",2"'-terpyridine-platinum(II)chloride.

Contents

Acknowledgements

I would like to extend my sincere gratitude to Mr *Craig Grimmer*, whose unwavering support, extensive patience and inquisitive mind has made the greatest impact on this work. Your input has been profound and your kindness unprecedented.

I would also like to acknowledge the following people:

Professor Igor Nikolaenko for being my dad and keeping your head when those around you (me in particular) where losing theirs. The generous time, effort and resources you devoted in helping to un-shroud the mystery behind these molecules is beyond measure.

Dr Desigan Reddy for providing me with all of the necessities required for scientific research and the room to learn what truly makes a good scientist.

Professor John Field for the never ending stream of probing questions that although difficult to answer, helped shape the theory of this thesis to what it is today. Your knowledge and insight have been indispensible.

Professor Siegfried Drewes for taking the time to proof read endless chapters and provide continuous encouragement.

Dr Matthew Akerman for all your help with the single crystal X-ray structure determinations.

To my fellow postgrads, thank you for the countless tea sessions and lunch walks, without you, research would have been impossible and life in general would have been very dull.

To my family, your unwavering belief, encouragement, patience and support are what fuel my tenacity and provide me with courage to take on challenging tasks and complete them.

Publications

- M. P. Akerman, C. D. Grimmer, V. I. Nikolayenko and D. Reddy, *Acta Cryst. Section E*, **2011**, E67(12), o3478-o3479.

- M. P. Akerman, C. D. Grimmer, V. I. Nikolayenko and D. Reddy, *Acta Cryst. Section E*, **2012**, submitted for publication.

- M. P. Akerman, C. D. Grimmer, V. I. Nikolayenko and D. Reddy, *Acta Cryst. Section E*, **2012**, in preparation.

Abbreviations List

A	Absorbance
A	Associative Mechanism
A	Pre-Exponential Factor
Aaa	$[Pt(diethylenetriamine)OH_2]^{2+}$
Aap	$[Pt(N\text{-}(pyridyl\text{-}2\text{-}methyl)\text{-}1,2\text{-}diaminoethane)OH_2]^{2+}$
AET	2-aminoethanediol
AIDS	Acquired Immune Deficiency Disorder
Apa	$[Pt(2,6\text{-}bis\text{-}aminomethylpyridine)OH_2]^{2+}$
App	$[Pt(2,2'\text{-}bipyridine)\text{-}(NH_3)(OH_2)]^{2+}$
br	Broad
BBR3464	Triplatin Tetranitrate
Bu	Butyl
C	Intrinsic Reactivity
c	Concentration
$CH_3PhPtCl$	$[Pt\{4'\text{-}(2'''\text{-}CH_3\text{-}Ph)\text{-}terpyridine\}Cl]^+$
$CF_3PhPtCl$	$[Pt\{4'\text{-}(2'''\text{-}CF_3\text{-}Ph)\text{-}terpyridine\}Cl]^+$
ClPhPtCl	$[Pt\{4'\text{-}(2'''\text{-}Cl\text{-}Ph)\text{-}terpyridine\}Cl]^+$
CMT	Carboethoxymethanethiol
COSY	Correlation Spectroscopy
C_q	Quarternary Carbon
D	Dissociative Mechanism
d	Double
dd	Doublet of doublets
DMF	Dimethyl formamide
DMSO	Dimethyl Sulfoxide
DMTU	1,3-Dimethyl-Thiourea
DNA	Deoxyribose Nucleic Acid
dt	Doublet of triplets
Dtdeg	*bis*[4'-(2,2′:6′,2″-terpyridyl)]-diethyleneglycol ether
ε	Molar Absorptivity
E_a	Arrhenius Activation Energy
Et_4dien	$(NH[CH_2CH_2N\text{-}(C_2H_5)_2]_2)$
$\Delta G^{\neq}$	Standard Gibb's Energy Change
$\Delta H^{\neq}$	Standard Enthalpy Change
HET	2-Hydroxyethanethiol
HOMO	Highest Occupied Molecular Orbital
HSAB	Hard Soft Acid Base Theory
HMBC	Heteronuclear Multiple Bond Correlation Experiment
HSQC	Heteronuclear Single Quantum Coherence Experiment
I	Interchange Mechanism
$\boldsymbol{I_a}$	Associatively Activated Intimate Mechanism
$\boldsymbol{I_d}$	Dissociatively Activated Intimate Mechanism
IR	Infra Red

l	Path Length
LUMO	Lowest Unoccupied Molecular Orbital
m	Medium, multiplet
MLCT	Metal to ligand charge transfer
MO	Molecular Orbital
n^{o}_{Pt}	Nucleophilicity
NMR	Nuclear Magnetic Resonance
NOESY	Nuclear overhauser enhancement spectroscopy
pap	[Pt(*bis*(2-pyridylmethyl)amine)OH_2]$^{2+}$
PGM	Platinum Group Metal
PhPtCl	[Pt{4'-Ph-terpyridine}Cl]$^{+}$
ppp	[Pt(terpyridine)OH_2]$^{2+}$
pK_a	Acid Dissociation Constant
PtCl	[Pt(terpyridine)Cl]$^{+}$
PtNCN	[Pt(1,3-di(2-pyridyl)benzene)Cl]
PtNNC	[Pt(6-phenyl-2,2′-bipyridine)Cl]
PtNNN	[Pt(terpyridine)Cl]
Py	Pyridine
R	Universal Gas Constant
ROESY	Rotating frame Overhauser enhancement spectroscopy
s	Strong, Singlet
$\Delta S^{\neq}$	Standard Entropy of Activation Change
SAR	Structure Activity Relationships
sh	Shoulder
SME_2	Methylsulfonyl methane
$\boldsymbol{S}$	Nucleophilic Discrimination Factor
T	Absolute Temperature
t	Triplet
Terpy	2,2′:6′,2″-Terpyridine
TU	Thiourea
TMTU	1,1,3,3,-Tetramethyl-2-Thiourea
UV	Ultra Violet
$\Delta V^{\neq}$	Partial Molar Volume Change
$\Delta V^{\neq}$	Volume of Activation Change
vs	Very strong
vw	Very weak
w	Weak

List of Figures

List of Tables

CHAPTER I
Introduction

Figure 1.1: Nugget of unrefined platinum metal.[1]

Platinum (***Figure 1.1***) is considered to have revolutionised the modern world. Its effects are evident in all facets of life, including vehicle emission control devices, industrial catalysts, electronics, jewellery and in smaller applications such as electrodes, anticancer agents, oxygen sensors, spark plugs and turbine engines.[2]

Its largest use is as a component of autocatalysis within the automobile industry. Due to the increasing global awareness of the detrimental effects of car exhaust fumes on the atmosphere, many countries have mandated legislation dictating a shift to green chemistry. New three-way catalysts based on platinum, palladium and rhodium were developed as multifunctional systems that could accelerate reaction rates, oxidise carbon monoxide (*Equation 1.1*) and unburnt hydrocarbons (*Equation 1.2*), and which are able to reduce the oxides of nitrogen (*Equation 1.3*).[3]

$$2CO + O_2 \xrightarrow{Pt,\ Pd,\ Rh} 2CO_2 \qquad \ldots 1.1$$

$$C_xH_{2x+2} + [(3x+1)/2]O_2 \xrightarrow{Pt,\ Pd,\ Rh} xCO_2 + (x+1)H_2O \qquad \ldots 1.2$$

$$2NO_x \xrightarrow{Pt,\ Pd,\ Rh} xO_2 + N_2 \qquad \ldots 1.3$$

The chemical industry, with specific regard to fuels and oils, has also found wide use for platinum as a catalyst: (i) for selective hydrogenation, (ii) in the oxidation of ammonia to nitric acid and (iii) as a dehydrogenation catalyst for chemical intermediates in the synthesis of plastics, synthetic fibres, silicone rubber, pesticides and dyes.[4–5]

Due to its low, but temperature dependent resistance, platinum has also found considerable application in the electronics industry. The glass manufacturing sector uses platinum in the vessels that channel molten glass in the production of fibreglass, liquid crystal displays and flat-panel displays.[5–6] Platinum is a precious metal commodity and also finds use in jewellery as a 90-95% alloy (often with ruthenium or iridium).[5] Approximately 38 % of the worlds platinum is used in the manufacturing of ornate jewellery .[7] Platinum finds further uses in the manufacturing of surgical instruments and medical implants.

Barnett Rosenberg's discovery in 1969 of the anticancer activity of *cis*-diaminedichloroplatinum(II) (*cis*-[$Pt(NH_3)_2Cl_2$]), cisplatin) propelled platinum chemistry into the foreground of chemical research.[8–15] Cisplatin and its derivatives proved to be particularly effective in the treatment of testicular, ovarian, head, neck, bladder, lung, prostate and cervical tumours. [4-5,16] This led to further studies on platinum complexes as anticancer agents and as a result, a greater need for mechanistic studies to help explain the activity of these complexes. This is validated by the representative number of publications associated with this field.[8–15]

The beneficiation of platinum is a multi-billion dollar industry and has played a fundamental role in strengthening the South African economy as 153 tons, or 76.5 %, of the world's platinum is mined in Southern Africa, providing its residents with countless employment opportunities.[3]

1.1 General Properties of Platinum

Platinum has six naturally occurring isotopes: ^{190}Pt, ^{192}Pt, ^{194}Pt, ^{195}Pt, ^{196}Pt and ^{198}Pt with the most abundant of these being ^{195}Pt, comprising 33.8 % of all platinum. It is a member of the platinum-group metals (PGMs) which also include iridium, palladium, osmium, ruthenium and rhodium (***Figure 1.2***). These metals are considered noble due to their high ionisation potentials and sublimation energies.[5] The most common oxidation states of platinum are +2 and +4. In the +2 oxidation state, platinum has 8 *d*-orbital electrons and consistently adopts a square-planar geometry due to the vacant dz^2 orbitals.[17] Platinum(IV) forms many thermally stable and kinetically inert complexes, most of which possess an octahedral geometry.

Characteristic reactions for platinum complexes include ligand substitution, reductive elimination and oxidative addition reactions.[17] The +1 and +3 oxidation states are less common, and are often stabilised by metal bonding in bi- or polymetallic species. Several barium platinides (BaPt, Ba_3Pt_2 and $BaPt_2$) have been synthesised in which platinum exhibits negative oxidation states ranging from −1 to −2.[18]

Platinum also exhibits negative oxidation states at surfaces that have been reduced electrochemically.[19] The negative oxidation states exhibited by platinum are unusual for metallic elements and may be attributed to the relativistic stabilisation of the *6s* orbitals.[20]

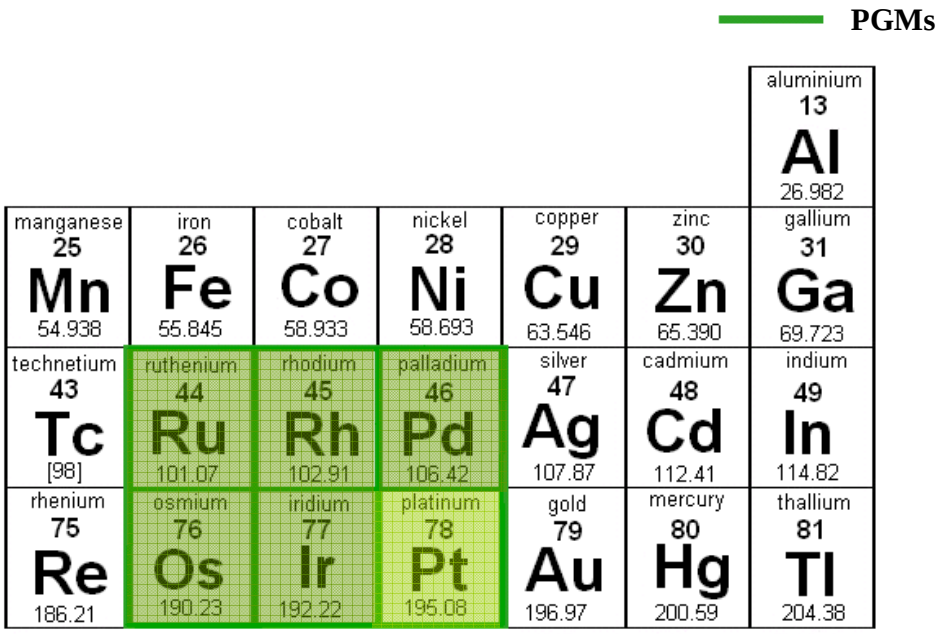

Figure 1.2: Portion of periodic table highlighting the platinum-group metals.[21]

1.2 Platinum(II)-Based Chemotherapy

Malignant neoplasm, or cancer, as it is more commonly known, is a class of diseases in which a group of cells display uncontrolled growth, invasion and metastasis.[22] It is these three factors that differentiate them from benign tumours. Cancer is a result of the formation of abnormalities in the genetic material of transformed cells.[22] These abnormalities may result from exposure to carcinogens, *e.g.* radiation or infectious agents.[22] Random errors in DNA replication and simple hereditary transfer are often also responsible.

Each year more people across the globe die of cancer, than of AIDS, tuberculosis, and malaria combined.[23] It is estimated that by 2030, 27 million new cancer cases and 17 million cancer deaths will occur each year worldwide. In light of statistics such as these, anticancer drug treatments continue to be a focal point of research. Patients diagnosed with cancer face the daunting task of choosing a course of treatment. Although surgery is an option, it is often ineffectual, highly traumatic and most importantly dangerous, as general anaesthesia is still considered a risk. Thus, in spite of the side-effects associated with radiotherapy and chemotherapy, these remain a better option due to their non-invasive nature.

1.2.1 First Generation Platinum(II)-Based Chemotherapy

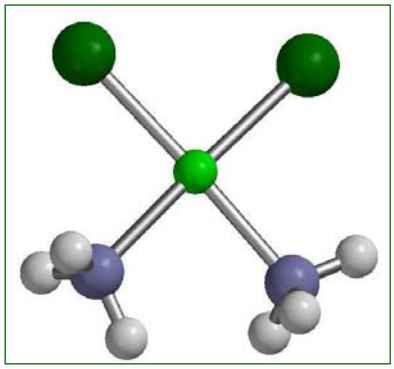

Cisplatin, (***Figure 1.3***) was first synthesised in 1844 but it was not until 1969 that its pivotal role in the development of platinum-based chemotherapy was discovered. This drug was approved by the Food and Drug Administration (FDA) in 1978[24] and is still in use to date. Cisplatin is used to treat ovarian cancer, small cell lung cancer, germ cell tumours and lymphomas.

Figure 1.3: Ball and stick structure of cisplatin $[Pt(NH_3)_2Cl_2]$.[25]

1.2.1.1 Mechanism of Action of Cisplatin

Outside the human cell, the chloride concentration is approximately 100 millimolar. This prevents the drug from hydrolysing, but once inside the cell, where the chloride concentration drops to between 4 and 20 millimolar, the chloride ligands of cisplatin are displaced and the complex is hydrolysed to its di-aqua form which is then capable of forming coordinate covalent bonds with purine bases on DNA.[26] These 1,2-intrastrand cross-links are believed to produce distortions to the natural structure of the double helix. If enough sequence errors are produced without repair, the cell will die following an apoptotic process (***Figure 1.4***). This process is not selective and cisplatin has been known to interact with non-cancerous cells and other biomolecules.

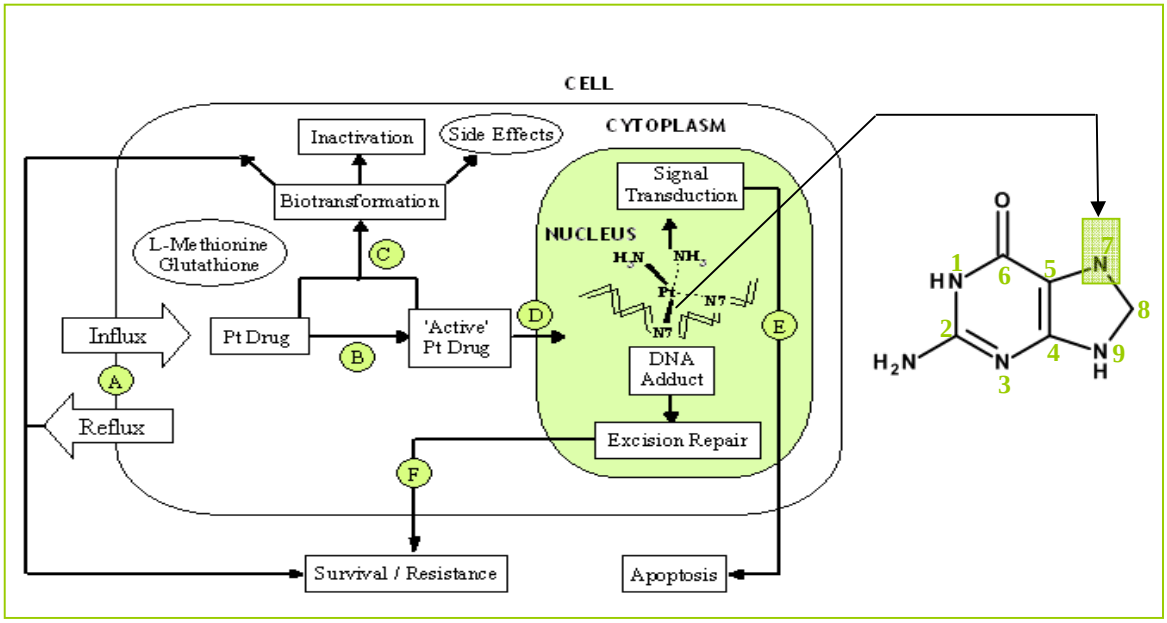

Figure 1.4: Schematic representation of cisplatin's proposed mechanism of action.[27]

Cisplatin's ability to act as an effective cytotoxic agent is dependent upon its bioavailability at the target site, and that in turn, is dependent upon the net uptake (***Figure 1.4***, ***A***) and the degree of detoxification by platinophilic agents, especially S-containing nucleophiles (***Figure 1.4***, ***C***). Upon entry to the cell cisplatin is slowly hydrolysed to form the reactive aqua species (***Figure 1.4***, ***D***). Platination occurs on the *N*7 of the guanine in DNA resulting in adduct formation. DNA damage may be detected by various sensors prompting a wide variety of different responses. If repair attempts are unsuccessful apoptosis (programmed cell death) (***Figure 1.4***, ***E***) will occur. Alternatively the Pt—DNA adduct will be adequately repaired so that the cells will survive (***Figure 1.4***, ***F***).[27]

1.2.1.2 Limitations of Cisplatin

As with any medicinal drug, adverse effects are unavoidable, and cisplatin is no exception. In spite of therapeutic success in the treatment of several types of tumours, its' effectiveness is severely hindered by undesirable side-effects such as nausea, alopecia (hair loss), neurotoxicity (nerve damage), ototoxicity (loss of hearing), nephrotoxicity (kidney damage) and mild myelosuppression (decrease in bone marrow activity resulting in decreased formation of red and white cells as well as blood platelets).[25]

Cisplatin's activity is also limited to a relatively narrow range of tumours. This is due to the fact that tumour resistance may be acquired during cycles of therapy, *e.g.* ovarian cancer and small cell lung cancer, or resistance may be intrinsic in patients with colorectal, prostate, non-small cell lung or breast cancer. [25] Neck, head and testicular cancers are sensitive to cisplatin treatment implying that acquired resistance may develop. A definitive explanation as to why resistance occurs has not yet been established. The general consensus is that resistance results from cisplatin being unable to reach its DNA target. [25]

1.2.1.3 Structure Activity Relationships (SAR)

Molecule-based hypotheses generally adhere to the notion that similar structured molecules possess similar activities. Cleare and Hoeschele[28-29] created SAR as conventional practices of medicinal chemistry which tried to adjust the effect or the potency of chemicals such as cisplatin by modifying their chemical structure. In essence these rules were considered a blue print that would yield success if followed.

The rules included:

i. Complexes exchange only some of their ligands quickly in reactions with biological molecules.
ii. Complexes should be electrically neutral, although the active form may be charged after undergoing ligand exchange in the organism.
iii. The geometry of these complexes is either square-planar or octahedral.
iv. Two *cis* monodentate or one bidentate leaving group (exchangeable ligands) are required; the corresponding *trans* isomer of the monodentate leaving groups is generally inactive.
v. The rates of exchange of these groups should fall into restricted regions, since too high a reactivity will mean that the chemical reacts immediately with the blood constituents and never gets to the tumour cells, while too low a reactivity would allow transportation to cells but would have no effect once there.
vi. The leaving groups should be approximately 3.4 Å apart on the molecule which is thought to correspond to the spacing between the steps of the Watson-Crick DNA ladder.
vii. The groups *trans* to the leaving groups should be strongly bonded *e.g.* relatively inert amine type ligands.

It was not long before exceptions to these rules were made. These include the high activity of leaving groups such as oxalate and malonate which were not encompassed; nor was the effect of cyclic amines, which decreased the solubility of the complexes, but markedly enhanced the anticancer activity. Also it has been shown that not all *trans* compounds nor all charged compounds are inactive.[30] It has also been established that only complexes with two amine ligands each carrying at least one H atom, are active.[30]

1.2.2 Second Generation Platinum(II)-Based Chemotherapy

Due to the shortcomings encountered with cisplatin, a second generation of synthetic analogues (based on the SAR described by Cleare and Hoeschele[28-29]) were created in an attempt to concentrate all the benefits of cisplatin whilst simultaneously eliminating the toxicity and resistance that had previously been experienced.[31-32] Examples of these analogues are given in ***Figure 1.5***. Carboplatin marketed under the trade name Paraplatin® (***Figure 1.5, a***) is an analogue of cisplatin in which the two chloride leaving groups are replaced by the more stable cyclobutanedicarboxylate ligand. This substitution results in decreased nausea, renal effects and nephrotoxicity. Furthermore unlike cisplatin, this drug does not require a rigorous pre-treatment hydration regime. Although less toxic, this synthetic analogue still induces toxicological problems such as myelosuppresion, neutropenia and anaemia.[31]

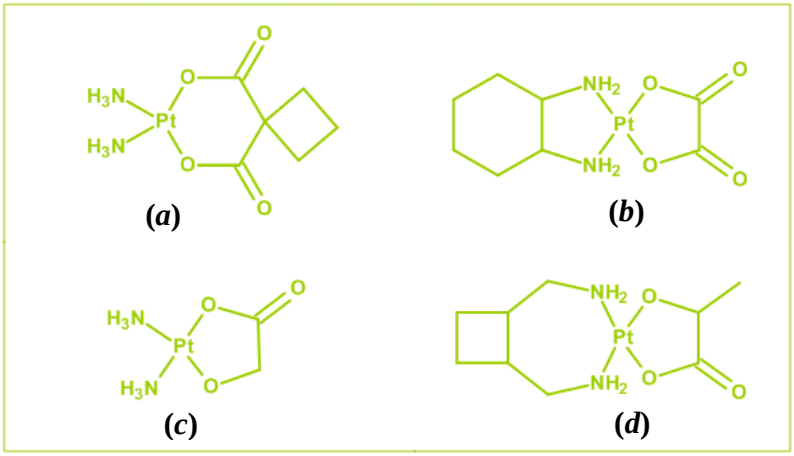

Figure 1.5: Some of the second-generation platinum(II) complexes investigated for their anticancer potential; Carboplatin (**a**), Oxaliplatin (**b**), Nedaplatin (**c**) and Lobaplatin (**d**).[32–34]

Oxaliplatin (***Figure 1.5, b***) has a lowered toxicity due to the slow hydrolysis of the malonate leaving group. This drug does not induce ototoxicity or myelosuppresion but side-effects do include tingling of the extremities, neuropathy, nausea and vomiting.[33] Both Nedaplatin (***Figure 1.5, c***) and Lobaplatin (***Figure 1.5, d***) offer lower toxicity and obey the structure activity relationships originally devised for anticancer candidates in the platinum family.[34] Nedaplatin is marketed under the name Aqupla® and is approved for use against ovarian cancer. Lobaplatin has been approved for treatment of small cell lung cancer, inoperable breast cancer and chronic myelogenous leukaemia. This drug has also completed phase II clinical trials in the European Union, Australia, United States of America, Brazil and South Africa for the treatment of various forms of cancer including oesophageal, lung and ovarian cancers.

1.2.3 Current Generation Platinum-Based Systems

It is clear that although second generation platinum(II) anticancer drugs alleviated some of the problems encountered with cisplatin, such as lowering the side-effects, broadening activity and overcoming certain types of resistance, none managed to resolve all the problems associated with the first generation drug.[35] It is because of this very reason that researchers deviated from the previously described SARs and began to focus on non-classical systems. Unlike their predecessors, non-classical systems are far too diverse for general structure activity relationships to be inferred. Thus, it is essential that one fully understands the mechanism of binding of a particular set of complexes to DNA.

Apart from adduct formation, molecules are able to bind to DNA through three distinct ways: groove binding, intercalation and insertion (***Figure 1.6***).[36] Groove binding (***Figure 1.6, a***) occurs when molecules bind into the minor groove of the DNA strand by partial intercalation or by hydrophobic interactions.[32] Molecules that partly unwind DNA and π-stack between two base pairs are known as intercalators (***Figure 1.6, b***). Once in position, they are maintained in place by hydrogen bonding and Van der Waal's forces.[36] Intercalators slot in to the major groove of the double helix with the intercalating ligand acting as a new base.[36] As no bases are excised the major groove widens. DNA insertion (***Figure 1.6, c***) involves separation and displacement of a base pair.[4]

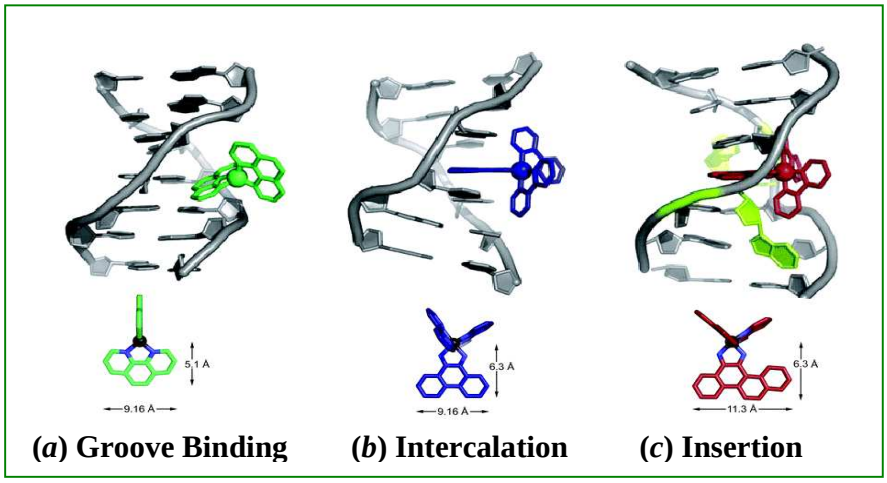

Figure 1.6: Diagram indicating non-covalent DNA binding modes; Groove Binding (***a***), Intercalation (***b***) and Insertion (***c***).[36]

1.2.3.1 Complexes Possessing Trans-Geometry

The prototype of a non-classical platinum complex is transplatin (***Figure 1.7, I***). This complex is devoid of anticancer activity. A possible explanation for this was that the *trans* isomer reacts much faster than its *cis* counterpart resulting in reduced selectivity and undesirable side reactions. Furthermore it is stereochemically impossible for the *trans* isomer to form 1,2-intrastrand cross-links between two adjacent purines (mode of binding for cisplatin).[4,31,37] It is interesting to note that transplatin attains cytotoxic properties comparable to cisplatin when treated cells are irradiated with UV light. This photo-activation results in the formation of intra-strand and DNA protein cross-links.[38] *Trans* complexes may be classified into three categories as seen in ***Figure 1.7***.[38]

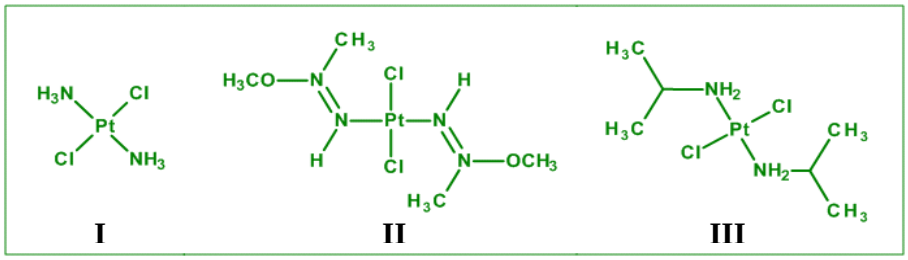

Figure 1.7: Representatives of non-classical platinum complexes possessing *trans* geometry; **I** transplatin, **II** transplatin analogue with iminoethers ligands and **III** *trans* configured complex with aliphatic amine ligands.[38]

1.2.3.2 Multinuclear Platinum(II) Complexes

Of all third or current generation complexes it is clear that multinuclear platinum complexes deviate the most from their originator, cisplatin. These complexes are comprised not of one, but rather two, or more, platinum centres, each possessing the ability to interact with DNA. The first dinuclear design was reported in 1988 and consisted of two *cis*-$PtCl_2(NH_3)_2$ units linked by a flexible diamine chain (***Figure 1.8: 2,2/t,t, 2,2/c,c and 2,2/c,t***).[39] Platinum complexes such as these are the most common of the non-classical systems and often exhibit high anticancer activity, broad cytotoxic profiles and are able to overcome cisplatin resistance.[40] Dinuclear complexes often possess a high charge (+4) whilst mononuclear complexes are generally neutral. This difference in charge ensures that dinuclear complexes have better solubility and thus faster uptake in the body.[41] Studies with these complexes have shown that hydrogen-bonding capacity, chain length, flexibility and the position of the leaving group (usually chloride) relative to the chain also appear to be major factors in designing multinuclear platinum anticancer drugs.[42–44]

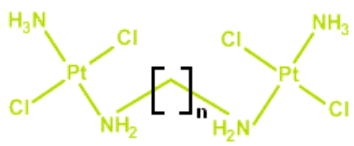

2, 2/t,t

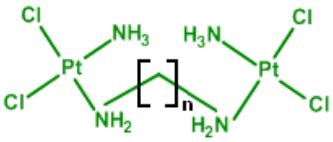

2, 2/c,c

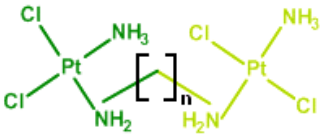

2, 2/c,t

Where n = 4, 5, or 6

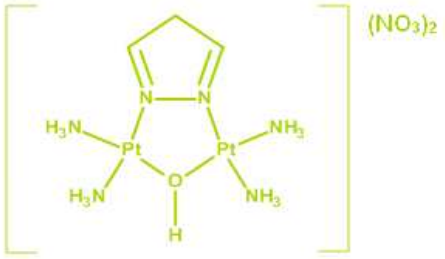

[{cis-$Pt(NH_3)_2$}(μ-OH)(μ-pz)]$(NO_3)_2$ **(pz)**

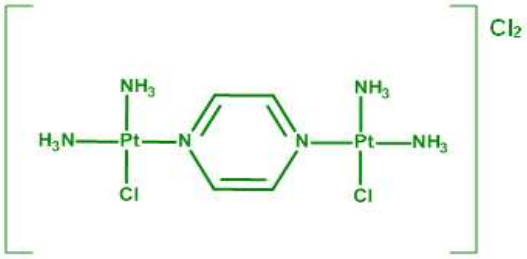

[{cis-$Pt(NH_3)_2Cl$}$_2$(μ-OH)(μ-pz)]Cl_2 **(pzn)**

Figure 1.8: Examples of multinuclear complexes with flexible (three possible isomers of *bis*-platinum(II) complexes possessing *trans,trans* (*t,t*), *cis,cis* (*c,c*) and *cis,trans* (*c,t*) geometries) and rigid (azole bridged **pz** and azine bridged **pzn**) spacers. [45]

Most dinuclear anticancer active platinum complexes described in the literature contain two types of bridges. There are flexible bridging ligands, such as aliphatic diamines, and there are rigid linkers such as azoles and azines (***Figure 1.8***: **pz** and **pzn**).[45–48] The complexes with flexible linkers are designed to form long-range cross-links on DNA, and those possessing rigid bridging ligands, are developed to minimise distortion of the DNA double helix in a 1,2-intrastrand cross-link.[43] Due to this mode of binding the induced distortion on DNA is much less severe.[49] The change of binding site numbers has resulted in a shift in which interstrand adduct formation now takes preference over the formation of the 1,2-intrastrand cross-linked adducts. A result of this is that multinuclear platinum complexes exhibit high cytotoxicity against tumours that are cisplatin resistant (both acquired and intrinsic).[49]

Triplatin tetranitrate (***Figure 1.9, BBR3464***) is a good example of a multinuclear platinum complex. This trinuclear platinum complex was first described by Nicholas Farrell in the 1990s and was the first platinum drug not based on the classical cisplatin template to enter clinical trials. The mode of action for BBR3464 is similar to that of cisplatin. Notable features include broad spectrum toxicity against a range of tumours, potency and a ten-fold lower maximum toleration dose.[28] Although BBR3464 exhibits improved functionality it also exhibits biotransformation and drug degradation.[50–51]

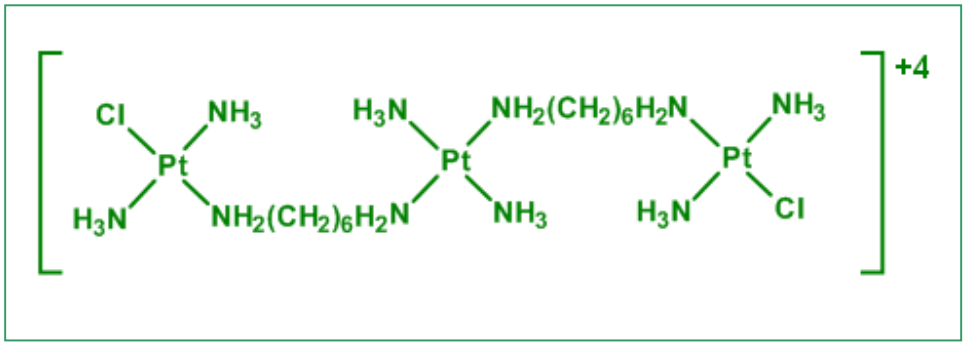

***Figure 1.9*:** Structure of triplatin tetranitrate (BBR3464) multinuclear platinum complex .[52]

1.3 Platinum(II) Terpyridine Complexes

1.3.1 General Synthetic Methodology of 2,2′:6′,2″-terpyridines

Terpyridine (terpy) was first synthesised by Morgan and Burnstall in 1932 by the oxidative coupling of pyridines.[53] Synthesis of 2,2′:6′,2″-terpyridines (***Figure 1.10***) has since been optimised and generally follows one of two methodologies. They can either be designed through the synthesis of the central ring or through the coupling of three pyridine rings. The main methodologies may then be separated into the following categories: (i) Condensation methodology[54–55]; (ii) Pyrolysis[56]; (iii) Todha methodology[57]; (iv) Metal mediated coupling reactions[58]; and (v) Sauer methodology (cycloaddition).[59] The condensation methodology is of particular interest as it pertains to the synthesis undertaken in this work.

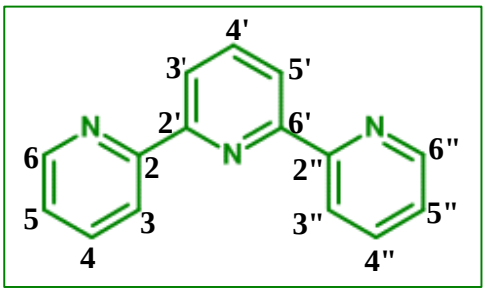

Figure 1.10: Diagram of a systematically labelled 2,2′:6′,2″-terpyridine molecule.[60]

The most efficient form of the condensation method was reported by Jameson and Guise[61] in which 2-acetylpyridine (***Table 1.1***, ***i)*** is reacted with *N*,*N*′-dimethylformamide dimethyl acetal to form the enaminone (***Table 1.1, ii)***. This enaminone is then condensed with the potassium salt of 2-acetylpyridine and the dimethyl amine is lost. The resulting 1,5-dione (***Table 1.1***, ***iii)*** is not isolated prior to the ring closure by ammonium acetate. The Kröhnke condensation [62] is another interesting synthetic method. The root of this reaction is the aldol condensation of 2-acetylpyridine (or a substituted derivative) (***Table 1.1, v)*** with an aldehyde in basic aqueous or alcoholic media to give an *α*, *β*-unsaturated ketone or enone (***Table 1.1, vi)***. Michael addition of a suitable enolate then affords a 1,5-dione (***Table 1.1, vii)***. Ring closure with ammonium acetate results in the formation of a dihydropyridine which undergoes oxidation to the desired terpyridines (***Table 1.1, viii)***.[60] Such a process is advantageous because it allows the production of symmetrical and unsymmetrical 2,2′:6′,2″-terpyridines.

Table 1.1: Schematic representation of 2,2′:6′,2″-terpyridine synthetic methodologies [54–62]

Condensation Methodology 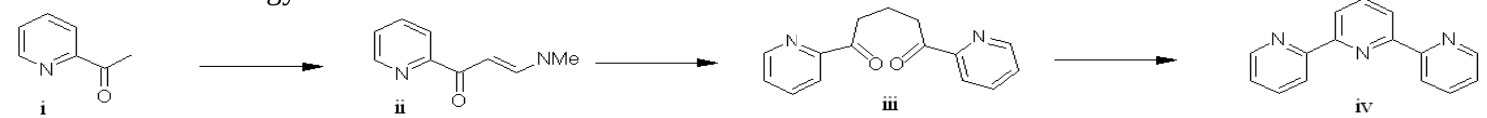 i ii iii iv
Kröhnke Methodology 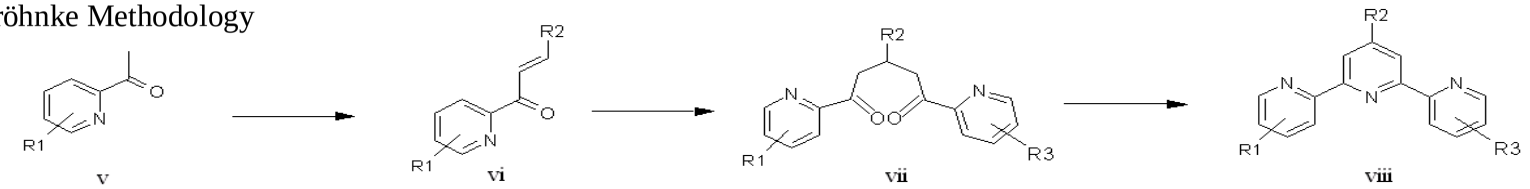 v vi vii viii
Pyrolysis 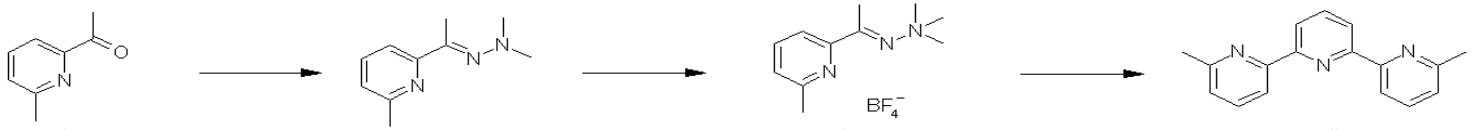 ix x xi xii
Todha Methodology 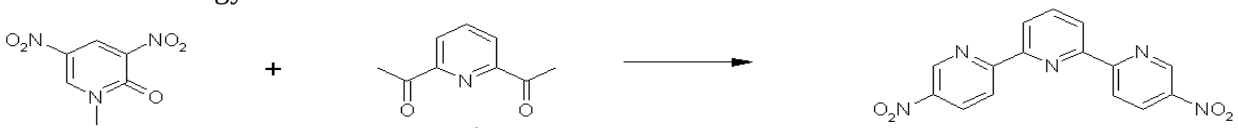 xiii + xiv xv
Metal–mediated Methodology 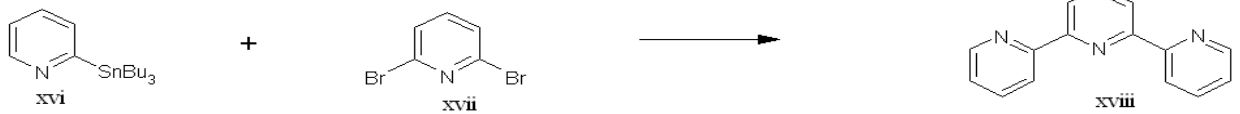 xvi + xvii xviii
Sauer Methodology 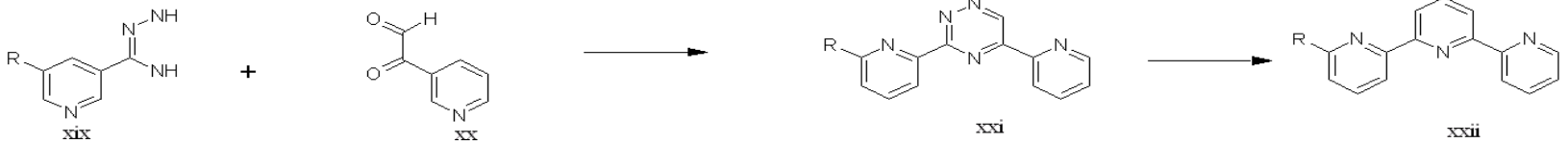 xix + xx xxi xxii

1.3.2 Functionalisation of the Terpyridine Fragment

2,2′:6′,2″-terpyridines may be functionalised at both the central and terminal pyridine rings by introducing substituted reagents in either the ring assembly or coupling procedures. The manner of functionalisation of these terpyridine derivatives, as discussed below, is organised according to their position on the ring.

1.3.2.1 Symmetrical Terminally Substituted Terpyridines

In an attempt to introduce functionality from the posterior end of the chelator, the highly unusual 3,3″-positions were functionalised by Benniston *et al*.[63–64] The 3,3″-di-*p*-tolyl-terpy was obtained from a six step synthesis that involved both coupling and ring closure (***Figure 1.11, 3,3")***.

To date, 4,4″-symmetrically functionalised terpyridines are known to exist with a variety of different substituents through an assortment of mechanisms (***Figure 1.11, 4,4")***. An example of such a system is the ring closure of the *bis*(chalcone) of 2,6-diacetylpyridine and *N*-phenacyl or *N*-methylpyridinium bromide which results in the analogous 4,4″-substituted compounds.[65]

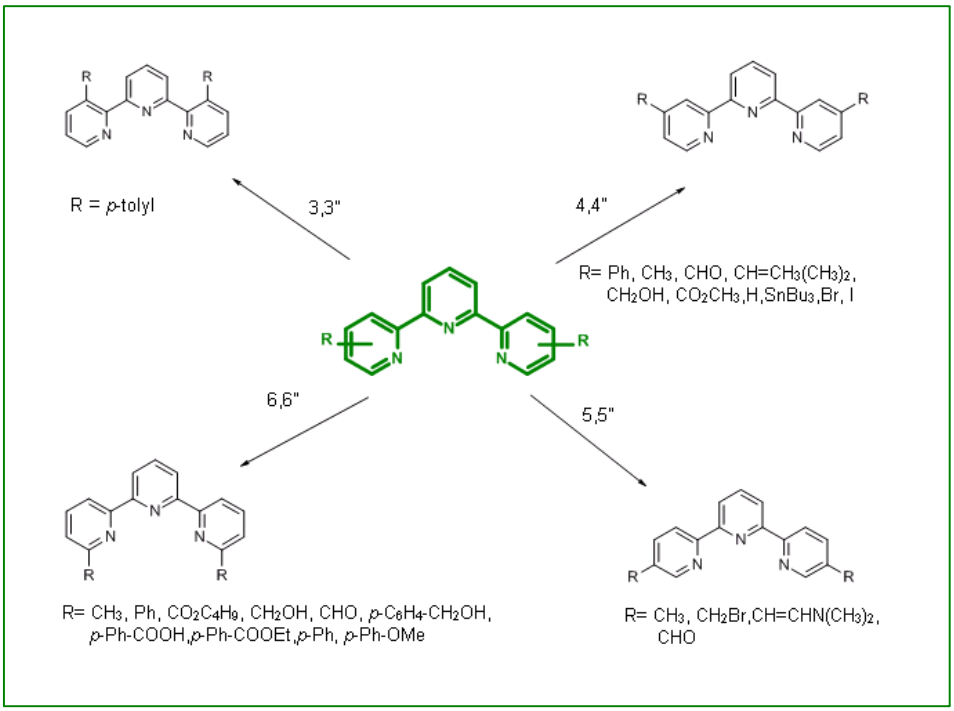

Figure 1.11: Symmetrical terminally substituted terpyridines.[63–65]

Heller and Schubert have also described the synthesis of 4,4″-dimethyl-terpy by a Stille-type cross coupling.[66] Sasaki *et al.* [67] synthesised 4,4″-diformyl-terpy by oxidation with H_2SeO_3 and the 4,4″-*bis*[(dimethylamino)methylidene]-terpy by conversion with Bredereck's[α] reagent. This compound was reduced by $NaBH_4$ in order to obtain the hydroxymethyl compound. 4,4"-*bis*(tributylstannyl)-terpy was prepared from 2,6-*bis*(1,2,4-triazin-3-yl)pyridine and tributyl(ethynyl)tin and upon subsequent treatment with Br_2 and I_2, the corresponding bromo and iodo compounds were synthesised (***Figure 1.11, 4,4"***).[68] 5,5″-dimethyl-terpy was synthesised through the coupling of 2-trimethylstannyl-5-methylpyridine and 2-bromo-5-methylpyridine.[69] Subsequent bromination with *N*-bromosuccinimide and azo-*bis*(isobutyronitrile) in carbon tetrachloride produced 5,5″-*bis*(bromomethyl-terpy). Sasaki *et al.*[67] have also described the synthesis of the 5,5″-*bis*[(dimethylamino)methylidene]-terpy and the 5,5″-diformyl-terpy ***(Figure 1.11, 5,5")***.[67]

6,6″-dimethyl-terpy can be synthesised through the Stille type cross-coupling of 2,6-dibromopyridine and 2-(tributylstannyl)-6-methylpyridine or through the use of a Kröhnke ring closure reaction involving different Mannich[β] salts.[70–71] 6,6″-di-*n*-butoxydicarbonyl-terpy may be synthesised from 6,6″-dibromo-terpy, carbon monoxide and $[PdCl_2(PPh_3)_2]$ in $^{n}BuOH$ and $^{n}Bu_3N$.[72–73] Reduction of this newly synthesised compound with $NaBH_4$ results in the formation of 6,6″-*bis*(hydroxymethyl)-terpy. The subsequent oxidation of 6,6″-*bis*(hydroxymethyl)-terpy with oxalyl chloride and dimethyl sulfoxide in dichloromethane yielded the 6,6″-diformyl-terpy. Benniston *et al.*[63] have published the preparation of 6,6″-*bis*[4-(hydroxymethyl)phenyl]-terpy by a ring-forming reaction (***Figure 1.11, 6,6")***.

α *Tert*-butoxy bis(dimethylamino)methane.

β A Mannich salt is a beta amino-ketone which is formed in the reaction of an amide or aldehyde with a carbonic acid.

1.3.2.2 Uniform All-Ring Substituted Terpyridines

A symmetrically functionalised 2,2′:6′,2″-terpyridine with one chloride atom at each pyridine ring has been prepared by combining 4,4′,4″-trinitro-2,2′:6′,2″ terpyridine, *N*-oxide and an excess of acetyl chloride in glacial acetic acid (***Figure 1.12***, ***4,4′,4″)***. [74]A palladium-catalysed coupling of 4-(5-nonyl)pyridine produced the 4,4′,4″-*tris*(5-nonyl)-terpy.[75–76] A Kröhnke condensation has been used to synthesise the 4,4′,4″-triphenyl-derivatised terpy.[63] Trimethyl substituted terpyridines (***Figure 1.12***, ***5, 4′,5″*** and ***Figure 1.12***, ***6, 4′,6″)*** have been synthesised using a Stille-type cross-coupling between the corresponding 4-, 5- and 6-methyl-2-(tributylstannyl)pyridines and 2,6-dibromo-4-methylpyridine.[60]

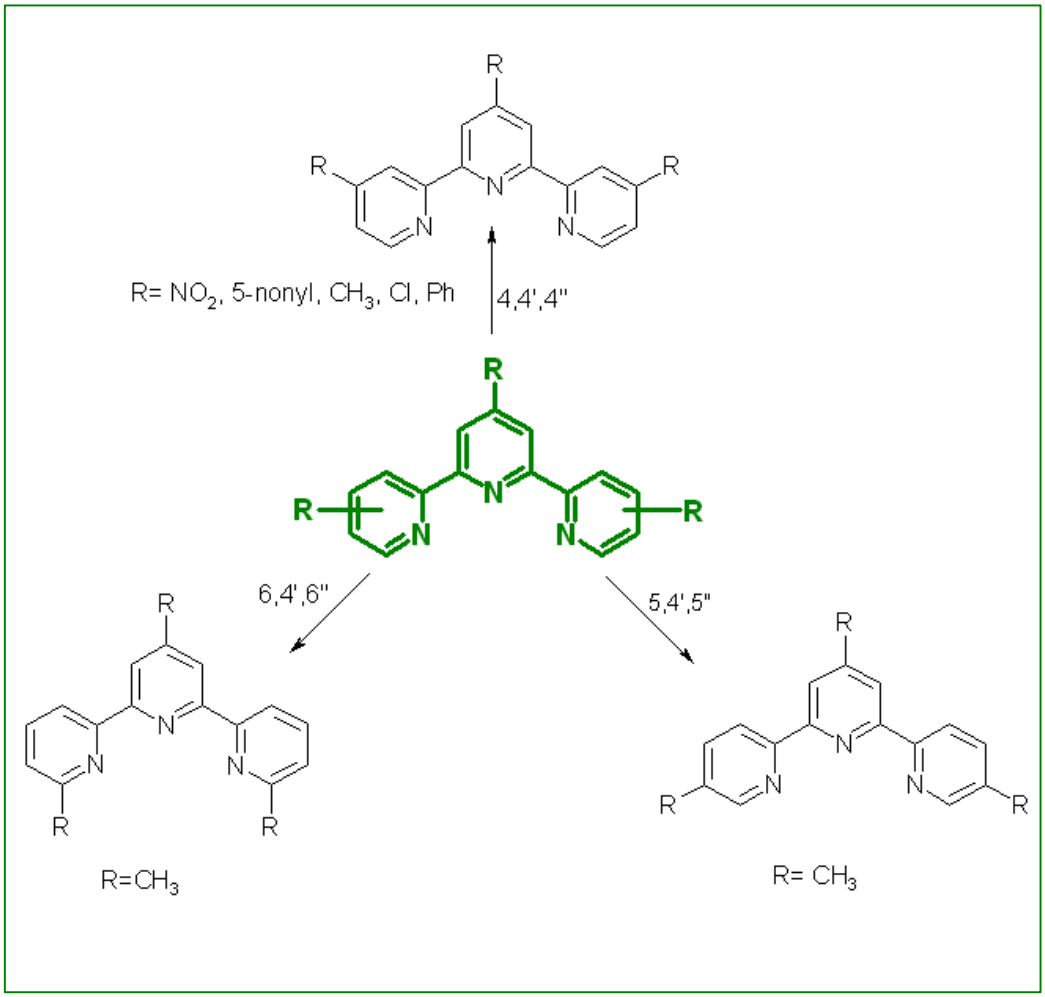

Figure 1.12: Uniform all-ring substituted terpyridines.[60, 63, 65, 74–75]

1.3.2.3 Asymmetric Terminally Substituted Terpyridines

A number of terpyridine complexes are known in which there are different substituents on the terminal rings. The 6-bromo-6″-methyl-terpy is one such molecule and was synthesised using the Kröhnke methodology (***Figure 1.13, 6,6″***).[77] Through application of the appropriate 1,2,4-triazines, Sauer *et al.*[68] were able to synthesise 4-tributylstannyl-terpy in a [4+2] cycloaddition with tributyl(ethynyl)tin. The tributylstannyl group can subsequently be replaced with a bromo or iodo group using Br_2 or I_2 respectively (***Figure 1.13,*** **(4,4″(a), 4,4″(b)**).

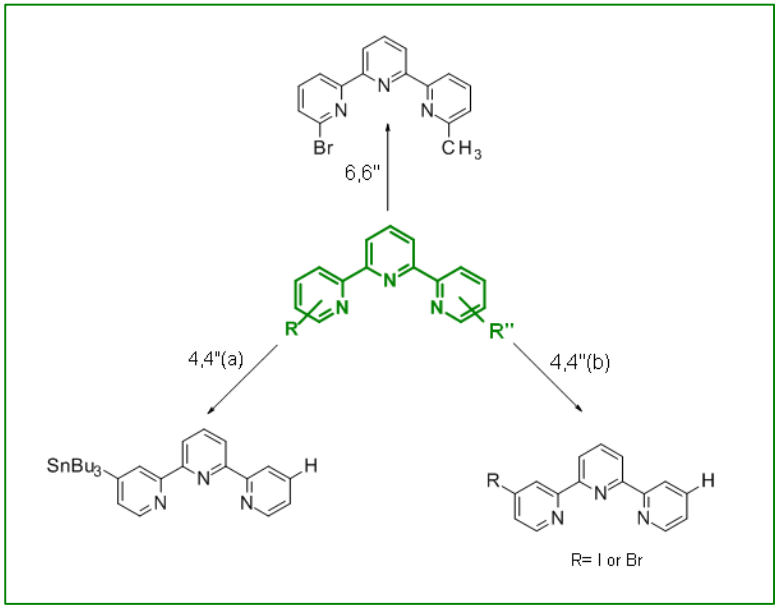

Figure 1.13: Asymmetric terminally substituted terpyridines.[66,77]

1.3.2.4 Multifunctional Terpyridines with Variable Substituents

2,2′:6′,2″-terpyridines bearing dissimilar functional groups at the 4′-position and on the outer pyridine rings have recently become an expanding field of terpyridine derivative preparation. Due to the sheer magnitude of functionalised terpyridines available only a select few will be discussed. Fallahpour *et al.*[78–79] have reported the treatment of 2,2-diacetyl-4-ethoxypyridine with paraformaldehyde and dimethylamine in DMF to yield a Mannich salt observed as pink crystals. The reaction of this Mannich salt with *N*-(methylacetyl)pyridinium chloride in ethanol resulted in the formation of 4′-ethoxy-6,6″-dimethyl-2,2′:6′,2″ terpyridine. Similar Kröhnke preparations resulted in the remaining molecules depicted in ***Figure 1.14***.

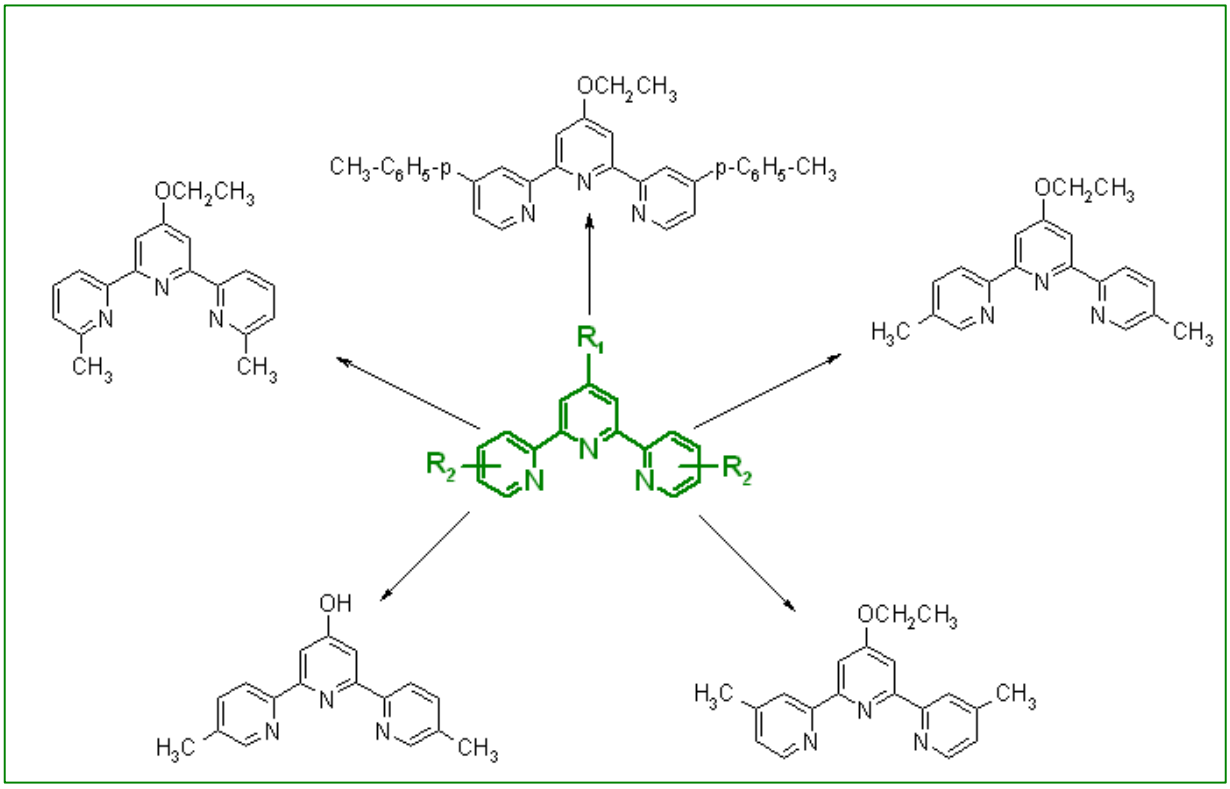

Figure 1.14: Multifunctional terpyridines with variable substituents.[65,78–79]

1.3.2.5 4′-Functionalised Terpyridines

Of the terpyridines discussed thus far, those functionalised at the 4′ position are generally considered the most notable and have particular relevance to this project. These functionalised terpyridines may be classified into two groups: 4′-aryl-substituted terpyridines and 4′-terpyridinyl ethers.

4′-aryl substituted terpy complexes are numerous and varied. The first example of this is the 4′-(2,5-dimethoxyphenyl)-terpy (***Figure 1.15****, A(I))* which was prepared by Colbran *et al.*[80–81] Macrocycles have also been attached to the 4′-aryl-substituted terpyridines. Ward *et al.*[82] have described the preparation of 4′-phenyl-substituted terpyridines with aza-18-crown-6 groups (***Figure 1.15,*** *A(II))*. Martinez-Manez *et al.*[83] have reported similar systems functionalised with 1,4,8,11-tetraazacyclotetradecane (***Figure 1.15,*** *A(III))*.

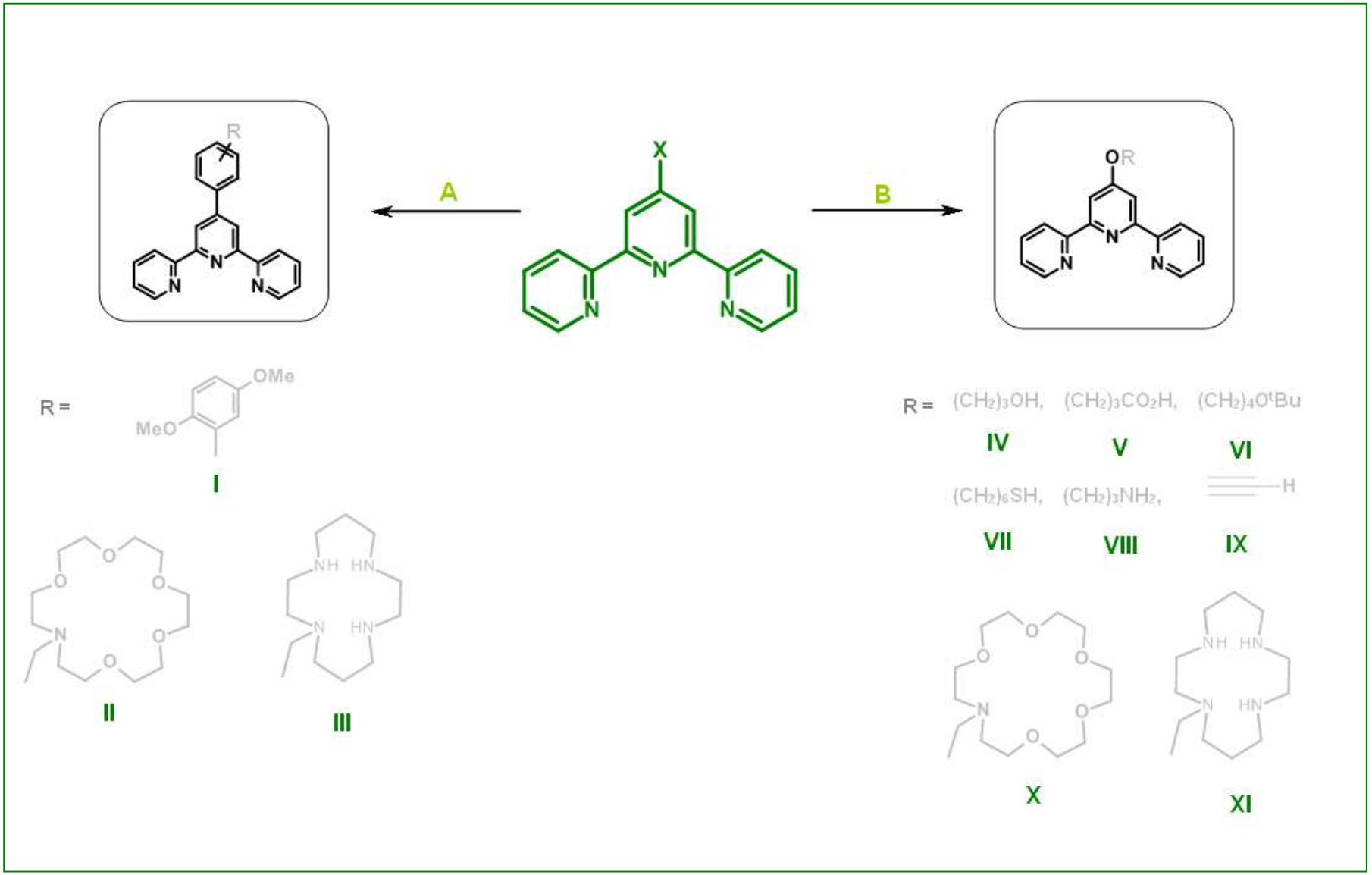

Figure 1.15: Types of 4′-functionalised terpyridines.[63,72–75]

4′-Terpyridinyl ethers are an essential class of terpyridine derivatives due to their convenient accessibility either by condensation reactions with 4′-hydroxyterpyridines, or through nucleophillic aromatic substitution of the 4′-haloterpyridines by primary alcohols (and analogues). A vast variety of functionalised terpyridinyl ethers have been synthesised and a small number is discussed here. Sampath *et al.*[84] and Schubert *et al.*[85–86] have reported a number of linear 4′-terpyridinyl ethers with terminal hydroxyl, carboxy, *tert*-butoxy, thio and amino groups (***Figure 1.15,*** *B(IV-VIII))*. These compounds were prepared by the reaction of an alcohol with a suspension of a base (KOH or NaH) in a polar aprotic solvent (DMSO or DMF) and the subsequent introduction of 4′-chloro-2,2′:6′,2″-terpyridine. Constable *et al.*[87–88] reported the synthesis of the alkyne-functionalised terpyridine *(**Figure 1.15,** B(IX))*. The same authors also presented a new class of terpyridine ligands in which a sugar moiety is covalently linked to the terpyridine ligand. This was done in an attempt to probe molecular recognition events by the functionalisation of biomolecules by metal binding sites.[87–88]

Another illustration of sophisticated ether-linked functional groups was presented in the formation of a fullerene-functionalised 4′-terpyridine published by Schubert *et al.*[89–90] in order to investigate the special electronic properties of such compounds. The 4′-derivatisation of terpyridines with aza-crown macrocycles is considered important for their use as luminescent or electrical sensors and the preparation of di- or multitopic terpyridine ligands.

Martinez-Manez *et al.*[91] have reported similar systems functionalised with 1,4,8,11-tetraazacyclotetradecane (***Figure 1.15,*** *B(X))* from the reaction of the 4′-(bromomethyl)- 2,2′:6′,2″-terpyridine and cyclam. Ward *et al.*[82] have described the preparation of the 4′-substituted and 4′-phenyl substituted 2,2′:6′,2″ terpyridines with aza-18-crown-6 groups from the reaction of 4′-bromo-2,2′:6′,2″-terpyridine and 18-crown-6 (***Figure 1.15,*** *B(XI))*.

Modern ring-assembly and cross-coupling procedures enable the well-directed introduction of different functionalities into almost every position of the terpyridine ring system. Nevertheless, the number of terpyridine derivatives is still relatively easy to survey. The methods for terpyridine construction are only compatible with a few less reactive functional groups.

1.3.3 Proposed Metals for Binding Bis-Terpyridine

The choice of metal for coordination to terpyridine systems such as those reviewed above is critical as it is the metal that ultimately determines the characteristic features of the metal chelate. Although numerous metals have been used in conjunction with terpyridine ligands this review will focus on four *viz*. platinum, ruthenium, cadmium and copper.

Platinum is the most commonly associated metal with regard to terpyridine binding due to its many appealing characteristics *viz.* (i) synthetic methods for the preparation of platinum(II) complexes are relatively straightforward and economically viable[92]; (ii) square-planar d^8 platinum(II) derivatives with terpyridinyl analogues often exhibit intriguing photophysical and spectroscopic properties due their planar coordination geometry which permits easy access to important frontier orbitals of the metal centre, d^8—d^8 metal—metal interactions as well as π—π interactions between chromophores of the polypyridinyl platinum(II) complexes lead to extensive polymorphism[93–96]; (iii) platinum(II) terpyridine complexes have been shown to act as intercalating agents and thus are potential anticancer agents.[94]

Figure 1.16 shows a series of dinuclear alkynyl platinum(II) terpyridinyl complexes.[97–100] Studies have shown that both mono- and dinuclear alkynyl complexes show interesting *inter*molecular aggregation and oligomerisation phenomena in the solution state with drastic colour changes and luminescence enhancement caused by polymer-induced or solvent-induced self-assembly of the metal complexes. The remarkable spectroscopic changes observed upon variation of the solvent composition, counterion, and pH of the polyelectrolyte, is believed to be the result of tuneable solution-state intermolecular Pt—Pt interactions and π—π stacking. Yam *et al.*[100] showed that chain length plays an important role in governing the occurrence and extent of intermolecular aggregation. Complexes ***I*** and ***II*** (***Figure 1.16***) which have short bridges will not undergo self association or aggregation at room temperature. In contrast complexes ***III*** and ***IV*** (***Figure 1.16***) with longer flexible bridges can readily self-associate and aggregate.

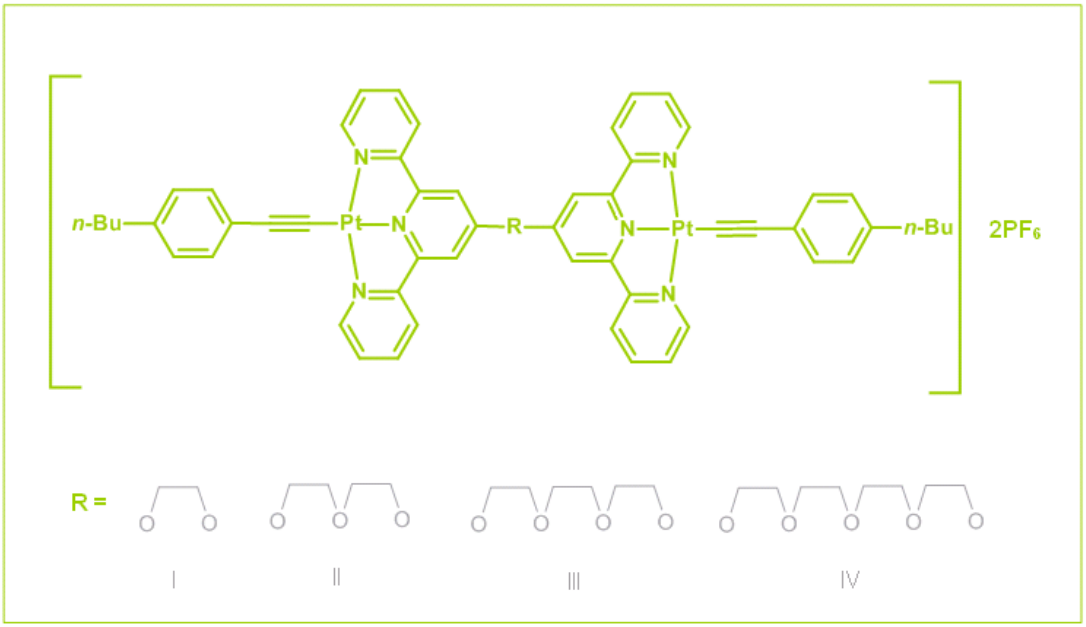

***Figure 1.16**:* Structure of the dinuclear alkynyl platinum(II) terpyridinyl complexes.[100]

Ruthenium is another promising choice of metal as it, like platinum, exhibits anticancer activity. An example of a dinuclear ruthenium terpyridinyl complex is shown in ***Figure 1.17***. Not only does this structure show anticancer activity, it also has the potential to act as a building-block for the self-assembly of supramolecular architectures. Metallomacrocycles of this nature have found applications as catalysts, sensors or receptors and in crystal engineering with metallocrowns, analogues of crown ethers in which backbone carbon atoms are replaced by metal ions.

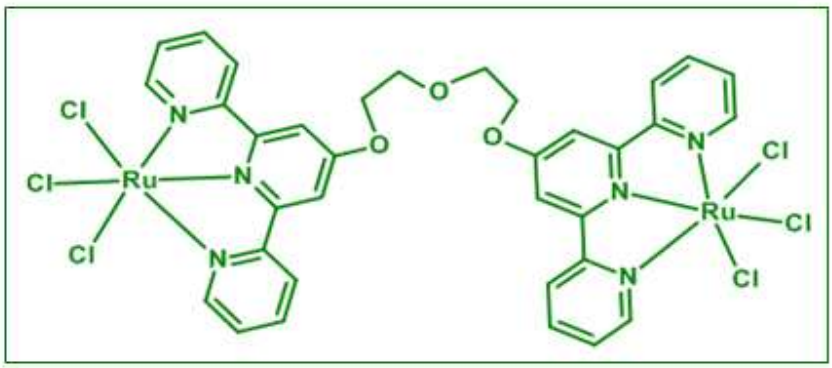

Figure 1.17: Structure of a dinuclear ruthenium(III) terpyridinyl complex which may be converted into the ruthenium(II) metallomacrocycle by addition of another equivalent of ligand.[101]

A challenging extension of the polynuclear concept was to introduce different metals at each of the binding sites, thus creating selective specificity and reactivity at each of the metal centres. One such example is the heterodinuclear ruthenium-platinum complex shown in ***Figure 1.18***. This complex consists of a ruthenium(II) cationic species as a light-absorbing unit linked to a reactive platinum centre through a short polyol bridging ligand. Work done by van der Schilden *et al.*[102] suggests that the platinum moiety is able to both intercalate and coordinate to the DNA without being hindered by the ruthenium unit, enabling a two-fold mechanism for binding to DNA. This is a unique example of a new series of potentially anticancer-active complexes of which variation of the terminal terpyridine ligand of the ruthenium unit offers great possibilities to improve noncovalent DNA binding modes as well as DNA coordination abilities. In view of the relatively long intramolecular ruthenium-platinum separation (14.5 Å), this approach can lead to compounds able to form delocalised long-range DNA adducts, thereby bestowing anticancer activity onto this new series of heterodinuclear ruthenium-platinum complexes.[102]

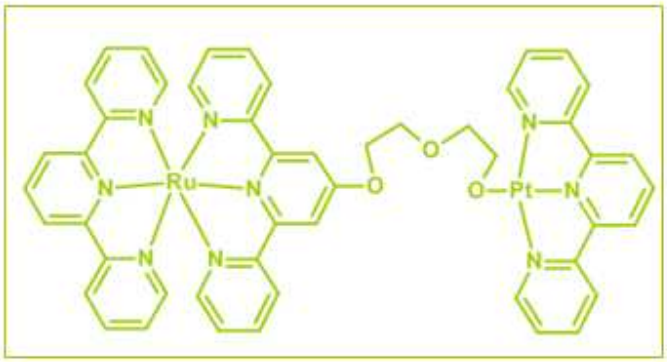

Figure 1.18: Structure of a heterodinuclear ruthenium(II)-platinum(II) complex. [(terpy)Ru(dtdeg)PtCl] capable of selective specificity and reactivity at each metal centre.[102]

Cadmium and copper have also been used to coordinate terpyridine systems. ***Figure 1.19*** shows examples of *bis*-terpyridinyl cadmium and copper complexes. This octahedral cadmium molecule is similar to the ruthenium complex discussed above, and may act as a metallo-supramolecular building block. Studies on the incorporation of such ligands into polymers with special photochemical properties as well as their attachment to metal surfaces and nanoparticles are currently in progress. [103–104]

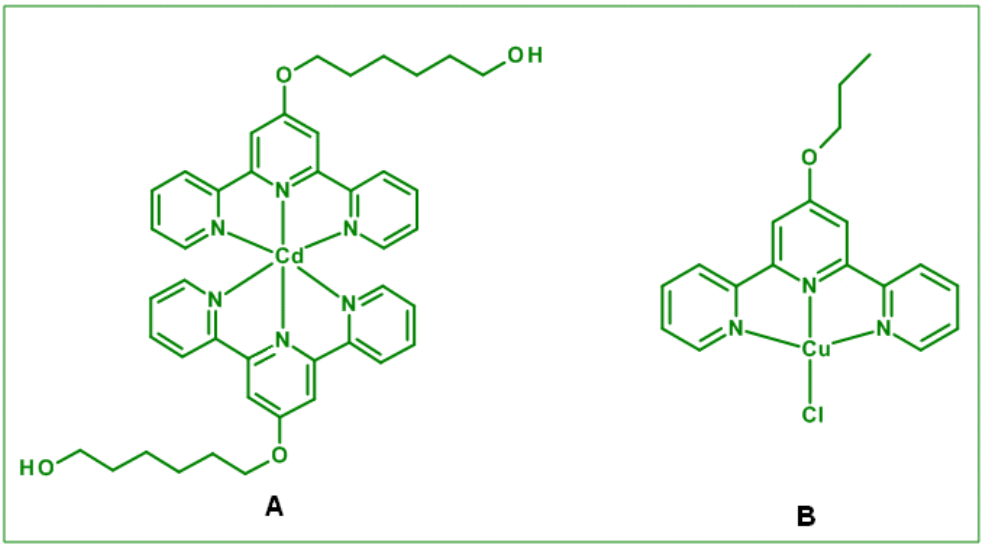

***Figure 1.19**:* Structure of cadmium and copper terpyidinyl complexes.[103–104]

1.3.4 Role of Platinum(II) Terpyridine Complexes in Biological Chemistry

The attractiveness of using platinum(II) terpyridines in biological studies is due to the useful properties of platinum(II) terpyridine probes. These properties include: the large platinum nucleus leading to high-scattering for X-ray diffraction studies, the spin-active ^{195}Pt nucleus for NMR spectroscopy and the long wavelength light absorption and emission for monitoring binding modes.[105] Pt(**X**terpy**Y**]$^{+}$ complexes (where **X** represents the substituent on the terpyidine chelate and **Y** represents the ligand at the fourth coordination site) are prevalent in the bioinorganic research field as these complexes have been shown to interact with biomolecules.[105–106] Their affinity can be explained by their ability to π-stack with other π-systems and by the fact that the **Y** ligand can be removed by a nucleophile, providing the molecule with an optimum attachment site. Lippard and co-workers[107] provided the first evidence in 1974 that platinum(II) terpyridine complexes can bind to DNA when they studied the interactions of the complex [Pt(terpy)(HET)]$^{+}$ (HET: 2-hydroxyethanethiol) with calf thymus DNA.[105] They showed that the complex intercalated between the base pairs of DNA by demonstrating that the interaction resulted in competitive inhibition.[107] Furthermore work done by McFayden *et al.*[108] showed that the platinum in these complexes was involved in binding to DNA as the free terpyridine ligands did not intercalate at physiological pH.[106]

Lippard and co-workers[109] investigated the intercalative ability of a variety of platinum(II) terpyridine complex cations of the type $[Pt(terpy)\mathbf{X}]^{n+}$ where n = 1 (**X** = Cl, HET, cysteine or carboethoxymethanethiol (CMT) or where n = 2, **X** = 2-aminoethanethiol (AET)).[106] Each of these complexes was shown to intercalate to DNA by their ability to unwind circular DNA and inhibit ethidium bromide binding. It was found that the AET complex had the highest binding constant (**Table 1.2)**. This is believed to be due to its dicationic charge which allows it to interact more strongly with the negatively charged DNA phosphate backbone.[106]

Table 1.2: Binding constants of platinum(II) terpy complexes to calf thymus DNA[105]

Complex	Medium	K (M^{-1})
$[Pt(terpy)Cl]^{+}$	Tris[α]buffer	3.9×10^{5}
$[Pt(terpy)(HET)]^{+}$	pH 7.5, 0.2 M NaCl	1.2×10^{5}
$[Pt(terpy)(Cys)]^{+}$	pH 7.5, 0.2 M NaCl	1.0×10^{5}
$[Pt(terpy)(CMT)]^{+}$	pH 7.5, 0.2 M NaCl	5.0×10^{4}
$[Pt(terpy)(AET)]^{2+}$	pH 7.5, 0.2 M NaCl	4.3×10^{5}

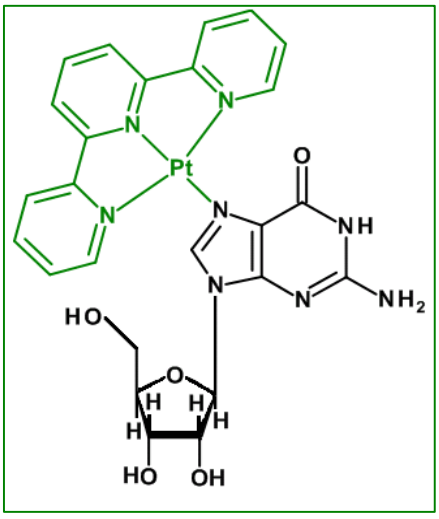

Figure 1.20: $Pt(terpy)^{2+}$ covalently bound to guanosine.[106]

Lippard and co-workers[109] showed that structural features such as size, steric effects of the complex, hydrogen bonding and the charge of the complex have an effect on the binding affinity of platinum(II) terpyridine complexes.

Figure 1.20 illustrates that $Pt(\mathbf{X}terpy)\mathbf{Y}]^{n+}$ complexes having a labile **Y** ligand which can undergo substitutions to bind covalently to nucleobases. Complexes where **Y** = Cl^{-}, H_2O, OH^{-} and pyridine derivatives have proven to react with nucleobases.[106] Lowe and co-workers[110] characterised the first platinum(II) terpyridine nucleobase complexes by NMR spectroscopy in their study on the reaction of $[Pt(terpy)Cl]^{+}$ and $[Pt(terpy)(4\text{-picoline})]^{2+}$ with nucleosides.[108]

[α] Tris(hydroxymethyl)aminomethane $(OHCH_2)_3CNH_2$

1.3.5 Mechanistic Investigations of Platinum(II) Terpyridine Complexes

Mechanistic studies of platinum(II) terpyridine complexes have focused on the influence of the terpyridine backbone on the reactivity of the metal centre through the addition of substituents onto the chelate or by adjusting the chelate itself to investigate the different effects of steric and electronic influences.

van Eldik *et al.*[111–112] investigated the effect of adding π-acceptor pyridine rings to the chelating ligand in their studies of the aqua substitution from [Pt(diethylenetriamine)OH_2]$^{2+}$ (**aaa**), [Pt(2,6-*bis*-aminomethylpyridine)OH_2]$^{2+}$ (**apa**), [Pt(*N*-(pyridyl-2-methyl)-1,2-diaminoethane)OH_2]$^{2+}$ (**aap**), [Pt(*bis*(2-pyridylmethyl)amine)OH_2]$^{2+}$ (**pap**), [Pt(2,2'-bipyridine)-(NH_3)(OH_2)]$^{2+}$ (**app**), and [Pt(terpy)OH_2]$^{2+}$ (**ppp**) by thiourea (**TU**), 1,3-dimethyl-thiourea (**DMTU**) and 1,1,3,3,-tetramethyl-thiourea (**TMTU**). The complexes are shown in ***Figure 1.21***. For the reaction with **TU**, the rate of substitution accelerated by a factor of 4 simply through the addition of a single pyridine ring in going from **aaa** to **aap**, a further increase in the reaction rate again by a factor of 4 was observed on the addition of a second pyridine ring (**pap**). On going from **aaa** to **ppp** the rate of the substitution reaction dramatically rose by four orders of magnitude with a general reactivity trend of **aaa** < **apa** < **aap** < **pap** < **app** < **ppp.**[111–112]

The electrophilicity of the metal centre (a result of electron back-donation to the ligand orbitals) determines complex reactivity. The significant increase in reactivity is the result of better electronic communication between the π-acceptor ligands when moving from **aaa** to **ppp**. The authors also showed that the π-acceptor on its own (in the *cis* or *trans* position) has only a minor impact on the rate of the substitution reaction because of the lack of direct electronic communication. Breaking this electronic communication between π-acceptor groups has recently been shown to slow the substitution reaction rate by a factor of 60.[113]

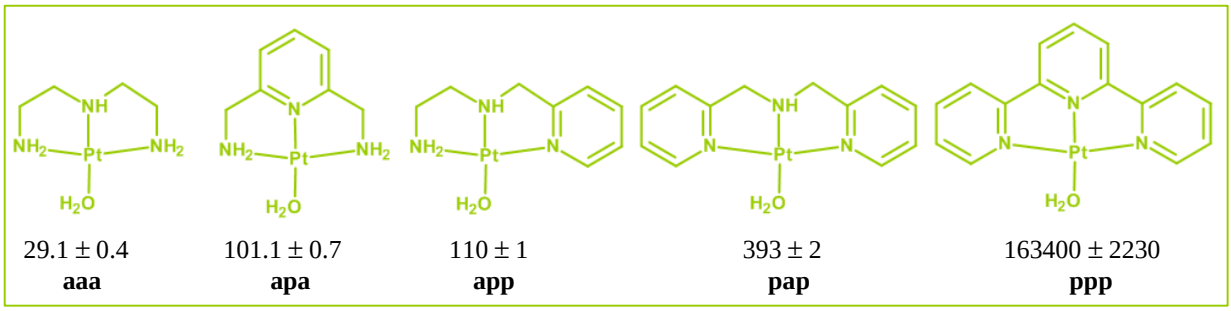

Figure 1.21: Complexes investigated by van Eldik *et al.* highlighting k_2 [$M^{-1}s^{-1}$] using the **TU** nucleophile.[111–112] (the $CF_3SO_3^-$ and ClO_4^- counterions are not shown).

Jaganyi *et al.*[114] extended the study on factors affecting the π-back donation effect of platinum(II) terpyridine complexes by attaching a substituent to the 4'-position of the chelate. Substitution kinetics of complexes such as those indicated in (***Table 1.3***) where studied with nucleophiles such as **TU**, **DMTU** and **TMTU**. **PtCl** was seen to react 1.2 times faster than **PhPtCl**. The observed decrease in reactivity of the **PhPtCl** can be explained by first considering the dihedral angle (***Figure 1.22***) between the phenyl ring and the terpyridine fragment which shows that any extension of π-backbonding towards the phenyl ring is absent since the phenyl ring is out of plane with respect to the terpyridine fragment. Thus the decrease in reactivity can only be due to the phenyl ring acting as an electron donating group which reduces the effectiveness of the terpyridine fragment as a π-backbonding system. This is further illustrated by the reactivity of **CH_3PhPtCl** in which the tolyl group in the 4'- position, being a slightly stronger σ-donor than the phenyl group, leading to a further decrease in reactivity at the metal centre. Conversely the reactivity of the complexes **ClPhPtCl** and **CF_3PhPtCl** is moderately enhanced since these are better electron withdrawing groups and thus increase the effectiveness of the terpyridine fragment as a π-backbonding system.

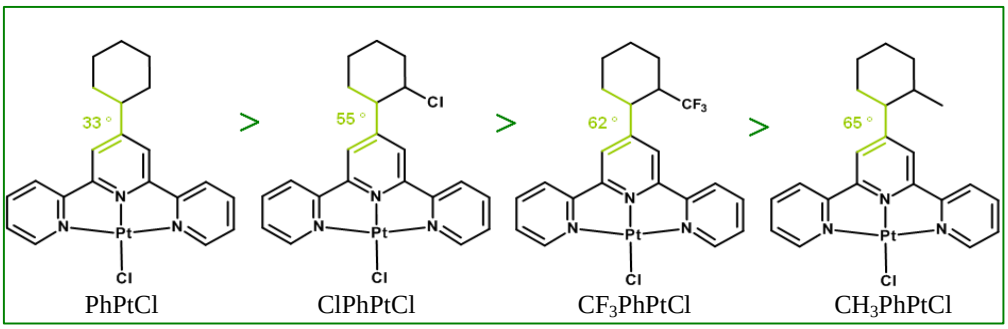

Figure 1.22: Diagram illustrating the effect of substituents on the dihedral angle.[114]

Table 1.3: Complexes with a substituent in the 4' position and there respective rate constants, dihedral angles and energy changes[114]

Complex	k_2 / $M^{-1}s^{-1}$ Nu = **TU**	**Dihedral Angle/°** (X-ray structure)	ΔE = $E_{HOMO} - E_{LUMO}$/eV
(**CH_3PhPtCl**), [Pt{4'-(2'''-CH_3-Ph)-terpy}Cl]$^+$	1222 ± 8	65	3.22
(**PhPtCl**) [Pt{4'-Ph-terpy}Cl]$^+$	1258 ± 13	33	3.22
(**PtCl**) [Pt(terpy)Cl]$^+$	1494 ± 10	–	3.29
(**ClPhPtCl**) [Pt{4′-(2‴-Cl-Ph)-terpy}Cl]$^+$	1765 ± 12	55	3.25
(**CF_3PhPtCl**) [Pt{4′-(2‴-CF_3-Ph)-terpy}Cl]$^+$	1933 ± 32	62	3.26

The experimental results were supported through computational modelling of the frontier molecular orbitals. The calculations showed that in the case of the complex with the strongest electron withdrawing group in the 4′-position of the terpyridine backbone *i.e.* **CF_3PhPtCl**, the majority of the electron density was centred away from the metal centre and toward the substituent in the 4′-position. This rendered the metal centre more reactive due to increased electrophilicty. The opposite was observed when electron-donating groups were situated at the 4′-position. For **CH_3PhPtCl**, the electron density was concentrated more towards the metal centre resulting in reduced electrophilic character and subsequently decreased reactivity. Indeed, the authors have shown that lowered reactivity of complexes bearing electron donating groups at the 4′-position can be explained in terms of the HOMO-LUMO (highest molecular orbital, lowest molecular orbital) gap which is increased for electron-donating groups, but reduced for electron-withdrawing groups. [114]

Jaganyi *et al.*[115] further elaborated on this work through their studies on the substitution kinetics of $[Pt(terpy)Cl]^+$ and $[Pt(^tBu_3terpy)Cl]^+$ with the nucleophiles **TU**, **DMTU**, **TMTU**, iodide (I^-) and thiocyanate (SCN^-), showing that the extent of π-backbonding can be controlled by the introduction of an electron-donating group at the 4, 4′ and 4″ positions of the terpyidinyl backbone.[104] Their results showed that the reaction rate decreases by a factor of 3.3 with **TU** ongoing from $[Pt(terpy)Cl]^+$ to $[Pt(^tBu_3terpy)Cl]^+$. They attributed this decrease in the rate of the substitution to the electron-donating groups in $[Pt(^tBu_3terpy)Cl]^+$ which leads to the reduction of π-acceptor effect of the terpy ligand, resulting in a less electrophilic complex.

Furthermore, computational calculations (***Table 1.4***) using complexes containing either electron-donating or electron-withdrawing groups in 4, 4′, 4″ positions, showed that the introduction of electron-donating groups have the effect of decreasing the positive charge on the metal centre, as well as increasing the HOMO-LUMO gap of the ground state, making the complex less reactive. Introducing electron-withdrawing groups increases the positive charge on the metal centre and decreases the HOMO-LUMO gap of the ground state, enhancing the reactivity of the complex. The authors concluded that by placing these substituents in both the *cis* and *trans* positions[115] the overall *trans*-influence is greater than the overall *trans*-effect and the overall π *cis*-effect is greater than the overall π *trans*-effect.

Table 1.4: Computational analysis of $[Pt(4,4',4''\text{-}R_3\text{-}terpy)Cl]^+$ analogues containing electron-donating (R = ^{t}Bu, H_2N, MeO or HO) or electron-withdrawing (R = Cl, NO_2, CF_3 or CN) groups in the ancillary positions of the terpyridine fragment[115]

	Electron donating groups (EDG)				**Terpy**	**Electron withdrawing groups (EWG)**			
	H_2N–	MeO–	^{t}Bu–	HO–	H	Cl–	CF_3–	CN–	NO_2–
Δ*E* = $E_{HOMO} - E_{LUMO}$/eV	3.43	3.45	3.41	3.40	3.29	3.21	3.14	2.95	2.87
NBO charge on Pt	0.7007	0.7168	0.7155	0.7131	0.7300	0.7368	0.7478	0.7569	0.7620

Studies have also been directed at analogous systems of platinum(II) terpyridine. In particular comparative mechanistic studies of complexes where one of the Pt—pyridinyl nitrogen bonds have been replaced by a Pt—phenyl carbon bond have demonstrated interesting behaviour.[113,116–117] Kinetic studies involving a Pt—C bond (as opposed to the Pt—N bond) are of considerable interest with most of the studied complexes having a single Pt—C bond that is located *trans* to the leaving group. These studies generally focus on the ability of the metal—carbon bond to labilise square-planar d^8 metal complexes through the kinetic *trans*-effect.[10,118–119] The reports showed that these complexes have a six fold increase in substitution reactivity. This is due to the σ-bound carbon ligands such as alkyl and aryl groups, having a large kinetic *trans*-effect.[43, 120–121] There are few reports on the *cis* effect with results often being contradictory.[106-107,114] This is attributed to the fact that platinum(II) complexes react at different rates depending on the σ-donor, π-acceptor and steric properties of the *cis* ligand. The general consensus is that the electronic effects of *cis* ligands is usually small when compared to that of the *trans* ligands in platinum(II) complexes.[11]

Jaganyi *et al.*[116] studied the ligand substitution of [Pt(4′-CF_3-Ph)-terpy]$^+$ (**CF_3PhPtCl**) and [Pt(4′-CF_3-Ph)-6-Ph-bipy] (**CF_3PhPtPhBpy**) with **TU**, **DMTU** and **TMTU**. When comparing the reactivity of the two complexes, the introduction of the Pt—C bond in the *cis*-position leads to a decrease in the rate of the chloride substitution by **TU** by a factor of 16.[118] This decrease in reactivity was attributed to the increase in electron density at the metal centre due to the σ-donating ability of the carbon atom, causing it to be less electrophilic than (**CF_3PhPtCl**). This leads to the repulsion of the incoming nucleophile.[113]

Furthermore, the results indicate that the *cis* and *trans* carbon σ-donors influence the lability of the leaving group differently. When the σ-donor is *trans* to the leaving group, the *trans*-effect takes control due to ground state labilisation and transition state stabilisation. This results in an elongation of the Pt—**X** bond (where **X** represents the leaving group) leading to an increase in the reaction rate.

The decrease in the reaction rate when the Pt—C bond is *cis* to the leaving group is due to the accumulation of electron density at the metal centre. This has less of an effect on the Pt—X bond length as there is no direct overlap of the orbitals of the two atoms *cis* to one another. This indicates that the Pt—C *cis*-effect, unlike the *trans*-effect, does not increase ground state destabilisation of platinum(II) complexes.[116]

van Eldik *et al.*[117] extended this work by studying the ligand substitution behaviour of the complexes [Pt(6-phenyl-2,2′-bipyridine)Cl] (**PtNNC**), [Pt(1,3-di(2-pyridyl)benzene)Cl] (**PtNCN**) and [Pt(terpy)Cl] (**PtNNN**) with **TU**, **DMTU** and **TMTU** in order to get a better understanding of the different *cis*- and *trans*-effects. For **TU**, the **PtNCN** complex reacted 30 times faster than **PtNNN**, and 455 times faster than the **PtNNC** complexes.[117] The σ-*cis*-effect is, therefore, larger than the corresponding σ-*trans*-effect (see *Chapter 3.5.2-3.5.3*). When the Pt—C bond is *trans* to the leaving group, the π-acceptor effect from the pyridyl/phenyl rings is small but still significant. The reactivity of this complex is thus the highest due to the highly destabilised ground state (labilisation of Pt—Cl by *trans* influence).[117] When the Pt—C bond is *cis* to the leaving group (**PtNNC**), the σ-donor effect of the carbon weakens the π-acceptor effect significantly. The σ-donor ability of the carbon counteracts the electron-withdrawing affect of the π-acceptor and is reflected by the reduced reactivity of the **PtNNC** complex in comparison to the **PtNCN** complex.

1.4 Aims of Current Study

If one is to consider all the multinuclear platinum(II) complexes discussed already it is clear that multinuclear systems are the next logical step in the sequential progression toward finding a anticancer drug that can match cisplatins effectivity without the adverse side-effects. Recent studies [53,122–123] on BBR3464 and its analogues, (which have monodentate amine ligands around the platinum centres and leaving groups of *trans* geometry to the alkanediamine linker), have shown degradation *in vitro* studies *via* liberation of the alkanediamine bridge. This happens when strong *trans*-effect ligands like the sulfur-containing biomolecules, whose *in vivo* prevalence is quite notable, substitute the leaving groups on the platinum(II) centres. Mambanda *et al*. observed similar behaviour with their series of [{Pt(H_2O)}2(*N*,*N*,*N*',*N*'-tetrakis(2-pyridylmethyl)-N(CH_2)$_n$N](CF_3SO_3)$_4$ complexes.[124] As a result of these findings *bis*-terpyridine complexes become particularly interesting as the chelating terpy has the potential to provide thermodynamic stability to the two platinum centres resulting in an accelerated or perhaps even decelerated, reaction rate as well as retaining the overall complex structure once inside a biological entity.

Of the terpyridine work previously described, terpyridines functionalised at the 4'-positions were considered the most notable. As a result, we propose to study a series of novel *bis*-terpyridine systems functionalised at the 4′-position with a α,ω-alkyldiol linker of systematically varied length. The flexible spacer will form an integral part of the core backbone of the carrier ligand framework around each platinum(II) centre, as well as being the linking structural entity between the two platinum(II) centres. It should theoretically confer structural flexibility on the metal complexes. By doing this, we hope to ascertain how the length of the spacer which is attached at the 4'-position influences reactivity at the metal centre as well as determining the optimum chain length for maximum effectivity.

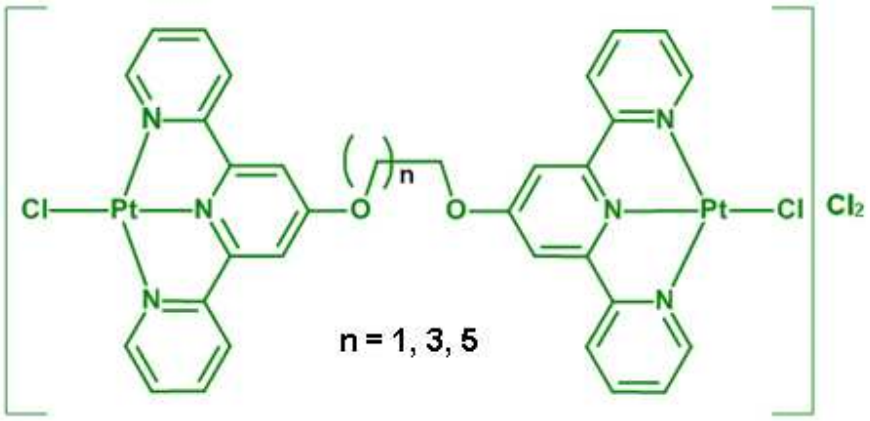

Figure 1.23*:* Proposed structure of *bis*[4'(2,2′:6′,2″-terpyidinyl)-*n*-diol].

This project was undertaken with the intention of achieving several goals. The first is to utilise a modified version of the method previously described by Van der Schilden *et al.*[125] and Constable *et al.*[101] to synthesise and successfully characterise a series of novel ligands each comprising two 2,2′:6′,2″-terpyridine domains linked through a flexible α,ω-alkyldiol derived spacer of variable length (**Figure 1.23**). Secondly, coordination of platinum(II) to each of the two terpyridine domains was attempted using a modification of a literature method described by Suntharalingam *et al.*[126] After full characterisation of the dinuclear complexes the reactivity was investigated through a detailed kinetic and mechanistic study in an effort to rationalise the effect of the bridging ligand on the reactivity of the metal centres.

1.5 References

1. http://www.popsci.com/science/article/2010-04/have-modern-sceintests-made-any-advancements-alchemy., Retrieved 2011-02-17.
2. M. W. George, *Platinum-Group Metals, 2008, U.S.A Geological Survey Mineral Commodity Summary.,* http://minerals.usgs.gov/minerals/pubs/commodity/platinum/mcs-2008-plati.pdf., Retrieved 2011-04-05.
3. P. J. Loferski, *Minerals Yearbook: Platinum-Group Metals*, U.S.A, Geological Survey, **2009**.
4. F. R. Hartley, *Chemistry of the Platinum Group Metals Recent Developments*, Elsevier, Amsterdam, **1991**, pp. 9, 23-30, 547-570.
5. R. J. Seymour and J. I. O'Farrelly, *Kirk-Othmer Encyclopedia of Chemical Technology, Platinum-Group metals*, Wiley, **2001,** pp. 1-33.
6. Z. Xiao and A. R. Laplante, *Minerals Engineering*, **2004**, *17*, 961-965.
7. P. J. Loferski, *Minerals Yearbook: Platinum-Group Metals*, United States Geological Survey, **2007**.
8. A. Sigel and H. Sigel., *Metal Ions in Biological Systems*, Marcel Dekker Inc., New York, **1996**, *33*, pp. 339-342.
9. D. T. Richens, *Chem. Rev.*, **2005**, *105*, 1961–2002.
10. M. L. Tobe and J. Burgess, *Inorganic Reaction Mechanisms*, Addison Wesley Longman Ltd., Essex, **1999**, pp. 30-43, 70-112.
11. J. D. Atwood, *Inorganic and Organometallic Reaction Mechanisms*, Wiley-VCH Inc., New York, 2nd Ed., **1997**, pp. 43-61.
12. R. B. Jordan, *Reaction Mechanisms of Inorganic and Organometallic Systems,* Oxford University Press Inc., **1991**, pp. 29-74.
13. R. G. Wilkins, *Kinetics and Mechanism of Reactions Transition Metal Complexes*, VCH, Weinheim, 2nd Ed., **1991**, pp. 199-201, 221, 232-242.
14. R. J. Cross, *Adv. Inorg. Chem.*, **1989**, *34*, 219-292.
15. M. W. George, *Mineral Yearbook 2006: Platinum-Group Metals*. United States Geological Survey. http://minerals.usgs.gov/minerals/pubs/commodity/platinum/myb1-2006-plati.pdf. Retrieved 2011-04-04

16. B. Lippert, *Cisplatin. Chemistry and Biochemistry of a Leading Anticancer Drug*, Wiley-VCH, Weinheim, **1999**, pp. 3-27,111-131,159-177.
17. D. F. Shriver and P. W. Atkins, *Inorganic Chemistry* 3rd, Ed. Oxford University Press, **2002**, pp. 285, 308-309, 490, 627.
18. A. Karpov, M. Konuma and M. Jansen, *Chem. Commun*., **2006**, 838-840.
19. J. Ghilane, C. Lagrost, M. Guilloux-Viry, J. Simonet, M. Delamar, C. Mangeney and P. Hapiot, *J. Phys. Chem*., **2007**, *111*, 5701-5707.
20. M. Jansen, *Solid State Sciences*., **2005**, *7*, 1464-1474.
21. P. Atkins and J. de Paula, *Atkins' Physical Chemistry* 7th Ed, Oxford University Press, **1978**, pp. 1150.
22. J. Cairns, *Cancer Science and Society*, W. H. Freeman and Company, USA, **1978**, pp. 15-31, 35-39.
23. http://www.webmd.com/cancer/news/20081209/global-cancer-deaths-double-2030., Retrieved 2011-04-05.
24. Editorial (P. Sadler, D. A. Juckett, and J. W. Judge), *Dalton Trans*., **2009**, 10648–10650.
25. L. Ronconi and D. Fregona, *Dalton Trans*., **2009**, 10670-10680.
26. http://www.wikipedia.org/wiki/Triplatin_tetranitrate., Retrieved 2011-04-19.
27. N. K. Summa PhD Thesis: *Thermodynamic and Kinetic Studies on Biotransformation Reactions of Medical Relevant Mono- and Polynuclear Platinum(II) complexes*, Friedrich Alexander Universität, Erlangen Nürnberg, **2006**.
28. M. J. Cleare and J. D. Hoeschele, *Plat. Met. Rev*., **1973**, *17*, 2–13.
29. M. J. Cleare and J. D. Hoeschele, *Bioinorg. Chem*., **1973**, *2*, 187–210.
30. B. Lippert, *Cisplatin: Chemistry and Biochemistry of a Leading Anticancer Drug*, WILEY–VCH, Zurich, **1999,** 19.
31. T. Hambley, *Coord. Chem. Rev*., **1997**, *166*, 181–223.
32. M. Galanski and B. K. Keppler, *Anticancer Agents in Medicinal Chemistry*., **2007**, *7*, 55.
33. N. J. Wheate, R. I. Taleb, A. M. Krause–Heuer, R. L. Cook, S. Wang, V. J. Higgins and J. R. Aldrich–Wright, *Dalton Trans*., **2007**, 5055–5064.
34. K. S. Lovejoy and S. J. Lippard, *Dalton Trans*., **2009**, 10651–10659.
35. P. Heringova, J. Woods, F. S. Mackay, J. Kasparkova, P. J. Sadler and V. Bradec, *J. Med. Chem*., **2006**, *49*, 7792–7798.

36. B. M. Zeglis, V. C. Pierre and J. K. Barton, *Chem. Commun*., **2007**, 4565–4579.
37. G. Natile and M. Coluccia, *Coord. Chem. Rev*., **2001**, *216–217*, 383–410.
38. M. A. Jakupec, M. Galanski, V. B. Arion, C. G. Hartinger and B. K. Keppler, *Dalton Trans*., **2008**, 183–194.
39. *Cisplatin: Chemistry and Biochemistry of a Leading Anticancer Drug*, Wiley–vch, Zurich, **1999**, pp. 479–496.
40. G. V. Kalayda, S. Fakih, H. Bertram, T. Ludwig, H. Oberleithner, B. Krebs and J. Reedijk, *J. Inorg. Biochem*., **2006**, *100*, 1332–1338.
41. Q. Liu, Y. Qu, R. Van Antwerpen and N. Farrell, *Biochemistry*, **2006**, *45*, 4284–4256.
42. S. A. De Pascali, D. Migoni, P. Papadia, A. Romano, S. Marsigliante, A. Pellissier, S. Chardon–Noblat, A. Ciccarese and F. P. Fanizzi, *Dalton Trans*., **2008**, 5911–5921.
43. O. F. Wendt and L. I Elding, *J. Chem. Soc*., *Dalton Trans*., **1997**, 4725–4731.
44. J. K. Burdett, *Inorg*. *Chem*., **1977**, *16*, 3013–3025.
45. N. P. Farrell, Y. Qu and M. P. Hacker, *J. Med. Chem*., **1990**, *33*, 2179–2184.
46. N. P. Farrell, S. G. de Almeida and K. A. Skov, *J. Am. Chem. Soc*., **1988**, *110*, 5018–5019.
47. N. P. Farrell and Y. Qu, *Inorg. Chem*., **1989**, *28*, 3416–3420.
48. S. Komeda, M. Lutz, A. L. Spek, M. Chikuma and J. Reedijk, *Inorg*. *Chem*., **2000**, *39*, 4230–4236.
49. I. Lakomska, H. Kooijman, A. L. Spek, W. Shen and J. Reedijk, *Dalton Trans*., **2009**, 10736–10741.
50. http://www.wikipedia.org/wiki/Triplatin_tetranitrate., Retrieved 2011–04–19.
51. N. K. Summa, J. Maigut, R. Puchta and R. van Eldik, *J. Am. Chem. Soc*.**, 2007**, *129*, 2094–2104.
52. J. Reedijk, *Chem. Commun*., **1996**, 801–806.
53. H. Hofmeier and U. S. Schubert, *Dalton Trans*., **2004**, 373–399.
54. C. Hollins, *Synthesis of Nitrogen Ring Compounds*, Van Nostrand, London, **1924**, 227–230.
55. A. E. Tschitschibabin, *J. Prakt. Chem*., **1924**, *107*, 122–125.
56. G. R. Newkome and D. L. Fishel, *J. Org. Chem*., **1972**, *37*, 1329–1336.
57. Y. Todha, M. Eiraku, T. Nakagawa, Y. Usani, M. Aiga, T. Kawashima, K. Tani, H. Watanabe and Y. Mori, *Bull. Chem. Soc. Jpn*., **1990**, *63*, 2820–2827.

58. Editorial (F. Diederich and P. J. Stang), *Metal–Catalyzed Cross Coupling Reactions*, Wiley–VCH, Weinheim, **1998**, pp. 877–885.
59. G. R. Pabst and J. Sauer, *Tetrahedron*, **1999**, *55*, 5067–5088.
60. R. A. Fallahpour, *2,2':6',2''– Terpyridines and their Metal Complexes*. University of Basel, Switzerland **2003**.
61. D. L. Jameson and L. E. Guise, *Tetrahedron Lett*., **1991**, *32*, 1999–2002.
62. F. Kröhnke, *Synthesis*, **1976**, *1*, 1–24.
63. A. C. Benniston, *Tetrahedron Lett*.**, 1997**, *47*, 8279–8282.
64. A. C. Benniston, L. J. Farrugia, P. R. Mackie, P. Mallinson, W. Clegg and S. J. Teat, *Aust. J. Chem*., **2000**, *53*, 707–713.
65. M. Heller and U.S. Schubert, *Eur. J. Org. Chem*., **2003**, *6*, 947–961.
66. M. Heller and U. S. Schubert, *Synlett*., **2002**, *5*, 751–754.
67. I. Sasaki, J. C. Daran and G. G A. Balavoine, *Synthesis*, **1999**, *5*, 815–820.
68. J. Sauer, D. K. Heldmann and G. R. Pabst, *Eur. J. Org. Chem*., **1999**, *1*, 313–321.
69. U. S. Schubert, C. Eschbaumer and G. Hochwimmer, *Synthesis*, **1999**, *5*, 779–782.
70. E. C. Constable, C. E. Housecroft, T. Kulke, C. Lazzarini, E. R. Schofield and Y. Zimmermann, *J. Chem. Soc*., *Dalton Trans*.**, 2001**, 2864–2871.
71. M. Heller and U.S. Schubert, *Eur. J. Org. Chem*., **2002**, *5*, 571–574.
72. A. El–Ghayoury and R. Ziessel, *J. Org. Chem*., **2000**, *65*, 7757–7763.
73. A. El–Ghayoury and R. Ziessel, *Tetrahedron Lett*., **1998**, *39*, 4473–4476.
74. S. E. Hobert, J. T. Carney and S. D. Cummings, *Inorg. Chim. Acta*., **2001**, *318*, 89–96.
75. K. Matyjaszewski, T. E. Patten and J. Xia, *J. Am. Chem. Soc*., **1997**, *119*, 674–680.
76. G. Kickelbick and K. Matyjaszewski, *Macromol. Rapid Commun*., **1999**, 341–346.
77. R. Chotalia, E. C. Constable, M. J. Hannon and D. A. Tocher, *J. Chem. Soc*., *Dalton Trans*., **1995**, 3571–3580.
78. R. A. Fallahpour, M. Neuburger and M. Zehnder, *Polyhedron*, **1999**, *18*, 2445–2454.
79. R. A. Fallahpour and E. C. Constable, *Org. Biomol. Chem.*, **1997**, *16*, 2263–2264.
80. G. D. Storrier, S. H. Colbran and D. C. Craig, *J. Chem. Soc., Dalton Trans*., **1998**, 1351–1363.
81. G. D. Storrier, S. B. Colbran and D. B. Hibbert, *Inorg. Chim Acta*, **1995**, *239*, 1–2.

82. B. Whittle, S. R.Batten, J. C. Jeffrey, L. H. Rees and M. D. Ward, *J. Chem. Soc., Dalton Trans*., **1996**, 4249–4255.
83. M. E. Pabilla–Tosta, J. M. Lloris, R. Martinez–Manez, A. Benito, J. Soto, T. Pardo, M. A. Miranda and M. D. Marcos, *Eur. J. Inorg. Chem*., **2000**, 741–748.
84. U. Sampath, W. C. Putnam, T. A. Osiek, S. Touami, J. Xie, D. Cohen, A. Cagnolini, P. Droege, D. Klug, C. L. Barnes, A. Modak, J. K. Bashkin and S. S. Jurisson, *J. Chem. Soc*., *Dalton Trans*., **1999**, 2049–2058.
85. U. S. Schubert, P. R. Andres and H. Hofmeier, *Polym. Matz. Soc. Eng*., **2001**, *85***,** 510–511.
86. U. S. Schubert, C. Eschbaumer, O. Hien and P. R. Andres, *Tetrahedron Lett*., **2001**, *42*, 4705–4707.
87. E. C. Constable, C. E. Housecroft, L. A. Johnston, D. Armspach, M. Neuburger and M. Zehnder, *Polyhedron*, **2001**, *20*, 483–492.
88. D. Armspach, E. C. Constable, C. E. Housecroft, M. Neuburger and M. Zehnder, *J. Organomet. Chem*., **1997**, *550*, 193–206.
89. A. El–ghayoury, A. P. Schenning, P. V. Hal, C. Weidl, J. V. Dongen, R. A. Janssen, U. S. Schubert and E. W. Meijer, *Thin Solid Films*, **2002**, *97*, 403–404.
90. U. S. Schubert, C. H. Weidl, A. Cattani, C. Eschbaumer, G. R. Newkome, E. He, E. Harth and K. Müllen, *Polym. Prepr*., **2000**, *41*, 229–230.
91. M. E. Padilla–Tosta, J. M. Lloris, R. Martinez–Manez, A. Benito, J. Soto, T. Pardo, M. A. Miranda and M. D. Marcos, *Eur. J. Inorg. Chem*., **2000**, 741–748.
92. a) V.W. W. Yam, R. P. L. Tang, K. M. C. Wong, K. K. Cheung, *Organometallics*, **2001**, *20*, 4476–4482; b) V.W.W. Yam, R. P. L. Tang, K. M. C. Wong, X. X. Lu, K. K. Cheung, N. Zhu, Chem. *Eur. J*., **2002**, *8*, 4066–4076; c) V. W.W. Yam, K. M. C. Wong, N. Zhu, *Angew. Chem.*, **2003**, *115*, 1438; *Angew. Chem. Int. Ed*., **2003**, *42*, 1400–1403; d) K. M. C. Wong, W. S. Tang, B. W. K. Chu, N. Zhu, V.W. W. Yam, *Organometallics*, **2004**, *23*, 3459–3465.
93. A. Hofmann, L. Dahlenburg and R. van Eldik, *Inorg. Chem*., **2003**, *42*, 6528–6538.
94. A. Hofmann, D. Jaganyi, O. Q. Munro, G. Liehr and R. van Eldik, *Inorg. Chem*., **2003**, *42***,** 1688–1700.
95. a) J. W. Schindler, R. C. Fukuda, A.W. Adamson, *J. Am. Chem. Soc*., **1982**, *104*, 3596–3600; b) V. M. Miskowski, V. H. Houlding, C. M. Che, Y. Wang, *Inorg. Chem*.,

1993, *32*, 2518–2524; c) H. K. Yip, H. M. Lin, Y. Wang, C. M. Che, *Inorg. Chem.*, **1993**, *32*, 3402–3407.

96. a) D. M. Roundhill, H. B. Gray, C. M. Che, *Acc. Chem. Res.*, **1989**, *22*, 55–61; b) V. M. Miskowski, V. H. Houlding, *Inorg. Chem.*, **1989**, *28*, 1529–1533; c) V. H. Houlding, V. M. Miskowski, *Coord. Chem. Rev.*, **1991**, *111*, 145–152
97. J. A. Bailey, M. G. Hill, R. E. Marsh, V. M. Miskowski, W. P. Schaefer and H. B. Gray, *Inorg. Chem.*, **1995**, *34*, 4591–4599.
98. G. T. Morgan and F. H. Burnstall, *J. Chem. Soc.*, **1934**, 1498–1500.
99. M. Howe–Grant and S. Lippard, *Inorg. Syntheses.*, **1980**, *20*, 101–105.
100. V. W. Yam, K. H. Chan, K. M. Wong and B. W. Chu, *Angew. Chem. Int. Ed.*, **2006**, 6169–6173.
101. E. C. Constable, C. E. Housecroft, M. Neuburger, S. Schaffner and C. B. Smith, *Dalton Trans.*, **2005**, 2259–2267.
102. K. Van der Schilden, F. Garcia, H. Kooijman, A. L. Spek, J. G. Haasnoot and J. Reedijk, *Angew. Chem. Int. Ed.*, **2004**, *43*, 5668–5670.
103. X. Liu, E. J. L. McInnes, C. A. Kilner, M. Thorton–Pett and M. A. Halcrow, *Polyhedron*, **2001**, *20*, 2889–2900.
104. U. S. Schubert, C. Eschbaumer, O. Hien and P. R. Andres, *Tetrahedron Lett.*, **2001**, *42*, 4705–4707.
105. S. D. Cummings, *Coord. Chem. Rev.*, **2009**, *253*, 449–478.
106. S. D. Cummings, *Coord. Chem. Rev.*, **2009**, *253*, 1495–1516.
107. K. W. Jennette, S. J. Lippard, G. A Vassiliades and W. R. Bauer, *Proc. Natl. Acad. Sci. U.S.A.*, **1974**, *71*, 3839–3843.
108. W. D. McFadyen, L. P. Wakelin, I. A. Roos and V. A. Leopold, *J. Med. Chem.*, **1985**, *28*, 1113–1116.
109. M. Howe–Grant, K. C. Wu, W. R. Bauer and S. J. Lippard, *Biochem*istry, **1976**, *15*, 4339–4346.
110. G. Lowe and T. Vilaivan, *J. Chem. Soc., Perkin Trans.*, **1996**, *1* 1499–1503.
111. D. Jaganyi, A. Hofmann, and R. van Eldik, *Angew. Chem. Int. Ed.*, **2001**, *40*, 1680–1683.
112. A. Hofmann, D. Jaganyi, O. Q. Munro, G. Liehr, and R. van Eldik, *Inorg. Chem.*, **2003**, *42*, 1688–1700.

113. R. Romeo, M. R. Plutino, L. M. Scolaro, S. Stoccoro and G. Minghetti, *Inorg. Chem.*, **2000**, *39*, 4749–4755.
114. D. Jaganyi, K. L. De Boer, J. Gertenbach and J. Perils, *Int. J. Chem. Kinetics*, **2008**, *40*, 808–818.
115. D. Reddy and D. Jaganyi, *Dalton Trans.*, **2008**, 6724–6731.
116. D. Jaganyi, D. Reddy, J. A. Gertenbach, A. Hofmann and R. van Eldik, *Dalton Trans.*, **2004**, 299–304.
117. A. Hofmann, L. Dahlenburg and R. van Eldik, *Inorg. Chem.*, **2003**, *42*, 6528–6538.
118. F. Basolo, J. Chatt, H.B. Gray, R. G. Pearson and B. L. Shaw, *J. Chem. Soc.*, **1961**, 2207–2215.
119. G. Alibrandi, D. Minniti, L. M Scolaro and R. Romeo, *Inorg. Chem.*, **1988**, *27*, 318–324.
120. R. Gosling and M. L Tobe, *Inorg. Chem.*, **1983**, *22*, 1235–1244.
121. L. Canovese and M. L. Tobe, *J. Chem. Soc., Dalton Trans.*, **1985**, 27–30.
122. M. E. Oehlsen, Y. Qu and N. Farrell, *Inorg. Chem.*, **2003**, *42*, 5498–5506.
123. V. Vacchina, L. Torte, C. Allievi and R. Lobeinski, *J. Anal. At. Spectrom.*, **2003**, *18*, 884–890.
124. A. Mambanda, D. Jaganyi, S. Hochreuther and R. van Eldik, *Dalton Trans.*, **2010**, *39*, 3595–3608.
125. K. van der Schilden, PhD Thesis: *Design and Development of Polynuclear Ruthenium and Platinum Polypyridyl Complexes in Search of New Anticancer Agents*, Leiden University, Netherlands, **2006**.
126. K. Suntharalingam, A. J. P. White and R. Vilar, *Inorg. Chem.*, **2009**, *48*, 9427–9435.

CHAPTER II
Reaction Kinetics

2.1 Introduction

A chemical reaction is defined as a process of the transformation of reactants into products, for which a balanced or stoichiometric chemical equation may be written.[1-2] Quantitative studies of chemical reactions generally belong to one of two distinct categories, the first being thermodynamic methods which usually involve studies related to the actual occurrence of the reaction. These studies do not take into account how quickly or slowly the reaction proceeds but rather the direction in which the reaction travels.[1,3] Studies are performed on systems that are at steady state with static concentrations. The standard enthalpy change ($\Delta H^{\neq}$) or the standard Gibbs energy change of a reaction ($\Delta G^{\neq}$) are the quantities measured in thermodynamic methods.[1,4]

The second method focuses on the rapidity with which a chemical reaction proceeds and is known as chemical kinetics ("kinetics" from the Greek word *kīnētikos*, which means movement or change). Here measurements are made under dynamic conditions in which the concentrations of the reactants and products are changed as a function of time.[1,3] Studies of the dependence of the rate on a range of factors can provide an empirical basis on which one might predict the reaction rate.[1,3-4] Furthermore such studies may provide relevant information about the detailed manner in which the chemical reaction takes place. They may demonstrate that a reaction does not occur in a certain way, or they may show that the total chemical process represented in the stoichiometric equation comes about through a particular succession of events.[5]

It is the subject matter of this second group of studies that forms the basis of this chapter and, more importantly, a principle component of this dissertation. The term kinetics is used to denote the study of a reaction and its parameters, but more importantly, to identify the variables that influence how quickly that chemical reaction will take place.[1]

Such variables include: reactant concentration, ionic strength, pH, solvent type, temperature and pressure.[6]

- Controlling and understanding the effect that the concentration has on a reaction is fundamental to a kinetic study, as a change in concentration of a reagent will lead to a change in the rate of the reaction.

- When a bimolecular reaction between two species occurs in a medium of high dielectric permittivity, the rate constant is found to depend on the ionic strength of the solution. Establishing and maintaining the ionic strength of a solution ensures that the overall ionic concentration and charge in the solution remains constant during the course of the reaction.

- The pK_a values for a molecule can be determined through a pH study. This is critical as different species will exist at different pH values and it is essential that one is certain of which species is being monitored.

- Solvents play a crucial role in the course of chemical reactions, since it may affect the reaction by acting as a reactant, or by forming a solvent cage around the molecule thereby changing the kinetics of the reaction.

- Temperature-dependent studies enable the entropy and enthalpy of a reaction to be determined. These values may provide an indication of the substitution mechanism for the reaction.

- From pressure dependent studies the volume of activation is determined, leading to the assignment of a mechanism for the reaction.

Thus, kinetics encompasses experimental measurements as well as empirical and theoretical methods to interpret these measurements. Another important aspect of kinetic studies is that they provide some of the information required to resolve the mechanism of a reaction.[1,5] These methods encompass a variety of systems including: complexation, acid-base and redox reactions.[3]

2.2 Rate Law

The reaction rate is defined simply as the rate of change of concentration of reactants or products.[7] The units of rate are stated as molarity per second (M s^{-1}).[8-9]

$$\textbf{Rate} = -\frac{d[\textbf{reactant}]}{dt} = \frac{d[\textbf{product}]}{dt} \qquad \textbf{…2.1}$$

The rate law illustrates the dependence of the reaction rate on the reagent concentrations.[8-9] For the general reaction:

$$\mathbf{A} \xrightarrow{k} \mathbf{B}$$

The rate can be expressed as

$$\text{Rate} = k[\text{A}]^{\alpha}[\text{B}]^{\beta} \qquad \textbf{…2.2}$$

where k is the rate constant whose units depend on the rate law, and the exponents α and β are experimentally determined partial orders with respect to A and B respectively.

The exponents in the rate law are not necessarily linked to stoichiometric coefficients in balanced reactions.[8-9] The rate law is important as it gives information on the concentrations of reagents needed to get to the product by the lowest energy pathway.[8-9] The overall order of a rate law is described as the sum of the exponents in the rate law.[8-9]

2.3 Integrated Rate Laws

2.3.1 First-Order Reactions

First-order reactions are considered the most simple of all integrated rate laws, thus reaction conditions are generally manipulated in order to allow reactions to follow first order reaction kinetics.[8-9]

A first-order reaction,

$$\mathbf{A} \xrightarrow{k_1} \mathbf{P}$$

will have the following rate law:

$$\text{Rate} = k_1[\text{A}]_t = -\frac{d[\text{A}]}{dt} \qquad \textbf{...2.3}$$

this can be rearranged to give:

$$-\frac{d[\text{A}]}{[\text{A}]_t} = k_1 dt \qquad \textbf{…2.4}$$

Equation 2.4 can be integrated from time at 0 (t = 0) to any time, t (t = t)

$$\int_{[X]_0}^{[X]_t} \frac{d[\mathbf{A}]}{[\mathbf{A}]_t} = -k_1 \int_0^t dt \qquad \textbf{…2.5}$$

$$\ln\frac{[\text{A}]_t}{[\text{A}]_0} = -k_1 t \quad \textbf{or} \quad \ln[\mathbf{A}]_t = -k_1 t + \ln[\mathbf{A}]_0 \qquad \textbf{…2.6}$$

Since *Equation 2.6* is a linear expression ($y = mx + c$), a plot of $\ln[\text{A}]_t$ versus t gives a slope from which the rate constant, k_1 can be found.[8-9]

The advantage of a first-order rate law is that any physical parameter that is proportional to concentration, *viz.* absorbance, volume, pressure or conductivity can be used directly to measure the first order rate constant.[6,8-9] One such example is when a reaction is characterised by a change in absorbance from (E_0 to E_∞) during the reaction, then

$$\ln\frac{[\text{A}]_t}{[\text{A}]_0} = \ln\frac{(\text{E}_t - \text{E}_\infty)}{(\text{E}_0 - \text{E}_\infty)} = -k_1 t \qquad \textbf{…2.7}$$

where, E_0, E_t and E_∞ are the absorbance measurements for the reactant A at time t = 0, t, and infinity (∞) respectively. Thus, a plot of $\ln\{(E_\infty\text{-}E_t)/(E_o\text{-}E_\infty)\}$ versus t can be used to determine (k_1).

2.3.2 Reversible First-Order Reactions

Certain reactions do not go to completion but rather attain an equilibrium where some of the products is converted back into starting material and the reaction is said to be reversible.[8-9]

$$\mathbf{A} \underset{\boldsymbol{k_{-1}}}{\overset{\boldsymbol{k_1}}{\rightleftharpoons}} \mathbf{B}$$

The rate law for the above reaction would follow the form of:

$$\text{Rate} = \frac{d[\text{B}]}{dt} = -\frac{d[\text{A}]}{dt} = k_1[\text{A}]_t - k_{-1}[\text{B}]_t \qquad \textbf{…2.8}$$

At time t = 0, no product has formed, hence $[B]_0 = 0$ and $[A]_t = [B]_0$, therefore at any time during the reaction:

$$[\text{B}]_t = [\text{A}]_0 - [\text{A}]_t \qquad \textbf{…2.9}$$

The substitution of *Equation 2.9* into *Equation 2.8* yields:

$$-\frac{d[\text{A}]}{dt} = k_1[\text{A}]_t - k_{-1}([\text{A}]_0 - [\text{A}]_t) \qquad \textbf{…2.10}$$

As no nett reaction occurs at equilibrium,

$$-\frac{d[\text{A}]}{dt} = 0 \qquad \textbf{…2.11}$$

Substituting *Equation 2.10* into *2.8* and applying *Equation 2.11* results in:

$$k_1[\text{A}]_{eqm} = k_{-1}[\text{B}]_{eqm} = k_{-1}([\text{A}]_0 - [\text{A}]_{eqm}) \qquad \textbf{…2.12}$$

which can also be written as:

$$[\text{A}]_0 = \frac{k_1 + k_{-1}}{k_{-1}}[\text{A}]_{eqm} \qquad \textbf{…2.13}$$

The substitution of *Equation 2.13* into *Equation 2.10* results in the following:

$$-\frac{d[\text{A}]}{dt} = (k_1 + k_{-1})[\text{A}]_t - (k_1 + k_{-1})[\text{A}]_{eqm} \qquad \textbf{…2.14}$$

Separation of the variables, results in the following expression:

$$\frac{d[\mathrm{A}]}{([\mathrm{A}]_t - [\mathrm{A}]_{eqm})} = -(k_1 + k_{-1})dt \qquad \textbf{…2.15}$$

Integrating this equation from $t = 0$ to $t = \mathrm{t}$:

$$\int_{[\mathrm{A}]_0}^{[\mathrm{A}]_t} \frac{d[\mathrm{A}]}{([\mathrm{A}]_t - [\mathrm{A}]_{eqm})} = -(k_1 + k_{-1})\int_0^t dt \qquad \textbf{…2.16}$$

$$\ln\left(\frac{[\mathrm{A}]_t - [\mathrm{A}]_{eqm}}{[\mathrm{A}]_0 - [\mathrm{A}]_{eqm}}\right) = -(k_1 + k_{-1})t \qquad \textbf{…2.17}$$

Rearrangement of *Equation 2.17* results in:

$$\ln([\mathrm{A}]_t - [\mathrm{A}]_{eqm}) = -(k_1 + k_{-1})t + \ln([\mathrm{A}]_0 - [\mathrm{A}]_{eqm}) \qquad \textbf{…2.18}$$

$$\ln([\mathrm{A}]_t - [\mathrm{A}]_{eqm}) = k_{obs}t + \ln([\mathrm{A}]_0 - [\mathrm{A}]_{eqm}) \qquad \textbf{…2.19}$$

Where $k_{obs} = k_1 + k_{-1}$

As *Equation 2.19* is in the form of the linear equation $y = mx + c$, a plot of $\ln([A]_t - [A]_{eqm})$ versus t is a straight line with a slope equal to k_{obs}.[8-9] The individual rate constants k_1 and k_{-1}, can be determined from the equilibrium constant, which is a rate of the formed product concentration and the starting material left at equilibrium which is expressed as:

$$K_{eqm} = \frac{k_1}{k_{-1}} \qquad \textbf{…2.20}$$

However the problem encountered with first-order reversible reactions is that it is difficult to measure $[A]_{eqm}$ accurately.[6,8-9]

2.3.3 Second-Order Reactions

Second-order kinetics are predominantly used for interpreting the reactions of complexes.[8-9] A second-order reaction which is first order with respect to each of the two starting materials in a bimolecular reaction is described in the reaction equation below:

$$\mathbf{A} + \mathbf{B} \xrightarrow{k_2} \mathbf{P}$$

The above second-order reaction has the following rate law:

$$\text{Rate} = -\frac{d[\text{A}]}{dt} = k_2[\text{A}]_t[\text{B}]_t \qquad \textbf{…2.21}$$

Equation 2.21 can be rewritten as follows:

$$\frac{d[\text{A}]}{[\text{A}]_t[\text{B}]_t} = -k_2 dt \qquad \textbf{…2.22}$$

Following reaction stoichiometry, if the initial concentrations of **A** and **B** are $[\text{A}]_0$ and $[\text{B}]_0$, then when the concentration of **A** drops to $[\text{A}]_0 - x$, where x refers to the amount of product produced at time t, the concentration of **B** must drop to $[\text{B}]_0 - x$. The rate equation for the reaction can thus be rewritten[10]:

$$-\frac{d[\text{A}]}{dt} = k_2([\text{A}]_0 - x)([\text{B}]_0 - x) \qquad \textbf{…2.23}$$

As $[\text{A}]_t = [\text{A}]_0 - x$, it means that $-\frac{d[\text{A}]}{dt} = \frac{dx}{dt}$ and hence *Equation 2.23* can be expressed as:

$$\frac{dx}{dt} = k_2([\text{A}]_0 - x)([\text{B}]_0 - x) \qquad \textbf{…2.24}$$

or

$$\frac{dx}{([\text{A}]_0 - x) - ([\text{B}]_0 - x)} = k_2 dt \qquad \textbf{…2.25}$$

Integrating *Equation 2.25* between the limits $x = 0$ and $x = x$ gives the following:

$$\int_0^x \frac{dx}{([A]_0 - x)([B]_0 - x)} = k_2 \int_0^t dt \qquad \textbf{…2.26}$$

Provided $[A]_0$ is not equal to $[B]_0$, *Equation 2.27* is obtainable:

$$\frac{1}{[A]_0 - [B]_0} \ln \frac{[B]_0([A]_0 - x)}{[A]_0([B]_0 - x)} = k_2 t \qquad \textbf{…2.27}$$

Equation 2.27 can be simplified:

$$\frac{1}{[A]_0 - [B]_0} \ln \frac{[B]_0[A]_t}{[A]_0[B]_t} = k_2 t \qquad \textbf{…2.28}$$

Thus $[A]_0$, $[B]_0$, $[A]_t$ and $[B]_t$ must be known for k_2 ($M^{-1}s^{-1}$) to be determined. In most kinetic experiments this is time-consuming and sometimes difficult to achieve.[8-9] To bypass this problem second-order reactions are usually studied under *pseudo* first-order conditions.[6,8-10]

P*seudo* first-order conditions occur when one reaction partner is selected in a large excess, *i.e.* $[B]_0 >> [A]_0$ (at least ten-fold excess) such that its concentration remains almost constant during the course of the reaction. Under *pseudo* first-order conditions the rate law simplifies to a first order expression[6,8-10] and *Equation 2.23* can be written as follows:

$$-\frac{d[A]}{dt} = k_2[A]_t[B]_t = (k_2[B]_0)[A]_t = k_{obs}[A]_t \qquad \textbf{…2.29}$$

where, $k_{obs} = k_2[B]_0$

Plotting ln[A] versus *t* gives a straight line with a slope of k_{obs}. A series of k_{obs} values can be determined by varying the concentration of **B**.[6,8-10] Then by using $k_{obs} = k_2[B]_0$, a plot of k_{obs} *vs* $[B]_0$ will give a straight line with a slope of k_2.[6,8-10]

2.3.4 Reversible Second Order Reactions

Some second order reactions may not go to completion but rather attain equilibrium:

$$\mathbf{A + B} \underset{k_{-2}}{\overset{k_2}{\rightleftharpoons}} \mathbf{P}$$

The reaction is said to possess mixed order behavior as the forward reaction is second order whilst the reverse reaction is first order. This difficulty is resolved by selecting *pseudo* first-order conditions for the forward reaction, *viz.* $[B]_0 >> [A]_0$.[8-9] The equation can then be simplified to a reversible first-order reaction.

Using *pseudo* first-order conditions, the rate law can be written as follows:

$$-\frac{d[A]}{dt} = k_2[A]_t[B]_t - k_{-2}[P]_t \qquad \textbf{…2.30}$$

To simplify this equation, it can be assumed that there is no product present initially and that the stoichiometry is 1:1:1, so that at any time, *t*, the mass balance must be:

$$[A]_t = [A]_0 - [P]_t$$

and $$[B]_t = [B]_0 - [P]_t \qquad \textbf{…2.31}$$

At equilibrium:

$$[A]_{eqm} = [A]_0 - [P]_{eqm}$$

and $$[B]_{eqm} = [B]_0 - [P]_{eqm} \qquad \textbf{…2.32}$$

From *Equations 2.31* and *2.32*,

$$[P]_t = [A]_0 - [A]_t$$

and $$[P]_{eqm} = [A]_0 - [A]_{eqm} \qquad \textbf{…2.33}$$

If the stoichiometry is not 1:1:1 then the appropriate stoichiometric coefficients must be used in the mass balance equations and in the rate law.

It is convenient to note that the forward and reverse rates are equal at equilibrium, which means that:

$$-\frac{d[\mathrm{A}]}{dt} = k_2[\mathrm{A}]_{eqm}[\mathrm{B}]_{eqm} - k_{-2}[\mathrm{P}]_{eqm} = 0 \qquad \textbf{…2.34}$$

And hence:

$$k_2[\mathrm{A}]_{eqm}[\mathrm{B}]_{eqm} = k_{-2}[\mathrm{P}]_{eqm} \qquad \textbf{…2.35}$$

Using *Equation 2.33*, *Equation 2.35* can be re-written as:

$$k_2[\mathrm{A}]_{eqm}[\mathrm{B}]_{eqm} = k_{-2}([\mathrm{A}]_0 - [\mathrm{A}]_{eqm}) \qquad \textbf{…2.36}$$

Rearranging *Equation 2.36* leads to:

$$k_{-2}[\mathrm{A}]_0 = k_2[\mathrm{A}]_{eqm}[\mathrm{B}]_{eqm} + k_{-2}[\mathrm{A}]_{eqm} \qquad \textbf{…2.37}$$

Substituting *Equation 2.33* into *Equation 2.30* followed by substitution of *Equation 2.37* in the resulting equation gives:

$$-\frac{d[\mathrm{A}]}{dt} = k_2[\mathrm{A}]_t[\mathrm{B}]_t - k_2[\mathrm{A}]_{eqm}[\mathrm{B}]_{eqm} - k_{-2}[\mathrm{A}]_{eqm} + k_{-2}[\mathrm{A}]_t \qquad \textbf{…2.38}$$

Substituting $[\mathrm{B}]_t$ and $[\mathrm{B}]_{eqm}$ from *Equations 2.31* and *2.33* into *Equation 2.38* and using the approximations $k_2[\mathrm{A}]_t[\mathrm{A}]_0 \approx k_2[A]_{eqm}[\mathrm{A}]_0$ and $k_2[\mathrm{A}]_t^2 \approx k_2[\mathrm{A}]_{eqm}^2$ gives:

$$\begin{aligned} -\frac{d[\mathrm{A}]}{dt} &= k_2[\mathrm{A}]_t[\mathrm{B}]_0 - k_2[\mathrm{A}]_{eqm}[\mathrm{B}]_0 - k_{-2}[\mathrm{A}]_{eqm} + k_{-2}[\mathrm{A}]_t \\ &= (k_2[\mathrm{B}]_0 + k_{-2})([\mathrm{A}]_t - [\mathrm{A}]_{eqm}) \end{aligned} \qquad \textbf{…2.39}$$

Rewriting *Equation 2.39* in terms of **A** and integrating gives:

$$\int_{[X]_0}^{[X]_t} \frac{d[\mathrm{A}]}{([\mathrm{A}]_t - [\mathrm{A}]_{eqm})} = -(k_2[\mathrm{B}]_0 + k_{-2})\int_0^t dt \qquad \textbf{…2.40}$$

Hence:

$$\ln\left(\frac{[A]_t - [A]_{eqm}}{[A]_0 - [A]_{eqm}}\right) = -(k_2[B]_0 + k_{-2})t = -k_{obs}t \qquad \textbf{…2.41}$$

Where $k_{obs} = k_2[B]_0 + k_{-2}$

Thus, plotting k_{obs} *vs* $[B]_0$ gives a straight line with a slope k_2 and intercept k_{-2}.

The equilibrium constant can be calculated by determining the ratio:

$$K_{eqm} = \frac{k_2}{k_{-2}} \qquad \textbf{…2.42}$$

A reversible process as described leads to a two-termed rate law. Another process which leads to this type of rate law is two parallel reaction paths where one is independent of $[B]_0$.[6,8-9]

2.4 Temperature Dependence and Activation Parameters

The temperature dependence of a rate constant is often studied in an attempt to harness more information about the energetics of a particular reaction. This results in the determination of a reaction's activation parameters.[8-9] For more complex rate laws, this may involve a study of concentration dependence of the rate at various temperatures, to determine the temperature dependence of different species in the rate law.[8-9] The Arrhenius equation, or Transition State Theory is used to analyse the experimental data of rate constants as discussed below.

2.4.1 Arrhenius Equation

Generally the rate of a chemical reaction is accelerated by an increase in temperature. The effect is normally represented in terms of the variation of a rate constant k with temperature, which frequently follows the Arrhenius equation[8-9]:

$$k = A\boldsymbol{e}^{\left(-\frac{E_a}{RT}\right)} \qquad \textbf{…2.43}$$

where A is the pre-exponential factor, E_a is the activation energy (J mol^{-1}), R is the universal gas constant (8.315 J K^{-1} mol^{-1}) and T is absolute temperature (K).

The rate constant, k, is determined by carrying out experiments at varying temperatures and it is generally expected to increase with increasing temperature.[8-9] A plot of ln k versus $\left(\frac{1}{T}\right)$ according to the following equation, which is the natural log of *Equation 2.43*

$$\ln k = \ln A - \frac{E_a}{R} \cdot \left(\frac{1}{T}\right) \qquad \textbf{…2.44}$$

gives a straight line of slope $-\frac{E_a}{R}$ and intercept of ln A. The Arrhenius equation is valuable in systems where the experimental rate constant is thought to be a combination of rate constants.[9]

2.4.2 Transition State Theory

The erection of potential energy surfaces stimulated interest in a more detailed picture of reactive collisions than Simple Collision Theory could provide. Focus was placed on the transient molecular configuration at the top of the energy barrier, and in 1935 a new method of calculating rate constants was suggested independently by Evans and Polyani, and Eyring.[11] The Transition State Theory was developed for a simple dissociation process in the gas phase and made two essential postulates which may be summarised as follows[14-15]:

- In the course of the reaction of A with B, somewhere there will be a configuration of the nuclei of the constituent atoms such that the species so formed may spontaneously undergo reaction, either to the reaction products or back to the reactants A and B.

- This species, which is usually referred to as the transition state of the reaction, is assumed to be in effective equilibrium with the reactants.

If we assume the reaction adheres to the mechanism depicted below[9,11-12]:

With a reaction rate as follows:

$$-\frac{d[\mathrm{A}]}{dt} = \frac{k_b T}{h}[\mathrm{A}---\mathrm{B}]^* = \frac{k_b T}{h} K^{\neq}[\mathrm{A}][\mathrm{B}] \qquad \textbf{…2.45}$$

where k_b is Boltzmann's constant (1.38 x 10^{-23} J K^{-1}), T is absolute temperature (K), h is Planck's constant (6.626 x 10^{-34} J s^{-1}) and $K^{\neq}$ is the equilibrium constant.

The experimental second order rate constant k_2 can be written as:

$$k_2 = \frac{k_b T K^{\neq}}{h} \qquad \textbf{…2.46}$$

The free energy of activation, $\Delta G^{\neq}$, can be written as:

$$\Delta G^{\neq} = -\mathrm{RT}\ln K^{\neq} = \Delta H^{\neq} - T\Delta S^{\neq} \qquad \textbf{…2.47}$$

where $\Delta H^{\neq}$ and $\Delta S^{\neq}$ are the changes in enthalpy and entropy of activation respectively.

Substitution of *Equation 2.47* into *2.46* gives the following expression:

$$k_2 = \frac{k_b T}{h}\exp\left(-\frac{\Delta G^{\neq}}{RT}\right) = \frac{k_b T}{h}\exp\left(\frac{-\Delta H^{\neq}}{RT}\right)\exp\left(\frac{\Delta S^{\neq}}{R}\right) \qquad \textbf{…2.48}$$

Taking the natural log of *Equation 2.48* results in *Equation 2.49*

$$\ln\left(\frac{k_2}{T}\right) = \ln\left(\frac{k_b}{h}\right) - \frac{\Delta H^{\neq}}{RT} + \frac{\Delta S^{\neq}}{R} \qquad \textbf{…2.49}$$

Subsequent linearisation gives:

$$\ln\left(\frac{k_2}{T}\right) = \frac{-\Delta H^{\neq}}{R}.\frac{1}{T} + \left(\ln\frac{k_b}{h} + \frac{\Delta S^{\neq}}{R}\right) \qquad \textbf{…2.50}$$

A plot of $\ln\left(\frac{k_2}{T}\right)$ versus $\left(\frac{1}{T}\right)$ gives the enthalpy of activation $\Delta H^{\neq}$ from the slope and the entropy $\Delta S^{\neq}$ can be obtained from the intercept. This type of plot is called an Eyring plot.[1,9,12] It is important to remember that activation parameter values determined by different workers on the same system may not always agree.

This is due to the fact that a long extrapolation of the Eyring plot to $\frac{1}{T} = 0$ is required to determine the entropy of activation. Thus the accuracy of the values obtained is compromised.[8-9] Using a wide range of temperature values or determining the volume of activation (see *Section 2.4.3*) alleviates this problem.[8-9]

Although the value of $\Delta H^{\neq}$ is not very informative regarding the mechanism of the reaction it is generally accepted that the value for associative reactions is usually smaller than that for dissociative reactions ($\Delta H^{\neq}$ is used as a measure of the bond strength of the dissociating ligand).[8-9,13] The entropy of activation on the other hand is far more useful when determining the reaction mechanism. Values that are below −10 J $K^{-1}mol^{-1}$ indicate an associative reaction whilst values of $\Delta S^{\neq}$ that are greater than +10 J $K^{-1}mol^{-1}$ indicate a dissociative reaction. One must be careful in interpreting the mechanism for reactions that have a $\Delta S^{\neq}$ between −10 and +10 J $K^{-1}mol^{-1}$ as solvent re-organisation may also contribute, especially for polar solvents and charged metal complexes.[8-9,13]

2.4.3 Pressure Dependence and Volumes of Activation

In case where the entropy and enthalpy of activation may be neither large and positive nor large and negative, it is difficult to infer a mechanism. The volume of activation, $\Delta V^{\neq}$, is a supplement to the enthalpy and entropy of activation and becomes very useful when such a situation arises.[8-9,13] It is obtained by measuring the variation of the rate constant with pressure as indicated below[8-9,13]:

$$\left(\frac{\partial \ln k_2}{\partial P}\right)_T = -\frac{\Delta V^{\neq}}{RT} \qquad \textbf{…2.51}$$

where $\Delta V^{\neq}$ is the partial molar volume change when reactants are converted to the activated complex.

A plot of $\ln k_2$ *vs.* P is linear with a slope of $-\frac{\Delta V^{\neq}}{RT}$.[8-9] A positive volume of activation indicates a dissociative mechanism while a negative value is indicative of an associative substitution reaction. Unfortunately the volume of activation incorporates both the volume changes in the reactants and the volume changes in the surrounding solvent (electrostriction of solvent). This has the potential to cause discrepancies in the interpretation of volumes of activation.[6,11-12]

2.5 Experimental Kinetic Techniques

Reactions in solution make up an extensive proportion of the chemical reactions whose kinetics have previously been subjected to detailed investigation.[1] The choice of method for measuring reaction rates is critical and depends solely on the nature of the reaction. In other words, is the reaction fast or slow.[3] A reaction that proceeds to 50 % completion in 10 seconds or less is considered fast. Such reactions require specifically designed equipment that would enable rapid mixing as well as rapid data collection.[3] The conventional methods of analysis for slow reactions determine the reactant or product concentration as a function of time. Unfortunately even in 'slow' experiments the concentrations of the species change appreciably during the course of reaction.[3] This problem is eliminated by lowering the temperature to slow the reaction to allow a measurement to be taken, which is time-consuming, or by using an instrumental technique (spectrophotometry, conductometry or potentiometry) that continuously records concentration as the reaction proceeds.[1,3]

Due to the natural evolution of laboratory equipment, an increasing number of kinetic studies have been carried out by monitoring some physical property of a reaction mixture. Such techniques include infrared spectroscopy (IR), nuclear magnetic resonance spectroscopy (NMR), UV/Visible absorption spectrophotometry and stopped-flow analysis. Despite the abundance of techniques only the last two are discussed in detail below as the focus of this dissertation is on spectrophotometric analysis.[1,3]

2.5.1 UV/Visible Spectrophotometry

In a UV/Visible spectrophotometer, light from a continuous light source is passed through a monochromator (a prism, grating or filter) to select a particular wavelength.[16-20] The light of the selected wavelength with an intensity, I_0, strikes a sample in a cell called a cuvette of length, l. The intensity of the beam exiting the sample is I where $I \leq I_0$ as the sample absorbs the light.[16-20] In a double-beam spectrophotometer, light passes alternately through the sample and reference cuvettes. Using a reference cuvette containing pure solvent is important as it compensates for absorption due to the cuvette and solvent or light scattering.[16-20]A double-beam spectrophotometer, as shown in ***Figure 2.1***, manages to alternate between cuvettes by using a chopper which is a motor that rotates a mirror into and out of the light path. When the chopper is not deflecting the beam, the light passes through the sample and the detector measures the intensity; however, when the chopper deflects the beam through the reference cuvette, the detector reads the reference value. [16-20]The beam is chopped several times per second.

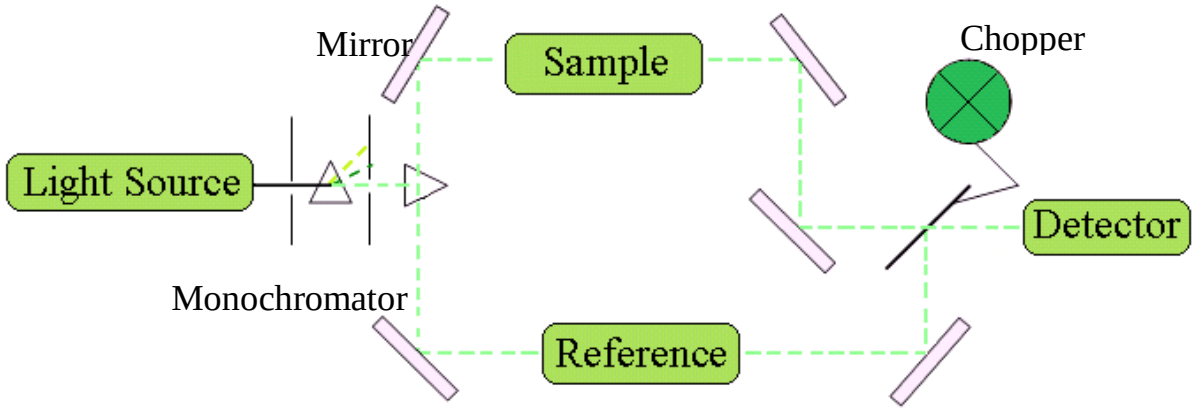

Figure 2.1: Schematic diagram of a double beam spectrophotometer.[19]

A spectrophotometer measures transmittance, T, which is defined as the fraction of the original light passing through the sample. [16-20]

$$T = \frac{I}{I_0} \qquad \textbf{…2.52}$$

Although transmittance, *T* is measured, absorbance is a more useful quantity and can be easily converted from transmittance

$$\mathrm{A} = \log\left(\frac{I_0}{I}\right) = -\log T \qquad \textbf{…2.53}$$

Absorbance is important because according to Beer's law given in *Equation 2.54*[16-20], it is directly proportional to the concentration of the sample:

$$\mathrm{A} = \varepsilon \cdot l \cdot c \qquad \textbf{…2.54}$$

Where A is the absorbance (it is dimensionless), *c* is the concentration of the sample (mol dm^{-3}), *l* is the pathlength (cm) and ε is the molar absorptivity ($Mol^{-1}dm^3\,cm^{-1}$).

For a first order reaction, *Equation 2.3*

$$\mathbf{X} \xrightarrow{k_1} \mathbf{Y}$$

The absorbance at any time t is

$$\mathrm{A}_t = \varepsilon_{\mathrm{X}}[\mathrm{X}]_t + \varepsilon_{\mathrm{Y}}[\mathrm{Y}]_t \qquad \textbf{…2.55}$$

where ε_{X} and ε_{Y} are the molar absorptivities of **X** and **Y** respectively.

Upon completion of the reaction, the absorbance will be

$$\mathrm{A}_\infty = \varepsilon_{\mathrm{X}}[\mathrm{X}]_\infty + \varepsilon_{\mathrm{Y}}[\mathrm{Y}]_\infty \qquad \textbf{…2.56}$$

Thus in kinetic analysis the following equation is used based on absorbance

$$\ln\frac{[\mathrm{X}]_0}{[\mathrm{X}]_t} = \ln\left(\frac{\mathrm{A}_0}{\mathrm{A}_t}\right) = k_1 t \qquad \textbf{…2.57}$$

where A_t is defined as absorbance of the reactant X at any time *t*.

The absorbance of a reaction is measured with time over a specific wavelength range. The observed rate constant for the reaction is determined by a least squares fit of an absorbance versus time plot at a specific wavelength. By monitoring the reaction at different concentrations of the reactant, the rate constant for the reaction at that temperature can be determined.

2.5.2 Stopped Flow techniques

Standard absorption spectrophotometry is often unable to monitor fast reactions as the time taken to mix the sample and take a reading is longer than the time needed for the reaction to occur.[3,5,8] An accepted and reliable method for monitoring rapid reactions is stopped-flow mixing (designed for the study of a reaction between two substances in solution).[3,5,8] This method involves mixing reagents rapidly and discontinuing the flow of the mixed solution abruptly. The evolution of the reaction is analysed near the mixer. [3,5,8,17]

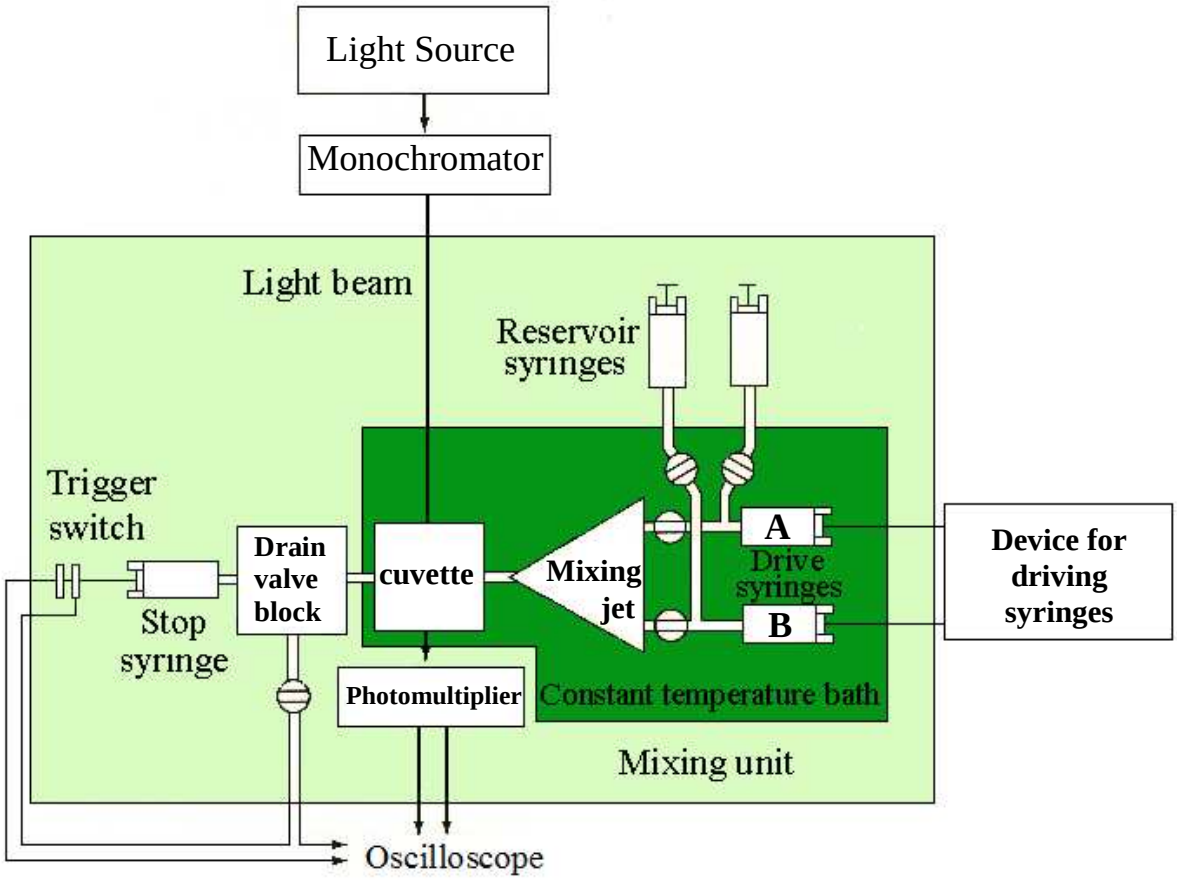

Figure 2.2: Schematic diagram of a stopped-flow apparatus.[3]

Syringes A and B (***Figure 2.2***) are filled and maintained with two separate solutions.[3,5,17] A pressure driven mechanism forces the plungers of the syringes down and a rapid stream of the two solutions passes into the mixing system and straight into the reaction cuvette. This ensures that mixing is complete within 1 ms.[3,5,17] The reaction solution then passes into the stop syringe.

This will eventually fill, causing the plunger to strike the stop block and instantly ceasing the flow, but leaving a recently mixed sample of solution in the observation cell. [3,5,17] Once the solution is stationary, an oscilloscope begins to take readings. The usual method of detection is UV/Visible spectrophotometry, and once the recording device starts, the amount of light transmitted through the observation chamber at a specific wavelength will change as the reaction proceeds. [3,5,17] A photomultiplier converts transmitted light into electric current and a computer interprets the data as an absorption versus time spectrum.

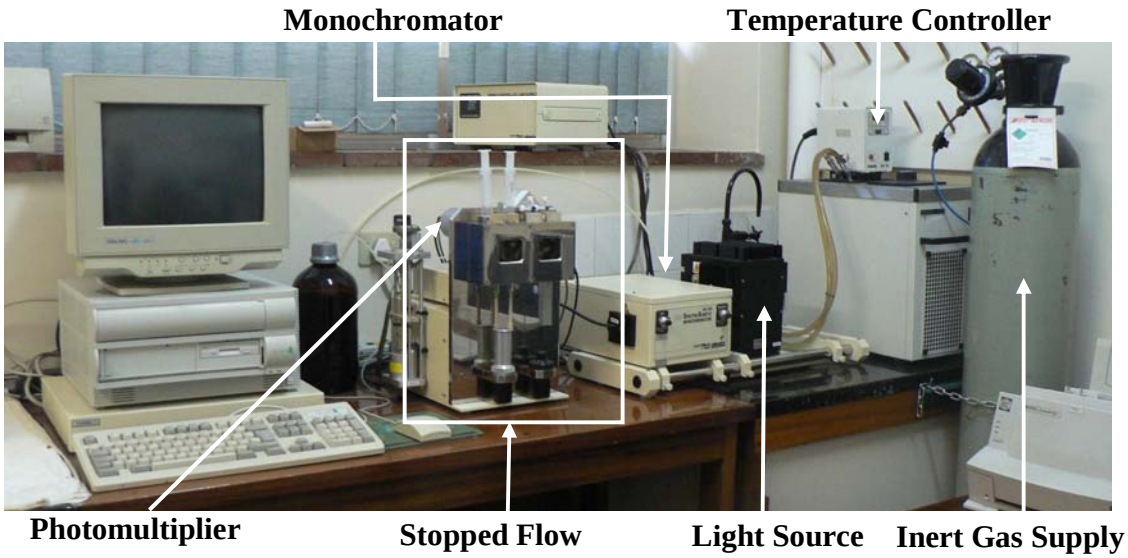

Figure 2.3: Photograph of a stopped-flow apparatus.

Stopped-flow analysis is a simple but highly advantageous technique. Not only does it allow very rapid first order reaction constants to be measured, $k \approx 40\ s^{-1}$, but it also does this in a simple and efficient (uses ≈ 0.2 ml volumes of solutions) manner.[17]

2.6 References

1. S. R. Logan, *Fundamentals of Chemical Kinetics*, Longman, Essex, **1996**, pp.1–30.
2. IUPAC, *Compendium of Chemical Terminology*, 2nd Ed. (the "Gold Book"), **1997**. Online corrected version, **2006**.
3. D. A. Skoog, D. M. West, F. J. Holler and S. R. Crouch, *Fundamentals of Analytical Chemistry* 8th Ed., Brooks/Cole – Thomson Learning, Inc., United States, **2004**, pp.718–734, 771–775, 878–894.
4. M. S. Silberberg, *Chemistry. The Molecular Nature of Matter and Change* 2nd Ed., McGraw–Hill, United States, **2000**, pp. 664–684.
5. K. J. Laidler, J. H. Meiser and B. C. Sanctuary, *Physical Chemistry*, Houghton Mifflin Company, United States, **2003**, pp. 363–376.
6. J. H. Espenson, *Chemical Kinetics and Reaction Mechanisms* 2nd Ed., McGraw–Hill, New York, **1995**, pp. 1–86.
7. J. Nicholas, *Chemical Kinetics: A Modern Survey of Gas Reactions*, Harper and Row, London, **1976**, pp. 1–16.
8. J. D. Atwood, *Inorganic and Organometallic Reaction Mechanisms* 2nd Ed., Wiley–VCH, New York, **1997**, pp. 1–32.
9. R. B. Jordan, *Reaction Mechanisms of Inorganic and Organometallic Systems*, Oxford University Press, New York, **1991**, pp. 1–17.
10. P. Atkins and J. de Paula, *Atkins' Physical Chemistry* 8th Ed., Oxford University Press, Oxford, **2006**, pp. 791–829.
11. a) H. Eyring, *J. Chem*., **1935**, *3*, 107–115; b) M. G. Evans and M. Polanyi, *Trans. Faraday Soc*., **1935**, *31*, 875–894.
12. S. Ašperger, *Chemical Kinetics and Inorganic Reaction Mechanisms*, 2nd Ed., Kluwer Academic/Plenum Publishers, New York, **2003**, *3*, pp. 14–23.
13. L. Helm and A. E. Merbach, *J. Chem. Soc*., *Dalton Trans*., **2002**, 633–641.
14. C. H. Langford, *Inorg. Chem*., **1979**, *18*, 3288–3289.
15. T. W. Swaddle, *Inorg. Chem*., **1980**, *19*, 3203–3205.
16. D. C. Harris, *Quantitative Chemical Analysis*, W.H Freeman and Company, San Francisco, **1982**, pp. 468–485.

17. R. G. Wilkins, *Kinetics and Mechanism of Reactions of Transition Metal Complexes* 2nd Ed., VCH Verlagsgesellschaft, Weinheim, **1991**, pp. 136–140.
18. H. H. Willard, L. L. Merritt, Jr., J. A. Dean and F. A. Settle, Jr., *Instrumental Methods of Analysis* 7th Ed., Wadsworth Publishing Company, California, **1988**, pp. 118–156, 159–162.
19. H. Bauer, G. D. Christian and J. E. O'Reilly, *Instrumental Analysis*, Allyn and Bacon, Inc., Boston, **1978**, pp. 167–188.
20. D.A. Skoog and D. M. West, *Principles of Instrumental Analysis*, 2nd Ed, Saunders College, **1980**, pp. 180–186.

CHAPTER III

Substitution Reactions

A simple substitution occurs when a ligand in the coordination shell is replaced by another from the environment causing no change in the oxidation state but rather a temporary change in the coordination number.[1-3] There are two important points that must be considered if one is to describe a single act of ligand substitution. The first highlights the changes in electron distribution that occur whilst bond-making and bond-breaking take place which is dependent less on the nature of the reaction centre and more on the nature of the entering and leaving groups. The second factor to consider is the timing (or molecularity) of the bond-making and bond-breaking process. In the seminal work by Ingold and Hughes[4], the modes of bond breaking were classified as either homolytic or heterolytic and the latter, further sub-divided according to the position of the bond electrons. Such processes were termed electrophilic and nucleophilic respectively and are represented below.

$$\begin{aligned} &M:L \longrightarrow M\cdot + L\cdot && \text{HOMOLYSIS} \\ &M:L \longrightarrow M^{+} + :L^{-} && \text{NUCLEOPHILIC HETEROLYSIS} \qquad \textbf{…3.1} \\ &M:L \longrightarrow M:^{-} + L^{+} && \text{ELECTROPHILIC HETEROLYSIS} \end{aligned}$$

Although effective for classifying carbon centres, this method could not be extended to the substitution reactions of inorganic systems. The reason for this is that heterolytic processes are in effect Lewis acid-base reactions wherein the reaction centre can behave as both a Lewis acid for nucleophilic processes and as a Lewis base for electrophilic processes. For nucleophillic processes, the reaction easily falls into the simple substitution reaction category. In the case of electrophilic attachment however, the reaction centre acts as a Lewis base and two formerly non-bonding electrons are brought into bonding which is comparable to a two-electron oxidation. When the ligand departs as a Lewis acid, electrophilic substitution is complete. It is also possible to stabilise the higher oxidation state intermediate by attaching a Lewis base (ligand) from the environment. Such events are often synchronous with the Lewis acid and base fragments residing on the same molecule. This process is termed oxidative addition and reductive elimination.[1]

3.1 Mechanistic Classification of Inorganic Substitution Reactions

Early kinetic investigations into the realm of transition metal substitutions, particularly those in solvents other than water, led to the realisation that kinetic order was not a good measure of molecularity as substitution frequently occurred within a pre-formed aggregate.[1] As a result, Langford and Gray[5] attempted to produce an operational way of defining inorganic reactions by introducing the concept of a stoichiometric mechanism which depends upon the identification of an intermediate species and which exists in three forms (***Figure 3.1***)[1,4]:

1. The first is a dissociative process (***D*** mechanism) and occurs when a reaction intermediate with a lower coordination number is formed.[1-2,6-8] In such a case the leaving group detaches before the attachment of the entering group occurs. [1-2,6-8] The rate of the reaction is insensitive to the entering group as the rate determining step is that of the bond breaking process. [1-2,6-8]

2. The second is the associative process (***A*** mechanism) which involves the formation of a reaction intermediate with an increased coordination number. [1-2,6-8] Here the entering group forms a bond to the metal centre before the leaving group has detached. Since bond formation is the rate determining step, the reaction is dependent on the entering group.[1-2,6-8]
3. The third and final form is an interchange process (***I*** mechanism), and is observed when bond-breaking and bond-making are synchronous and no intermediate is formed.

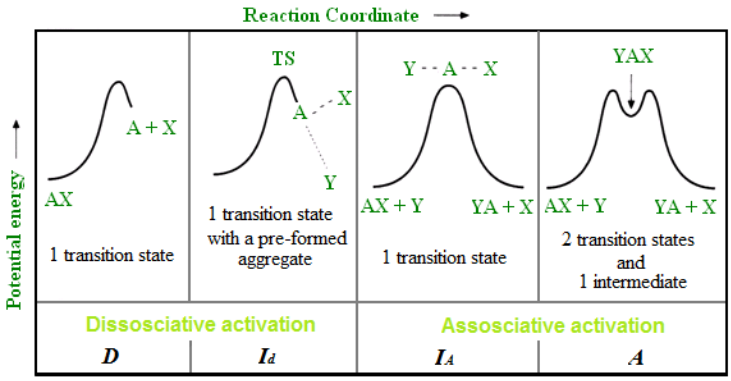

Figure 3.1: Relationship between the mechanism of substitution and associated energy profile according to the Langford-Gray nomenclature.[1]

The stoichiometric interchange mechanism can be further classified according to its intimate mechanism, an indication of the mode of activation.

1. A dissociatively activated intimate mechanism (***I_d***) (***Figure 3.2***, **I**) has a transition state where only very weak bonds exist between the metal centre and the entering group. [1-2,6-8] The entering group has a minor effect on the reaction rate resulting from solvent interactions in the ground state of any intermediate whilst bond breaking is more dominant.[1-2,6-8]

2. An assosciatively activated intimate mechanism (***I_a***) (***Figure 3.2,*** **II**) has a transition state in which there is significant bonding of the metal to the entering group.[1-2,6-8] This mechanism shows considerable sensitivity toward nature of entering group thus bond formation is more dominant.

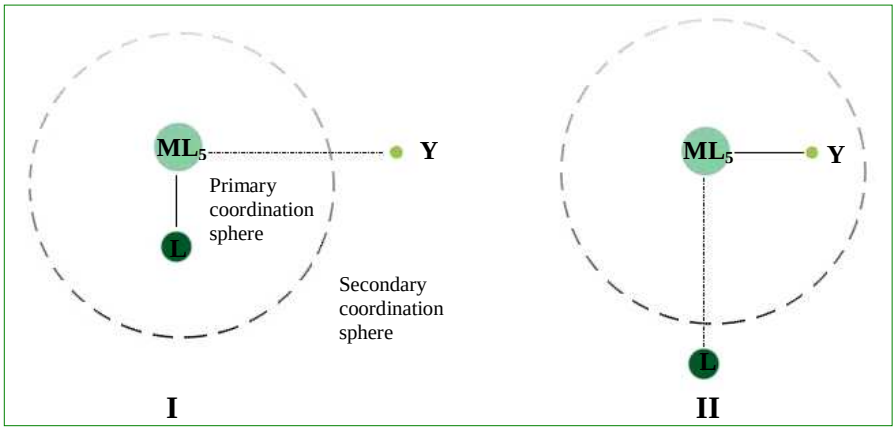

Figure 3.2: Diagram illustrating **I** dissociatively activated, and **II** associatively activated intimate mechanisms. [1-2,6-8]

3.2 Coordination Number and Mechanism of Substitution

One would assume that the more atoms or ligands surrounding a central atom, the harder it might be to bind another group, thus it is not unreasonable to imagine that a connection exists between the coordination number and the substitution mechanism. It is therefore reasonable to expect that centres with a higher coordination number should theoretically favour a dissociative mechanism whilst the opposite would be true for the associative mechanism. Unfortunately although a relationship does exist, it is not so straightforward.[1]

A combination of electronic and steric factors of the central atom and its ligands control the ground-state geometry, and as a result, the change on going to the transition state is also determined by the resultant of a number of factors.[1] It is thus not surprising that tetrahedral *sp*-block elements and first row *d*-block M^{2+} and M^{3+} centres employ $\boldsymbol{I_d}$ and $\boldsymbol{I_a}$ pathways.[1] The small discrepancies in energy between various geometries available to seven and eight coordinate species, permit *f*-block elements to react through associative or dissociative pathways.[1] With a few exceptions square-planar *d*-block complexes generally follow an associative mechanism.[1-3, 6-12, 13-14]

3.3 Substitution in Square-Planar Platinum(II) Complexes

For square-planar geometry to be favoured, special circumstances are required as this geometry does not represent the lowest energy arrangement of four ligands in an electrostatically bonded system.[1,3] The most common d^8 square-planar complexes are those in which the metal centre has a +2 oxidation state.[1] Of these, platinum is the most favoured when studying ligand substitution for square-planar metal centre's as it is resistant to redox reactions, has low reactivity which leads to the synthesis of a variety of complexes and reactions lead to kinetics which are simple and easy to interpret.[1,3,7] Palladium complexes are far more reactive, thus they are less favourable to study.[1,3] In some instances, simply substituting a platinum(II) centre for a palladium(II) centre can increase the rate constant by a factor of 10^5.[1,3,6]

During ligand substitution of square-planar platinum(II) complexes (***Figure 3.3***), the coordination number increases from four to five and the transition state adopts a trigonal bipyramidal conformation, given that the bond to the incoming ligand **Y** is formed prior to bond cleavage of the leaving group **X**, *ie*. The mechanism of substitution is associative in nature.[6-8,15]

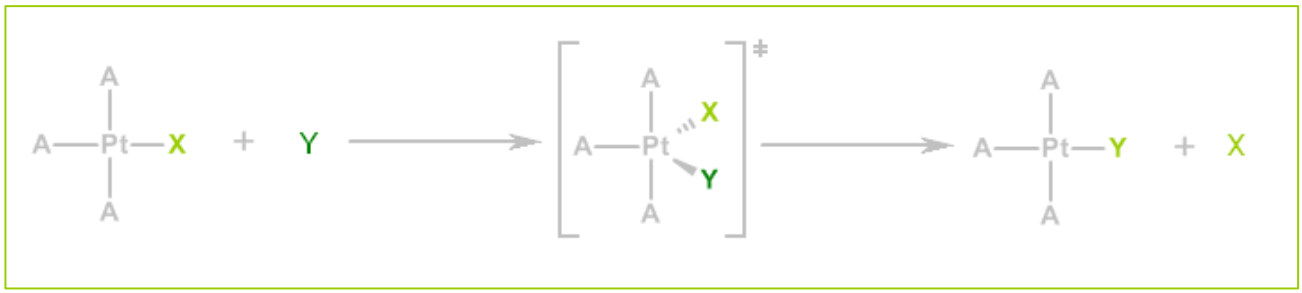

A = inert ligand

Figure 3.3: Schematic illustrating typical ligand substitution for a platinum(II) complex which follows an associative mode of activation proceeding through a trigonal bipyramidal transition state. [6-8,15]

3.4 The Kinetics and Mechanism of Substitution of Square-Planar Platinum(II) Complexes

Studies of square-planar platinum(II) complexes have generally focused on the substitution of one monodentate ligand with another. As a result, the rules that govern the kinetics and mechanism of substitution are based primarily on a simple type of substitution.[2,6,15]

The reaction,

$$\mathbf{[L_3M–X] + Y} \underset{}{\overset{k_1}{\rightleftharpoons}} \mathbf{[L_3M–Y] + X} \qquad \textit{(Charges omitted)}$$

has the following rate law:

$$-\frac{d[L_3MX]}{dt} = k_1[L_3MX] + k_2[L_3MX][Y] = \{k_1 + k_2[Y]\}[L_3MX] \qquad \textbf{…3.2}$$

Substitution reactions of square-planar complexes generally consist of two terms as is the case in *Equation 3.2*. The first term is first-order with respect to the metal complex, [L_3MX], whilst the second term is first-order in both the metal complex and the entering nucleophile, [Y].[2] In an attempt to simplify the substitution of square-planar platinum(II) complexes, *pseudo* first-order conditions are often adopted, thus *Equation 3.2* can be reduced to:

$$-\frac{d[L_3MX]}{dt} = \{k_1 + k_2[Y]\}[L_3MX] = k_{obs}[L_3MX] \qquad \textbf{…3.3}$$

where k_{obs} is the observed *pseudo* first-order rate constant and equates to (k_1 + k_2[*Y*]).

This is frequently referred to as a "typical rate law for square-planar substitution." This is only applicable in coordinating solvents under the conditions described above.

A plot of k_{obs} versus the concentration of the entering nucleophile, [*Y*], is linear with a slope equal to k_2 and an intercept equal to k_1. ***Figure 3.4*** shows some typical plots attained.

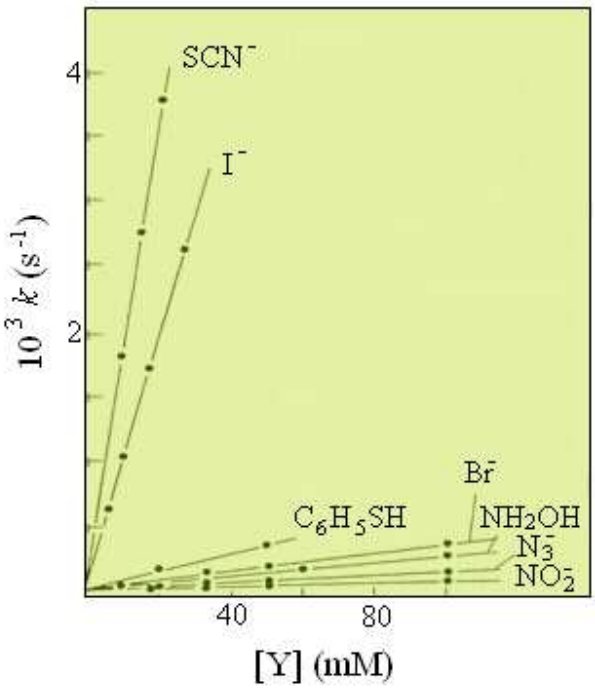

Figure 3.4: Plots of the *pseudo* first-order rate constants, k_{obs}, versus the concentration of the entering nucleophile, [*Y*], for the reaction of *trans*-[$Pt(py)_2Cl_2$] with a series of nucleophiles in methanol at 30.0 °C.[16]

The substrate is also capable of undergoing reversible solvolysis thus:

$$\mathbf{[L_3M–X] + S \rightleftharpoons [L_3M–S] + X}$$

It is often necessary to add an excess of **X** to suppress this. The kinetics are studied under conditions where **[X]** >> **[L_3M–X]** and the rate law takes on the form:

$$k_{obs} = \frac{k_1 k_Y [Y]}{k_X [X] + k_Y [Y]} + k_2 [Y] \qquad \textbf{…3.4}$$

The simpler expression is simply a limiting form of this when $k_Y[Y] >> k_X[X]$. At the other limit, when $k_X[X] >> k_Y[Y]$, the expression reduces to:

$$k_{obs} = \left\{ \frac{k_1 k_Y}{k_X [X]} + k_2 \right\} [Y] \qquad \textbf{…3.5}$$

The conditions of this approximation require that $k_1 >> k_2$ if the limiting form is to be anything other than $k_{obs} = k_2[Y]$.

k_1 is a rate constant that is independent of the incoming nucleophile, **Y**, whilst k_2 is the rate constant that is very sensitive to **Y** (for a given solvent at a fixed temperature). An important point to note is that the positive intercept, as observed in ***Figure 3.4***, may not always be attributed to k_1 (*Equation 3.3*) and might in fact reflect the rate constant for the reverse reaction, as shown in *Equation 3.2*.[17-18] Generally kinetic studies on the substitution behaviour of platinum(II) complexes are conducted in coordinating solvents such as methanol or water usually present in a large molar excess.[19] In circumstances where the contribution of the reverse reaction is negligible, the k_1 term may be ascribed to the solvolysis pathway[2,6-7,15]. Consequently the k_2 term is the product of direct nucleophilic attack by the entering nucleophile, **Y**, on the metal centre.

The reaction proceeds with a retention of stereochemistry, *i.e.* the ground state geometry of the complex is preserved with both the *cis* and *trans* ligands, relative to the leaving group, remaining in the trigonal equatorial plane. The k_1 term is obtained from the attack of a solvent molecule on the metal centre and also proceeds *via* a trigonal bipyramidal transition state. ***Figure 3.5*** illustrates the connection between these two reaction pathways.

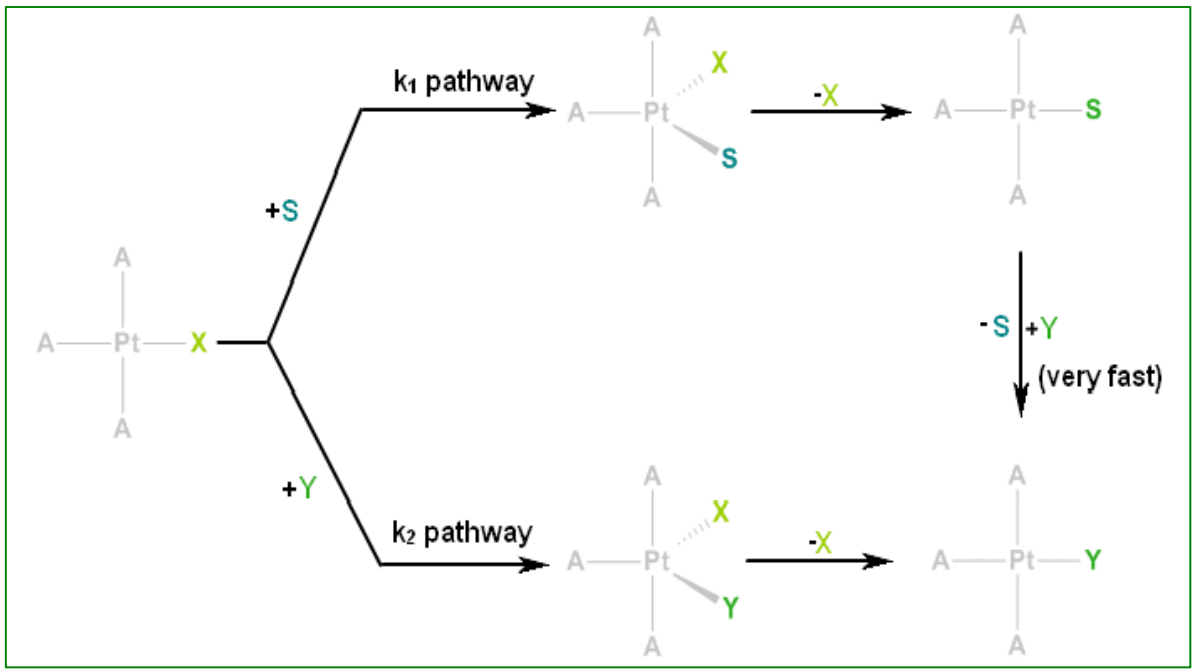

A = inert ligand
S = solvent

Figure 3.5: Schematic showing direct nucleophilic attack and solvolytic reaction pathways for the substitution reactions of platinum(II) complexes.[1-2]

3.5 Reactivity of Square-Planar Platinum(II) Complexes

The magnitude of the rate constant obtained from the substitution reaction of square-planar platinum(II) complexes is strongly dependent on a number of factors including:

- Nature of the entering group
- Nature of the *trans* ligand
- Nature of the *cis* ligand
- Solvent
- Nature of the leaving group
- Nature of the metal centre
- pH

Some of these will be discussed in further detail below.

3.5.1 Effect of the Entering Group

It is well documented that the rate of substitution for a reaction following an associative pathway is dependent upon the nucleophilicity, which is a quantitative measure of the reactivity of the entering group, *i.e.* the stronger the nucleophile, the greater the rate at which the substitution reaction for a particular platinum(II) complex will proceed.[1,3]

Although several nucleophilicity scales have been proposed, *e.g.* the Methyl-Hg(II) scale; Edwards' scale; Swain and Scott's scale (n_{Pt}) and the Drago E and C scale, the one found most applicable to the platinum(II) reaction centre was the n_{Pt} scale[1] and is defined as:

$$n_{Pt} = \log\left(\frac{k_2}{k_1}\right) \qquad \textbf{…3.6}$$

using kinetic data for the reaction[1,8],

$$\textit{trans}\text{-}[Pt(py)_2Cl_2] + Y^{n-} \longrightarrow \textit{trans}\text{-}[Pt(py)_2Cl(Y)]^{(n-1)} + Cl^-$$

Since k_2 (L mol^{-1} s^{-1}) and k_1 (s^{-1}) differ in their dimensions, the logarithmic representation was found to be inaccurate and, once it was accepted that the first-order pathway was an associative solvolysis, k_1 was replaced by a second-order constant giving[1,3,20]:

$$n^{o}_{Pt} = \log\left(\frac{k_2}{k_1^{o}}\right) \qquad \textbf{…3.7}$$

where $k_1^{o} = k_1[CH_3OH]$

At 30.0 °C, the concentration of methanol is 24.3 mol dm^{-3} and *Equation 3.7* can be reduced to:

$$n^{o}_{Pt} = n_{Pt} + \log 24.3 = n_{Pt} + 1.39 \qquad \textbf{…3.8}$$

Table 3.1 shows a number of important n^{o}_{Pt} values.[1]

***Table 3.1*:** A selection of n^{o}_{Pt} values listed according to the donor atoms[1]

Carbon		**Nitrogen**			
$C_6H_{11}NC$	6.34	NH_3	3.07	NO_2^-	3.22
CN^-	7.14	$PhNH_2$	3.16	C_5H_5N	3.19
		Imidazole	3.44	NH_2OH	3.85
		NH_2NH_2	3.86		
Oxygen		**Halogens**		**Phosphorous**	
MeOH	0.00	F^-	< 2.2	$(Et_2N)_3P$	4.57
MeO^-	< 2.4	Cl^-	3.04	$(MeO)_3P$	7.23
OH^-	< 2.4	Br^-	4.18	Ph_3P	8.93
		I^-	5.46	Et_3P	8.99
		Sulfur			
Me_2SO	2.56	(Ph)MeSO	2.90	Ph_2S	3.22
$(PhCH_2)_2S$	3.43	$(4\text{-}MeC_6H_4)_2S$	3.68	PhSH	4.15
Et_2S	4.52	Me_2S	4.87	$(CH_2)_5S$	5.02
SCN^-	5.75	SO_3^{2-}	5.79	PhS^-	7.17
$S_2O_3^{2-}$	7.34				
Arsenic		**Selenium**		**Antimony**	
Ph_3As	6.89	Me_2Se	5.70	Ph_3Sb	6.79
Et_3As	7.68	$SeCN^-$	7.11		

A number of interesting trends can be seen from the data provided in ***Table 3.1***. To begin with the nucleophilicities of the halides show typical soft acid-base behaviour, decreasing as one moves up the periodic table, **I^- > Br $^-$> Cl^- > F^-**.[1,3] Group 15 bases (except amines) are all excellent nucleophiles towards platinum(II) but nucleophilicity does decrease in the order **phosphines > arsines > stibines > amines** while hydroxides are too weak to produce a k_2 term.[1,3]

No relationship can be found between n^{o}_{Pt} (kinetic) and pK_a (thermodynamic).[1,3] In general, the most reactive nucleophiles are "soft"[α] which is why sulfur is a better donor than oxygen.[1,3,21-24]

It is of little use to introduce the concept of nucleophilicity scales if the order (quantitative or qualitative) is not maintained throughout a wide range of substrates. For many compounds it has been found that for a specific substrate, a plot of log k_2 for a particular nucleophile against its n^{o}_{Pt} value is linear.

$$\log k_2 = \boldsymbol{S}.n^{o}_{Pt} + \boldsymbol{C} \qquad \textbf{…3.9}$$

where k_2 is the second-order rate constant for the nucleophile, ***S*** is the nucleophilic discrimination factor and ***C*** is the intrinsic reactivity which can only be used effectively in reactions carried out in methanol (***C*** = log k_1−1.40)[1,3]

S is dependent upon the nature of the complex, reflecting its electrophilicity and steric hindrance towards incoming nucleophiles. The intrinsic reactivity, ***C***, of the complex is obtained as an intercept and represents the reactivity of the poorest nucleophilic reagent whose effect can be measured in solution. The trend that is usually observed is that complexes with a high ***C*** value are less discriminating in a reaction with different nucleophiles and consequently have a small ***S*** value. For complexes with a low ***C*** value, the reverse is often true.[16,25]

Quite soon after its introduction, the n^{o}_{Pt} scale showed its limitations as certain nucleophiles, *viz* $(NH_2)_2CS$, NO_2^- and $SeCN^-$, failed to follow the linear relationship previously described as their nucleophilicity was substrate dependent.[1,3] For example, the nucleophile might be less effective than expected from the n^{o}_{Pt} value when the effective nuclear charge of platinum is high while it might be more effective than expected if the effective nuclear charge of platinum is low.[1,3]

[α] The polarisability of a ligand is best explained using Pearson's "Hard Soft Acid Base" (HSAB) Theory which states that hard acids, *i.e.* those metal ions that are small, bear a high charge and possess a valence electron shell that is not easily distorted, prefer hard bases, *e.g.* Mg^{2+} and F^-. Similarly soft acids, *i.e.* those metal ions that are large, bear a low charge and possess a valence electron shell that is easily distorted or removed, prefer soft bases, *e.g.* Pd^{2+} and SCN^-.[22–24]

Another reason for such discrepancies can be attributed to steric hindrance.[26-27] Those complexes following an associative mode of substitution possess a transition state with an increased coordination number as a result of bonding between the metal centre and the entering group. Due to this, steric interactions in the transition state are increased. It is therefore not unusual to expect that sterically hindered complexes react slower due to transition state destabilisation by increased steric interactions.

3.5.2 Nature of the Trans Ligand

Another crucial factor in determining the rate of substitution in a square-planar complex is the effect of the *trans* ligand. At the turn of the century Alfred Werner was the first to notice the ability of certain ligands to promote substitution *trans* to themselves. However it was not until a quarter of a century later that Chernayev and his colleagues established the *trans*-effect, defining it as the effect of a coordinated ligand on the rate of replacement of a ligand *trans* to itself.[1,3,7,27] These groups labilise a ligand *trans* to themselves in order to facilitate substitution, (***Figure 3.6***). Thus, complexes in which the *trans* group influences the rate far more than the *cis* groups are considered to show the *trans*-effect.[27]

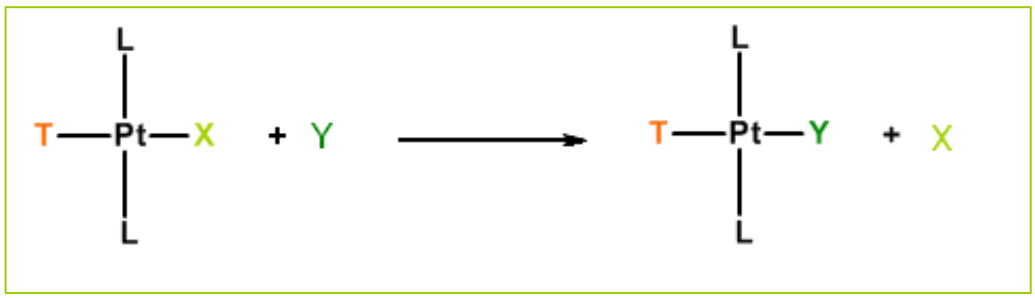

***Figure 3.6*:** Diagram illustrating ligand (T) ability to labilise the ligand *trans* to itself (X).[27]

The ascending order of the *trans*-effect of classic ligands is:[1,3,5,27-32]

$H_2O < OH^- < NH_3 \sim RNH_2 <$ pyridine $< Cl^- < Br^- < SCN^- \sim I^- \sim NO_2^- \sim SO_3^{2-} \sim PR_3 \sim SR_2 \sim SC(NH_2)_2 < CO \sim C_2H_4 \sim CN^-$ **…3.10**

Kinetically, the *trans*-effect can be large; a difference in rate of reaction of a factor of 10^6 can be found between a complex containing a good *trans* ligand and a poor *trans* ligand (***Table 3.2***).[27]

***Table 3.2*:** The kinetic *trans*-effect for neutral ligands

trans–[Pt(L)(am)Cl_2] + MeOH ⟶ *trans*–[Pt(L)(MeOH)Cl_2] + am	
L (neutral)	**10^3 k_1 (s^{-1})**
C_2H_4	6800
CO	1210
PR_3	15

It is imperative that one be able differentiate between the *trans*-**effect** and the *trans*-**influence** of a ligand. The *trans*-**effect** involves the effect of the ligand on the rate of substitution of the *trans* ligand and involves both the ground and transition state.[7] The *trans*-**influence** is the effect of the *trans* ligand only on the ground state properties such as bond lengths or infrared stretching frequencies.[7,27,33]

There have been many theories postulated in an attempt to explain the *trans*-effect. Amongst these was Grinberg's[33] theory, which stated that the primary charge on the platinum(II) metal induces a dipole in the *trans* ligand, causing an induced dipole in the metal.[33] This second dipole then repels the negative charge in the leaving group, **X** causing the **Pt—X** bond to lengthen and deteriorate (***Figure 3.7***). Thus a link is formed between the *trans* influence of **T** and its polarisability (*e.g.* $H^- \sim I^- > Cl^-$).[27]

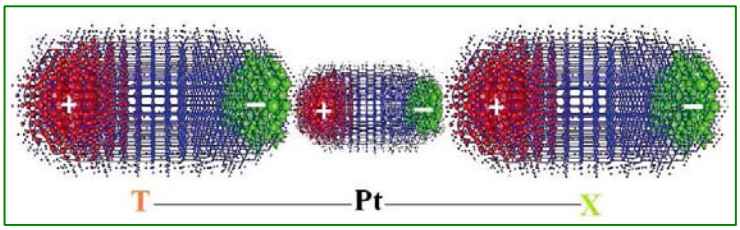

Figure 3.7: Induced dipoles over **T–Pt–X**.[27]

Unfortunately this electrostatic theory does not account for the fact that the induced dipole on platinum(II) should depend on the distance from **T** (the smaller the distance the bigger the dipole) and should also depend on the net charge of **T** more strongly than on its induced dipole moment.[27] This would lead to Cl^- having a greater *trans* effect than I^- which is not true. However, this objection can be eliminated if covalent bonding is taken into account with highly polarising ligands also able to form more covalent bonds to platinum(II).[2]

The π-bonding theory is another attempt in explaining the *trans*-effect and states that ligands with π-bonds, such as C_2H_4, PR_3 and CO (***Table 3.2***) stabilise the transition state for a reaction and therefore appear higher in the *trans*-effect series.[1,3,7,27] A pair of electrons are donated from the ligand to the metal centre creating a σ-bond whilst a π-bond is formed by the overlap of a filled *d* orbital on the metal and a vacant orbital of the ligand.[27] In the ground state, evidence indicates removal of electrons from the metal by the π-bonding would actually strengthen bonds of the other ligands instead of weakening the **Pt—X** bond.[27] Chatt *et al.*[34]and later Orgel[35-36] proposed π bonding stabilisation of the trigonal bipyramidal intermediate in the transition state to explain the *trans*-effect. Chatt stated that in the transition state, the incoming group brings in extra electron density and the removal of this added charge from platinum(II) by π-bonding of **T** will enhance the addition of **Y** and the reaction will happen more rapidly as the activation energy is lowered as shown in ***Figure 3.8***.[1,3]

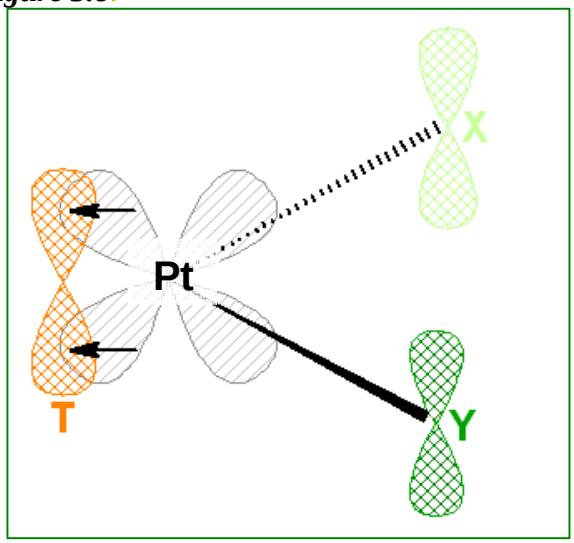

Figure 3.8: π-back donation from full metal *d*-orbitals to vacant orbitals of the *trans* ligand.[27]

Orgell supported this, stating that π-bonding reduces the electron density on platinum(II) along the **Pt—X** and **Pt—Y** direction which will lead to a retention of configuration.[27]

The π-*trans* effect is supported by Molecular Orbital Theory (MO). ***Figure 3.9*** illustrates a simplified MO diagram for $[PtCl_4]^{2-}$.[15] σ-bonding orbitals closely followed by π-bonding orbitals, are considered the two most stable molecular orbitals and are mainly located on the four chlorine atoms.[27,37]

Above these are the relatively stable anti-bonding orbitals, $\pi^*_{xz}, \pi^*_{yz}, \pi^*_{z^2}$, $\sigma^*_{z^2}$ and π^*_{xy} and the comparatively unstable $\sigma^*_{x^2-y^2}$ which come from the 5*d* atomic orbitals of platinum(II).[27,37] Situated above these at a higher energy are the anti–bonding orbitals σ^*_s, σ^*_x, σ^*_y and σ^*_z.[27,37] For square-planar complexes, π^*_{xz}, π^*_{yz} and π^*_{xy} are the only orbitals with the correct orientation for π-bonding.[38] On addition of **Y**, a trigonal bipyramidal intermediate forms ensuring that, π^*_{xz}, π^*_{yz}, π^*_{xy} and $\pi^*_{x^2-y^2}$ are now in the correct orientation for π-interactions and are shared in π-bonding with the three ligands, **T**, **X** and **Y** in the trigonal plane.[27] If the *trans* ligand is capable of bonding to the π* orbitals and delocalising the electronic charge to lower the energy, the transition state can undergo significant stabilisation as there are more filled π^* orbitals in the transition state than in the ground state.[27] Thus a good *trans* π-acceptor ligand will lower the activation energy for the reaction.

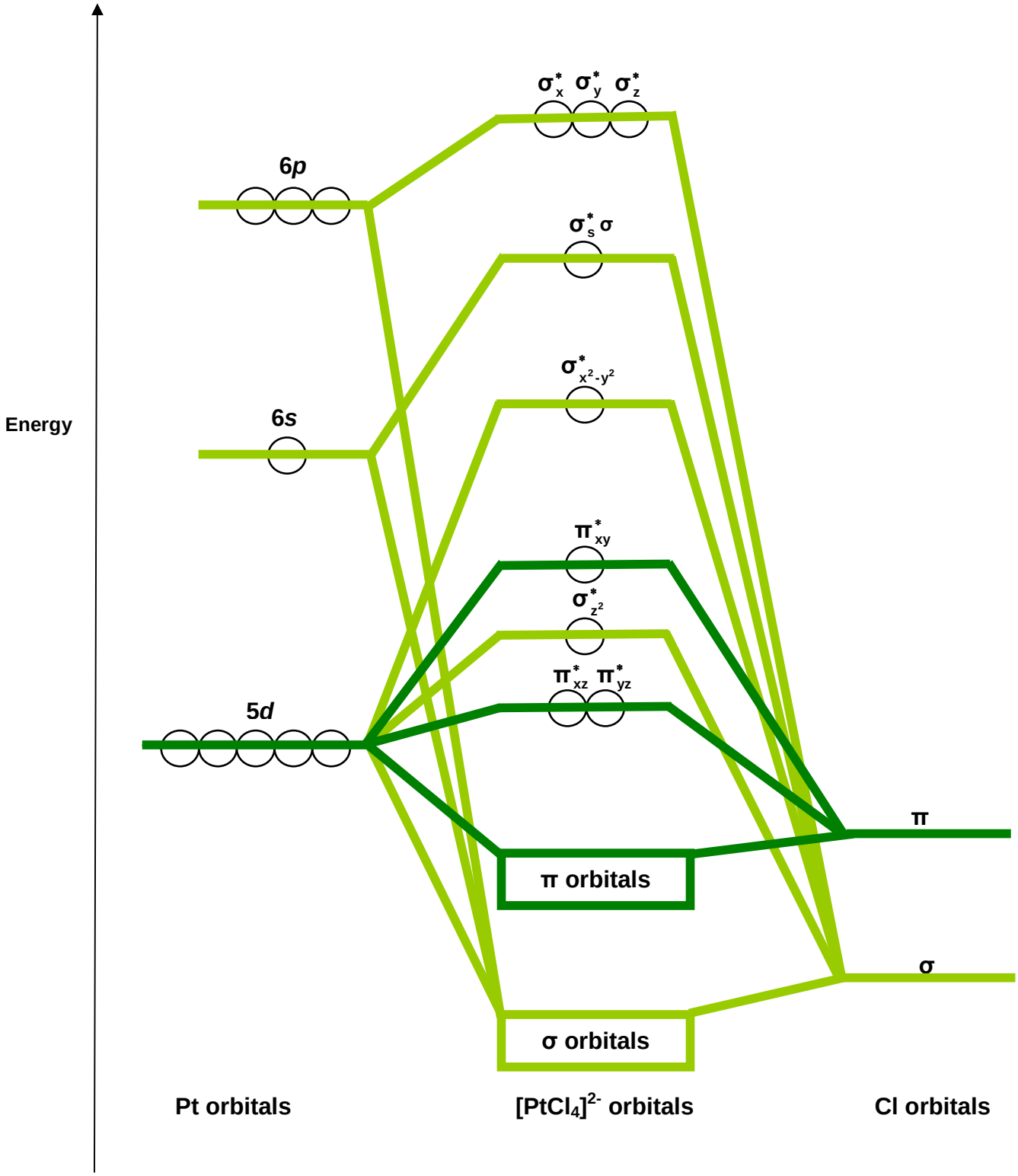

Figure 3.9: Molecular orbital (MO) diagram for $[PtCl_4]^{2-}$.[27,37]

Langford and Gray[5] used σ-bonding to explain the increased stabilisation of the trigonal bipyramidal intermediate.[1,27] In the ground state of a square-planar complex, there is only one p_x-orbital used to bond **T—Pt—X**. Upon addition of the entering group, **X** moves out of the *x*-axis into the trigonal plane.[1,27] This trigonal plane has two *p*-orbitals, (p_x and p_z) increasing the number of orbitals available for bonding. Since the ground state has only one *p*-orbital bonding two ligands whilst the transition state has two orbitals bonding three ligands, increased stability is observed in the transition state, (***Figure 3.10***).[1,27] As a result good σ-bonding ligands which can donate into the extra *p*-orbitals can stabilise the σ structure in the transition state through the *trans* effect.[1,5,27]

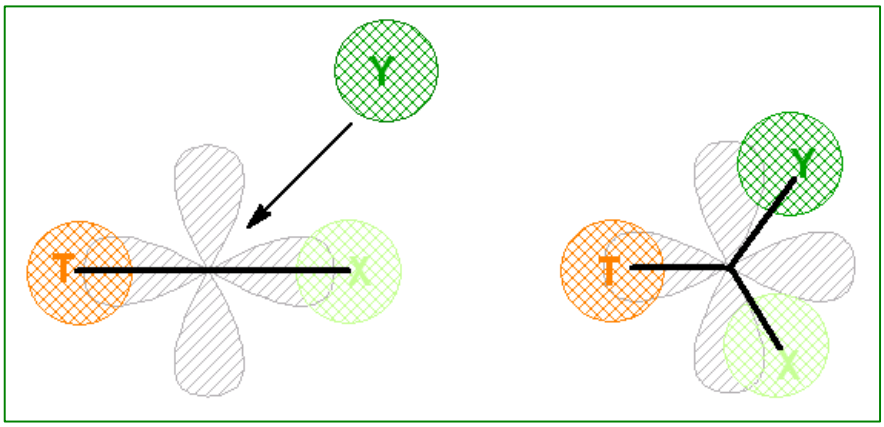

Figure 3.10: The Langford and Gray model for the *trans* effect.[1]

σ-bonding can also affect the ground state stability of a complex.[15] As previously discussed, the *trans* ligand and the leaving group share the same p_x orbital in the ground state, (***Figure 3.11***). A strong σ-donor *trans* ligand, such as CH_3^- or H^- would donate more electron density to the shared *p*-orbital, strengthening the **T—Pt** bond and weakening the **Pt—X** bond which would increase the rate of the reaction.[27]

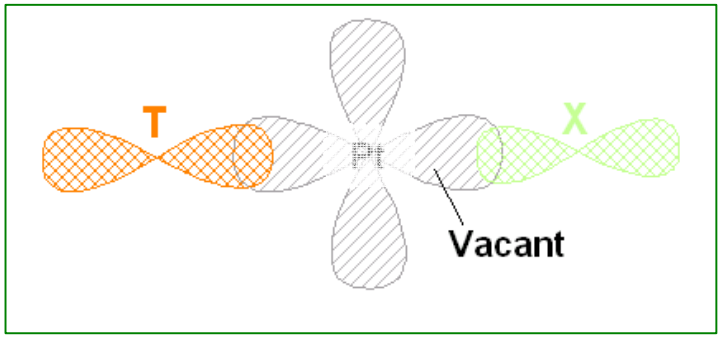

Figure 3.11: Diagram illustrating donation of electrons into the empty *p*-orbital of the metal by the *trans* and leaving groups of the square planar metal complex.[27]

3.5.3 Nature of the Cis Ligand

Although data on the *cis* effect is limited and often contradictory it is generally believed that the *cis* effect is much weaker than the *trans* effect.[39-41] *Cis* effects become pertinent when steric factors are involved as steric hindrance will exert a much bigger influence from the *cis* position when compared with the *trans* position.[1] This becomes more pronounced in the trigonal bipyramidal transition state as the *trans* group is in the equatorial plane with an angle of 120° between it and the incoming and leaving groups while the axial *cis* ligands are separated from the incoming and leaving groups by only 90°.[7] The increase of steric size often causes a decrease in the rate of substitution for an associative reaction.[1]

van Eldik and co-workers[42] studied the reaction kinetics of the complexes (***Figure 3.12***) [Pt(6-phenyl-2,2'-bipy)Cl] (**NCN**), [Pt(1,3-di(2-pyridyl)benzene)Cl] (**NCN**) and [Pt(terpy)Cl] (**NNN**) with **TU**, **DMTU** and **TMTU**. Alternating the position of the Pt—C bond indicated that in the *trans* position the complex reacted much faster than the standard terpyridine complex and much faster than its *cis* counterpart. This suggests that the Pt—C bond in the *cis* position activates the metal centre in a different way from that in the *trans* position. Jaganyi *et al.*[43] obtained similar results

Figure 3.12: Schematic structures of complexes studied by van Eldik *et al*. and the rate constants ($M^{-1}s^{-1}$) obtained with Thiourea in Methanol at 25 °C and 0.1 M ($LiSO_3CF_3$) ionic strength.[42]

3.5.4 Nature of the Leaving Group

The effect of the leaving group is very closely connected with the nature of the incoming nucleophile and the *trans* ligand thus it is difficult to quantify.[2] During a dissociative reaction the bond between the leaving group and the metal breaks in the transition state and thus these reactions depend heavily on the nature of the leaving group.[3,7] For an associative reaction, the effect of the leaving group is dependent on the degree to which bond breaking occurs in the transition state.[2,6] The following reaction has been studied in great detail in an attempt to ascertain the effect of the leaving group, **X**, on the rate of substitution:[10,44]

$$\mathbf{[Pt(dien)X]^{+} + Py \longrightarrow [Pt(dien)Py]^{2+} + X^{-}}$$

For entry of a particular nucleophile, the rate constant for the displacement of **X** decreases as shown in ***Table 3.3***):

$$NO_3^- > H_2O > Cl^- > Br^- > I^- > N^{3-} > SCN^- > NO_2^- > CN^- \qquad \textbf{...3.11}$$

Table 3.3: The effect of the leaving group, **X**, on the rate of substitution of $[Pt(dien)\mathbf{X}]^{+}$ with pyridine (py).[3,7,10,44]

X	$\boldsymbol{k_{obs}}$ **(s^{-1})**
NO_3^-	very fast
H_2O	1900
Cl^-	35
Br^-	23
I^-	10
N^{3-}	0.8
SCN^-	0.3
NO_2^-	0.05
CN^-	0.02

Leaving groups having a low nucleophilicity are considered easier to substitute than those having a high nucleophilicity. One such example is to compare CN^- and Cl^- as entering and leaving groups. The substitution of Cl^- by CN^- as the leaving group results in the reduction of the reaction rate by a factor of approximately 2000,[10] but when CN^- acts as the entering group, it is 10^4 times better than Cl^-.[16] Thus it is evident that metal-ligand bond-breakage is also significant for the reactivity of the complex even though the reaction rate is more sensitive to the nature of the entering group, as is expected for an associative reaction mechanism.

3.5.5 Nature of the Metal Centre

The nature of the reaction centre affects the rate of substitution of square planar complexes, thus to guarantee that effects are due only to a change in metal centre, only the isovalent ion reactivity's can be compared.[3] As a result, the only d^8 isovalent ions that can be compared are Ni(II), Pd(II), Pt(II) and Co(I), Rh(I) and Ir(I). The general trend that has been determined is Ni > Pd > Pt in the ratio $10^7-10^8:10^5-10^6:1$.[3,45] Although Tobe[3] has predicted that the smaller the effective nuclear charge on the metal, the greater the relative stability of the five-coordinate intermediate (Ir(I) > Pt(II) > Au(III)), no other adequate comparisons have been made.[3]

3.6 The Dissociative Mechanism for Square-Planar Platinum(II) Complexes

Substitution reactions of square-planar platinum(II) complexes rarely follow a dissociative reaction pathway, instead favouring the more common associative route. However, in spite of this, the dissociative pathway may be encouraged by promoting bond weakening, stabilising the intermediate of a lower coordination number or by preventing bond formation. This may be achieved using electronic or steric effects. Although weakly electronegative ligands can cause the *trans* metal-ligand bond to weaken by forming very strong bonds to the metal, there is no evidence that this causes a change in mechanism.[3]

A great deal of effort has gone into investigating the use of steric hindrance to discredit the associative mechanism. If sterically bulky ligands were chosen in the ground state, then the associative mechanism would be hindered, as the transition state for an associative reaction is more crowded than the ground state.[1,3] The reverse is true for the dissociative mechanism, as the transition state is less crowded than the ground state; thus the choice of bulky ligands in the ground state should speed up the reaction to relieve the steric strain.[1,3] There has been some success when using *N*-ethyl substituted diethylenetriamine[3] as the ethyl groups hinder the metal making an associative mechanism difficult to follow.[3] The steric hindrance is believed to be the reason why the reaction follows the less favourable dissociative mechanism.[3] A complete mechanistic changeover does not occur as five-coordinate complexes of Co(II) and Ni(II) with Et_4dien ($NH[CH_2CH_2N\text{-}(C_2H_5)_2]_2$) have previously been described.[3]

Romeo *et al.*[13,46] showed that in the case of the complexes of the type *cis*-$[Pt(L)_2R_2]$ (L = Me, Ph; R = thioethers or DMSO), the fourteen-electron intermediate common to a dissociative substitution mechanism is stabilised by the two strong σ-donor carbon groups. By replacing one of the thioethers with a good π-acceptor, the mechanism reverts to an associative pathway by removing electron density away from the metal centre and favouring formation of a five-coordinate eighteen-valence electron intermediate, which is typical for an associative mode of activation.

From comparative studies of the substitution reactions of the complexes *cis*-$[Pt(Ph)_2(SMe_2)_2]$ and $[Pt(2,2'\text{-biphenyl})(SMe_2)_2]$, the latter reacts approximately 100 times faster and follows a dissociative reaction pathway despite its presumed π-acceptor ability. It was concluded that in-plane disposition of simple aryl ligands does not result in increased electrophilicity of the platinum centre through π back-bonding.[47]

Another consequence of a mechanistic changeover for the substitution reactions of square-planar complexes is the stereochemistry of the products formed. The dissociation of a ligand from a square-planar complex gives rise to a three-coordinate, T-shaped intermediate (***Figure 3.13***). Intramolecular rearrangements of the "*cis*-like" T-shaped intermediate into the "*trans*-like" T-shaped intermediate and subsequent capture by a nucleophile can result in non-stereospecific reactions, unlike the associative pathway, which proceeds with a retention of stereochemistry.[1]

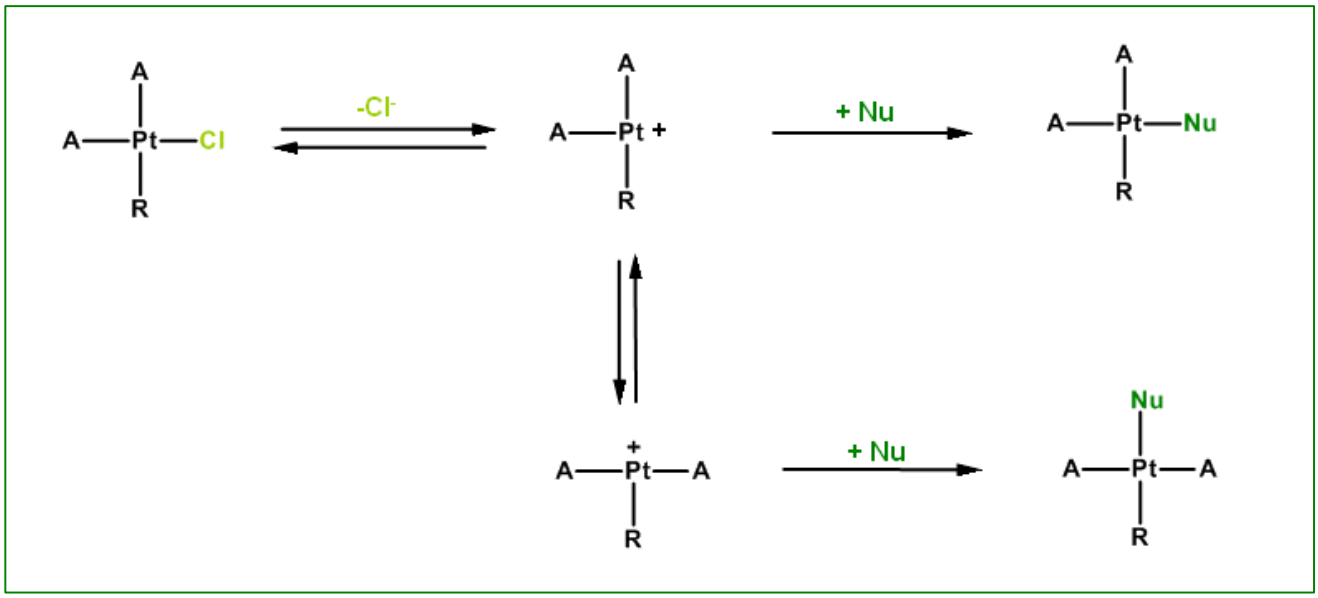

A = Inert ligand

Figure 3.13: Diagrammatic representation of the non-stereo specificity resulting in *intra*molecular rearrangements during the substitution reaction of a typical square-planar platinum(II) complex following a dissociative pathway.[15]

3.7 References

1. M. L. Tobe and J. Burgess, *Inorganic Reaction Mechanisms*, Addison Wesley Longman, Ltd., Essex, **1999**, pp. 30–43, 70–112.
2. R. G. Wilkins, *Kinetics and Mechanism of Reactions of Transition Metal Complexes* 2nd Ed., VCH, Weinheim, **1991**, pp. 199–201, 221, 232–242.
3. M. L. Tobe, Substitution Reactions in *Comprehensive Coordination Chemistry*, G. Wilkinson (Ed.), Pergamon Press, Oxford, **1987**, *1*, pp. 281–329.
4. C. K. Ingold and E. D. Hughes, *Structure and Mechanism in Organic Chemistry* 2nd Ed., Cornell University Press, Ithaca, New York, **1969**, pp. 241–243.
5. C. H. Langford and H. B. Gray, *Ligand Substitution Processes*, Benjamin, New York, **1965** pp. 7, 19.
6. S. Ašperger, *Chemical Kinetics and Inorganic Reaction Mechanisms* 2nd Ed., Kluwer Academic / Plenum Publishers, New York, **2003**, pp. 105–106, 108–110, 140–153.
7. J. D. Atwood, *Inorganic and Organometallic Reaction Mechanisms* 2nd Ed, Wiley–VCH, Inc., Canada, **1997**, pp. 43–62
8. R. B. Jordan, *Reaction Mechanisms of Inorganic and Organometallic Systems*, Oxford University Press Inc., New York, **1991**, pp. 29–74.
9. F. Basolo, *Coord. Chem. Rev*., **1996**, 151–161.
10. F. Basolo, H. B. Gray, R.G. Pearson, *J. Chem. Soc., Dalton Trans*., 1**960**, 4200–4203.
11. B. V. Petrović, M. I. Djuran, Z. D. Bugarčić, *Metal–Based Drugs*, **1999**, *6*, 355–360.
12. S. D. Cummings, *Coord. Chem. Rev*., **2009**, *253*, 449–478.
13. R. Romeo, *Comments Inorg. Chem*., **1990**, *11*, 21–57.
14. G. Faraone, V. Ricevuto, R. Romeo, M. Trozzi, *J. Chem. Soc*., **1971**, 18771–881.
15. R. A. Henderson, *The Mechanisms of Reactions at Transition Metal Sites*, Oxford University Press, Oxford, **1993**, pp. 2–21.
16. U. Belluco, L. Cattalini, F. Basolo, R. G. Pearson and A. Turco, *J. Am. Chem. Soc*., **1965**, *87*, 241–246.
17. P. Haake, S. C. Chan and V. Jones, *Inorg. Chem.*, **1970**, *9*, 19251–926.
18. J. K. Beattie, *Inorg. Chim. Acta*, **1983**, *76*, L69.

19. A. Peloso, *Coord. Chem. Rev.*, **1973**, *10*, 123–181.
20. D. K. Lin and C. S. Garner, *J. Am. Chem. Soc.*, **1969**, *91*, 6637–6643.
21. F. A. Cotton, G. Wilkinson and P. L. Gaus, *Basic Inorganic Chemistry* 3rd Ed, John Wiley & Sons, New York, **1995**, pp. 228–229.
22. R. G. Pearson, *J. Am. Chem. Soc.*, **1963**, *85*, 3533–3539.
23. R. G. Pearson, *J. Chem. Edu.*, **1968**, *45*, 643–648.
24. R. G. Pearson, *J. Chem. Edu.*, **1987**, *64*, 561–567.
25. U. Belluco, *Coord. Chem. Rev.*, **1966**, *1*, 111–117.
26. H. Krüger, and R. J. van Eldik, *Chem. Soc. Chem. Commun.*, **1990**, 330–331.
27. F. Basolo, J. Chatt, H. B. Gray, R. G. Pearson and B. L. Shaw, *J. Chem. Soc.*, **1961**, *419* 2207–2215.
28. F. A. Cotton, L. M. Daniels, C. A. Murillo and J. F. Quesada, *Inorg. Chem.*, **1993**, *32*, 48614–867.
29. I. I. Chernyaev, *Ann. inst. platine USSR*, **1926**, *4*, 261–285.
30. I. I. Chernyaev, *Ann. inst. platine. USSR*, **1926**, *4*, 243–275.
31. I. I. Chernyaev, *Ann. inst. platine. USSR*, **1927**, *5*, 102–118.
32. I. I. Chernyaev, *Ann. inst. platine. USSR*, **1928**, *6*, 55–97.
33. A. Grinberg, *Acta Physicochim*, **1935**, *3*, 573–582.
34. J. Chatt, L. A. Duncanson and L. M. Venanzi, *J. Chem. Soc.*, **1955**, 4456–4460.
35. L. E. Orgel, *J. Inorg. Nucl. Chem.*, **1956**, *2*, 137–140.
36. J. Chatt, G. A. Gamlen and L. E Orgel, *J. Am. Chem. Soc.*, **1959**, 1047–1049
37. C. W. Schwietert and J. P. McCue, *Coord. Chem. Rev.*, **1999**, *184*, 67–89.
38. R. Romeo, *Comments Inorg. Chem.*, **1990**, *11*, 21–57.
39. D. Jaganyi, A. Hofmann and R. van Eldik, *Angew. Chem., Int. Ed.*, **2001**, *40*, 1680–1683.
40. A. Hofmann, D. Jaganyi, O. Q. Munro, G. Liehr and R. van Eldik, *Inorg. Chem.*, **2003**, *42*, 1688–1700.
41. J. K. Burdett, *Inorg. Chem.*, **1977**, *16*, 3013–3025.
42. A. Hofmann, L. Dahlenburg and R. van Eldik, *Inorg. Chem.*, **2003**, *42*, 6528–6538.
43. D. Jaganyi, D. Reddy, J. A. Gertenbach, A. Hofmann and R. van Eldik, *Dalton Trans.*, **2004**, 299–304.
44. H. G. Gray and R. J. Olcott, *Inorg. Chem.*, **1962**, *1*, 481–485.

45. J. J. Pesek and W. R. Mason, *Inorg. Chem.*, **1983**, *22*, 2958–2959.
46. G. Alibrandi, G. Bruno, S. Lanza, R. Romeo and M. L. Tobe, *Inorg. Chem.*, **1987**, *26*, 185–190.
47. M. R. Plutino, L. M. Scolaro, R. Romeo and A. Grassi, *Inorg. Chem.*, **2000**, *39*, 2712–2720.

CHAPTER IV

Experimental

4.1 Materials and Methods

Reactions used in the synthesis of the novel *bis*-(4'-terpyridyl)-α,ω-alkyldiol ligands and coordination of these to platinum(II) were all carried out under an inert atmosphere of nitrogen using standard Schlenk techniques, unless otherwise stated. 4′-chloro-2,2′:6′,2″-terpyridine (99 %), 1,2-ethanediol (99 %), 1,4-butanediol (99 %), dimethyl sulfoxide (DMSO, 99.8 %), thiourea (TU, 99 %), 1,3-dimethyl-2-thiourea (DMTU, 99 %) and 1,1,3,3-tetramethyl-2-thiourea (TMTU, 98 %), were purchased from Aldrich. Diethyl ether (99 %), acetone (98 %), absolute ethanol (99 %),1,6-hexanediol (≥ 97 %), sodium chloride (NaCl, 99 %) and potassium hydroxide (KOH, 98 %), were purchased from Merck, whilst the potassium tetrachloroplatinate (K_2PtCl_4, 99.9 %) was purchased from Strem. The diols underwent further purification[1] before use. The terpyridinyl ligands were synthesised using a modified version of the method previously described by Van der Schilden[2] and Constable *et al*.[3] whilst coordination was attempted utilising an adapted version of a previously described literature method.[4]

4.2 Physical Measurement and Instrumentation

Elemental analyses were performed at the Institute for Inorganic Chemistry, University of Erlangen-Nürnberg Germany. Infrared spectra were recorded on a Perkin Elmer Diamond-Anvil ATR Spectrometer. Mass spectra were collected using a Waters Micromass LCT Premier TOF Mass Spectrometer. Raman spectra were recorded on a Delta Nu Advantage 532 instrument equipped with a 532 nm laser (Nd:Y:Ag crystal) and a CCD detector. Data were processed with Grams software.

NMR spectra were recorded on either a Bruker Avance III 500 or Bruker Avance III 400 spectrometer at the following frequencies: ^{1}H 500/400, ^{13}C 125/100, ^{195}Pt 107 MHz. ^{1}H and ^{13}C spectra of the ligands were recorded using a 5 mm BBOZ probe; ^{1}H and ^{1}H-detected "inverse" experiments on saturated solutions of the platinum complexes were recorded using a 5 mm TBIZ probe and ^{195}Pt spectra were recorded using a 5 mm BBOZ probe. All experiments were conducted at 30 °C unless otherwise specified. All chemical shifts are reported in units of ppm.

All proton and carbon chemical shifts are quoted relative to the relevant solvent signal (DMSO-d^{6}: ^{1}H, 2.50 ppm, ^{13}C, 39.5 ppm; $CDCl_3$: ^{1}H 7.26 ppm, ^{13}C, 77.0 ppm; CD_3CN: ^{1}H 1.93 ppm, ^{13}C 1.28 ppm). All ^{195}Pt shifts are reported relative to hexachloroplatinic acid (0 ppm). Proton-proton coupling constants are reported in Hertz.

X-ray diffraction data for all three ligands was collected on an Oxford Xcalibur2 CCD 4-circle diffractometer equipped with an Oxford Instruments Cryojet operating at 100(2) K, unless otherwise specified. The data was collected with Mo K_α (= 0.71073Å) radiation at a crystal-to-detector distance of 50 mm using omega scans at θ = 29.389 ° with 20 s exposures taken at 2.00 kW X-ray power with 0.75 frame widths. Data were collected and reduced using CrysAlis CCD and CrysAlis RED Version 1.7.1 respectively. The structures were solved by direct methods, using SHELXS-97[5-6] running under WinGX[7]. A semi empirical multi-scan absorption correction[8] was applied in all cases. All non-hydrogen atoms were refined anistropically. The position of the hydrogen atoms was calculated using the standard riding model of SHELXL-97.

All kinetic measurements were performed under *pseudo* first-order conditions. Trial UV/Visible absorption spectra were used to determine the suitable wavelength at which kinetic investigations could be performed; these were recorded using a Varian Cary 100 Bio spectrophotometer, and subsequently either the Varian Cary 100 Bio spectrophotometer with an online kinetic utility or an Applied Photophysics SX. 20MV stopped-flow system coupled to an online data acquisition system was used to monitor the kinetic process. All measurements were performed in a thermostated environment to within ± 0.1 °C. All data was graphically analysed using the software package Origin 7.5.[9]

4.3 Synthesis and Characterisation of the *Bis*-Terpyridine Ligands

4.3.1 Synthetic Route

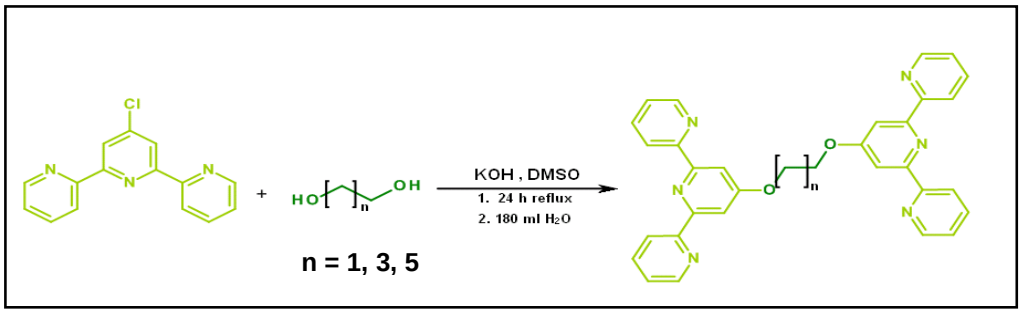

The corresponding α,ω-alkyldiol (102 mg, 1.13 mmol) was added to a suspension of potassium hydroxide (162 mg, 6.69 mmol) in DMSO (30 ml). The suspension was refluxed for 1 h after which 4′-chloro-2,2′:6′,2″-terpyridine (600 mg, 2.23 mmol) was added and the mixture was further refluxed for 24 hours. After cooling to room temperature, the brown mixture was poured onto ice cold water (180 ml). The resulting off-white precipitate was then filtered, and air dried.

4.3.2 Characterisation of bis-(4'-terpyridyl)-α,ω-alkyldiol Ligands

bis[4′-(2,2′:6′,2″-terpyridyl)]-*1,2-ethanediol* (**L1**)

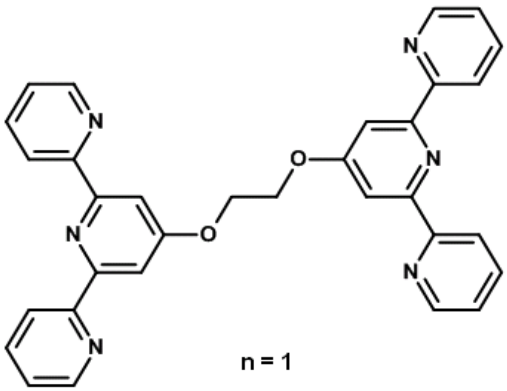

Yield : 54.7 mg, (78 %)

Elemental Anal. **Calcd. for $C_{32}H_{24}N_6O_2$**: C, 73.3 %; H, 4.61 %; N, 16.0 %.
Found: C, 72.9 %; H, 4.61 %; N, 16.1 %

IR (cm^{-1}) : 661.01(w), 699.19(w), 734.38(w), 742.25(m), 786.41(vs), 868.50(s), 884.40(w), 914.66(w), 987.67(w), 1038.30(m), 1088.47(w), 1201.76(s), 1251.94(w), 1328.81(m), 1370.30(w), 1407.54(m), 1441.83(w), 1467.68(w), 1561.96(vs), 1578.06(w), 2180.48(b), 2895.10(w), 2965.03(w), 3010.48(w), 3052.44(w)

HRMS : **Calcd. for $C_{32}H_{24}N_6O_2$**: 524.5719 g/mol

Found: 547.1858 g/mol [M + Na]

NMR (^1H) : 4.70 ppm (4 H); s; C_qOCH_2, 7.34 ppm, (4 H); m; NCHCH, 7.87 ppm (4 H); t; *J* = 7.1 Hz; NC_qCHCH, 8.14 ppm (4 H); s; NC_qCHC_qO, 8.63 ppm (4 H); d; *J* = 7.9 Hz; NC_qCHCH, 8.71 ppm (4 H); d; *J* = 4.1 Hz; NCH.

NMR (^{13}C) : 66.7 (2 C); t; C_qOCH_2, 107.9 (4 C); d; NC_qCHC_qO, 121.7 (4 C); d; NC_qCHCH, 124.0 (4 C); d; NCHCH, 137.3 (4 C); d; NC_qCHCH, 148.7 (4 C); d; NCH, 155.4 (4 C); s; NC_qCHCH, 156.8 (4 C); s; NC_qCHCqO, 167.0 (2 C); s; C_qO.

bis[4′-(2,2′:6′,2″-terpyridyl)]-*1,4-butanediol* (**L2**)

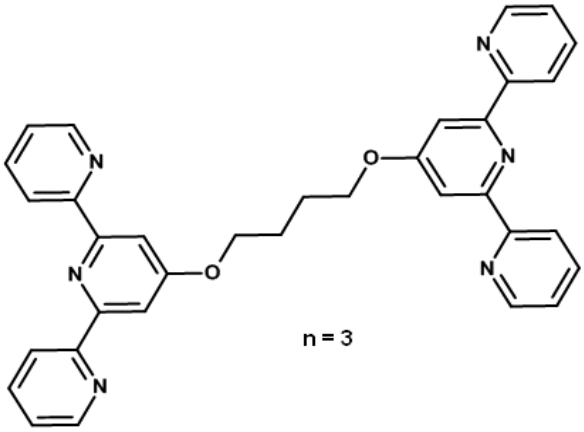

Yield: 72.3 mg, (71 %).

Elemental Anal.

Calcd for $C_{34}H_{28}N_6O_2$: C, 73.9 %; H, 5.11 %; N, 15.2 %.

Found: C, 73.5 %; H, 5.19 %; N, 15.1 %

IR (cm^{-1}) : 658.73(w), 702.61(m), 742.61(s), 789.66(vs), 863.76(w), 878.78(sh), 927.68(m), 1017.70(s), 1058.93(m), 1086.61(w), 1355.94(s), 1406.14(m), 1443.40(m), 1469.08(s), 1562.68(s), 1580.85(m), 2863.63(w), 2958.04(w).

HRMS : **Calcd for $C_{34}H_{28}N_6O_2$**: 552.2274 g/mol
Found: 575.2110 g/mol [M + Na].

NMR (^1H) : 2.05 ppm (4 H); brs; $C_qOCH_2CH_2$, 4.38 ppm (4 H); brs; C_qOCH_2, 7.48 ppm (4H), ddd; *J* = 7.5; 4.8; 0.9 Hz; NCHCH, 7.98 ppm (4 H); s; NC_qCHC_qO, 7.99 ppm (4 H); dt; *J* = 7.6; 1.7 Hz; NC_qCHCH, 8.59 ppm (4 H); d; *J* = 8.0 Hz; NC_qCHCH, 8.69 ppm (4 H); d; *J* = 4.8 Hz NCH.

NMR (^{13}C) : 25.1 (2 C); t; $C_qOCH_2CH_2$, 67.7 (2 C); t; C_qOCH_2, 107.0 (4 C); d; NC_qCHCqO, 121.0 (4 C); d; NC_qCHCH, 124.5 (4 C); d; NCHCH, 137.4 (4 C); d; NC_qCHCH, 149.2 (4 C); d; NCH, 155.0 (4 C); s; NC_qCHCH, 156.8 (4 C); s; NC_qCHCqO, 166.8 (2 C); s; C_qO.

bis[4′-(2,2′:6′,2″-terpyridyl)]-*1,6-hexanediol* (**L3**)

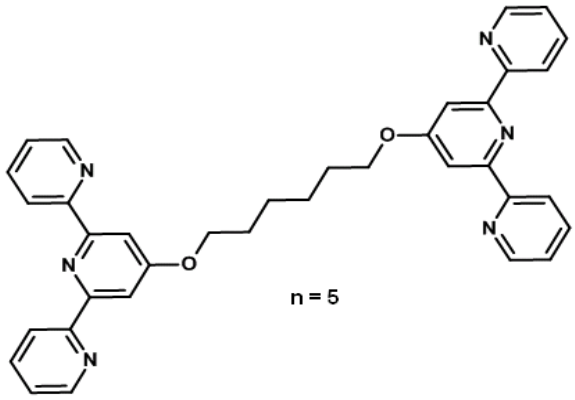

Yield: 88.1 mg, (66 %).

Elemental Anal.

Calcd. for $C_{36}H_{32}N_6O_2$: C, 74.5 %; H, 5.56 %; N, 14.5 %

Found: C, 74.1 %; H, 5.70 %; N, 14.3 %

IR (cm^{-1}) : 657.82(w), 698.04(m), 733.20(w), 752.81(sh), 790.51(s), 863.01(w), 884.57(w), 924.11(m), 1016.99(vs), 1092.00(m), 1126.16(sh), 1142.90(w), 1254.10(w), 1363.17(s), 1404.51(s), 1442.17(m), 1470.45(m), 1560.96(s), 1579.25(sh), 2941.32(m), 3436.72(b).

HRMS : **Calcd. for $C_{36}H_{32}N_6O_2$**: 580.2587 g/mol

Found: 603.2284 g/mol [M + Na].

NMR(^1H) : 1.62 ppm (4 H); m; $C_qOCH_2CH_2CH_2$, 1.92 ppm (4 H); m; $C_qOCH_2CH_2CH_2$, 4.26 ppm (4 H); t; *J* = 6.4 Hz; $C_qOCH_2CH_2CH_2$, 7.31 ppm (4 H); ddd; *J* = 7.6; 4.8; 1.0 Hz; NCHCH, 7.84 ppm (4H); dt; *J* = 7.7; 1.6 Hz; NC_qCHCH, 8.02 ppm (4 H); s; NC_qCHC_qO, 8.61 ppm (4 H); d; *J* = 7.9 Hz; NC_qCHCH, 8.68 ppm (4 H) d *J* = 4.3 Hz NCH.

NMR(^{13}C) : 25.8 (2 C); t; $C_qOCH_2CH_2CH_2$, 29.0 (2 C); t; $C_qOCH_2CH_2CH_2$, 68.1 (2 C); t; $C_qOCH_2CH_2CH_2$, 107.5 (4 C); d; NC_qCHC_qO, 121.3 (4 C); d; NC_qCHCH, 123.7 (4 C); d; NCHCH, 136.7 (4 C); d; C_qCHCH, 149.0 (4 C); d; NCH, 156.3 (4 C); s; NC_qCHCH, 157.1 (4 C); s; NC_qCHC_qO, 167.3 (2 C); s; C_qO.

4.3.3 Crystal Growth and Characterisation

Single crystals suitable for X-ray diffraction were grown by slow liquid diffusion of hexane into a chloroform solution of the respective *bis*-terpyridine ligands.

Table 4.1: Crystal data and structural refinement details for *bis*[4′-(2,2′:6′,2″-terpyridyl)]-1,4-butanediol, *bis*[4′-(2,2′:6′,2″-terpyridyl)]-1,2-ethanediol and *bis*[4′-(2,2′:6′,2″-terpyridyl)]- 1,6-hexanediol

Chemical Formula	$C_{32}H_{24}N_6O_2$	$C_{34}H_{28}N_6O_2$	$C_{36}H_{32}N_6O_2$
M_r (g mol^{-1})	524.57	552.62	580.67
Space Group	P-1	P-1	P b c a
Temperature (K)	296(2)	100(2)	100(2)
***a* (Å)**	6.312(4)	6.368(2)	15.139(5)
***b* (Å)**	10.260(2)	10.509(4)	11.428(5)
***c* (Å)**	10.320(2)	10.922(3)	16.760(5)
α (º)	94.050(3)	72.580(3)	90.000
β (º)	98.960(3)	78.561(3)	90.000
γ (º)	102.340(3)	77.438(3)	90.000
V (Å^3)	641.17(2)	673.64	2899.6(18)
Z	1	1	8
Radiation type	Mo*K*α	Mo*K*α	Mo*K*α
μ (mm^{-1})	0.088	0.088	0.085
Crystal size (mm)	0.16 x 0.09 x 0.06	0.4 x 0.4 x 0.3	0.4 x 0.2 x 0.2
R_{int}	6.31	5.27	3.96

4.4 Synthesis of *Bis*-Terpyridine Platinum(II) Complexes

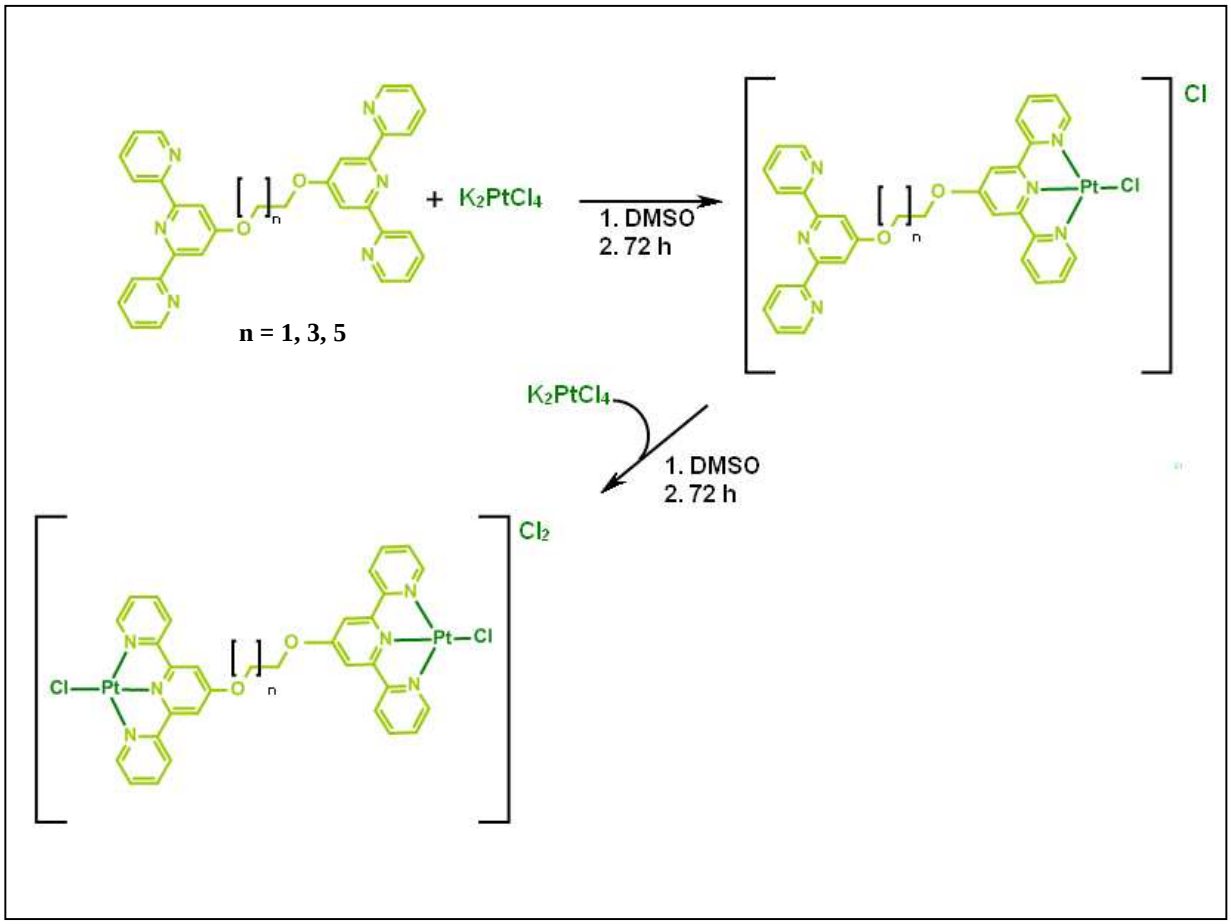

K_2PtCl_4 (36.3 mg, 0.0875 mmol) was added to DMSO (15 cm^3) at 50 °C. To this, a solution of the corresponding *bis*-(4'-terpyridyl)-α,ω-alkyldiol ligand (50.8 mg, 0.0875 mmol) in DMSO (30 cm^3) was added dropwise, and the resulting mixture was stirred for 72 h. A second equivalent of ligand (50.8 mg, 0.0875 mmol) was then added and the solution was stirred for a further 72 h. The orange solution was cooled and added dropwise to acetone (100 cm^3) upon which a super fine orange solid precipitated. The product was isolated by filtration, repeatedly washed with cold water and air dried.

4",4"'-[ethane-1,2-diyl*bis*(oxy)]-2',2":6",2"'-terpyridine-platinum(II)chloride **(L1-Pt)**

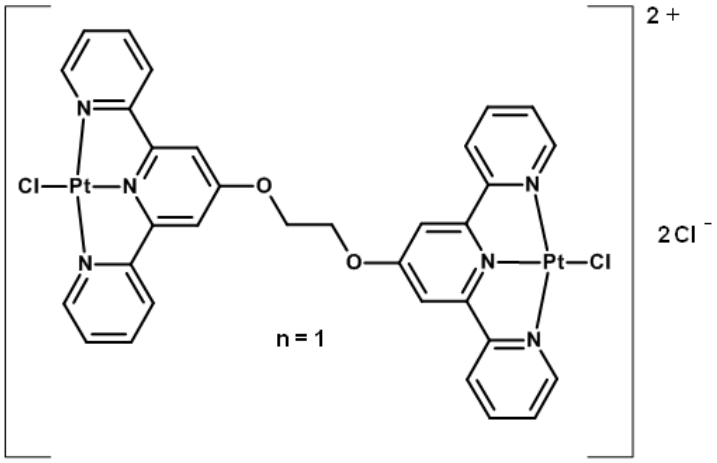

Yield: 28.5 mg, (62 %)

IR cm^{-1} : 732.08(w), 747.97(m), 840.36(w), 906.72(w), 936.41(w), 978.64(w), 1037.41(m), 1101.99(m), 1166.94(w), 1252.52(w), 1290.94(w), 1318.98(m), 1378.26(w), 1455.74(w), 1544.16(s), 1652.02(vs), 3202.49(w).

HRMS : **Calcd. for $C_{32}H_{24}N_6O_2Pt_2Cl_4$**: 985.0622 g/mol
Found: 492.5307 g/mol (M / z)

NMR(^{1}H) : 4.98 ppm (4 H); s; C_qOCH_2, 7.98 ppm (4 H); m; NCHCH, 8.45 ppm (4 H); s; NC_qCHC_qO, 8.52 ppm (4 H); dt; *J* = 7.9, 1.4 Hz; NC_qCHCH, 8.67 ppm (4 H); d; *J* = 7.8 Hz; NC_qCHCH, 8.97 ppm (4 H); dd; *J* = 5.8, 1.1 Hz; NCH.

NMR (HSQC) : 68.8 (2 C); t; C_qOCH_2, 111.5 (4 C); d; NC_qCHC_qO, 126.0 (4 C); d; NC_qCHCH, 129.7 (4 C); d; NCHCH, 142.9 (4 C); d; C_qCHCH, 151.8 (4 C) d; NCH.

NMR (HMBC) : 157.0 (4 C); s; NC_qCHCH, 158.6 (4 C); s; NC_qCHC_qO, 169.2 (2 C); s; C_qO.

4",4"'-[butane-1,4-diyl*bis*(oxy)]-2',2":6",2"'-terpyridine-platinum(II)chloride **(L2-Pt)**

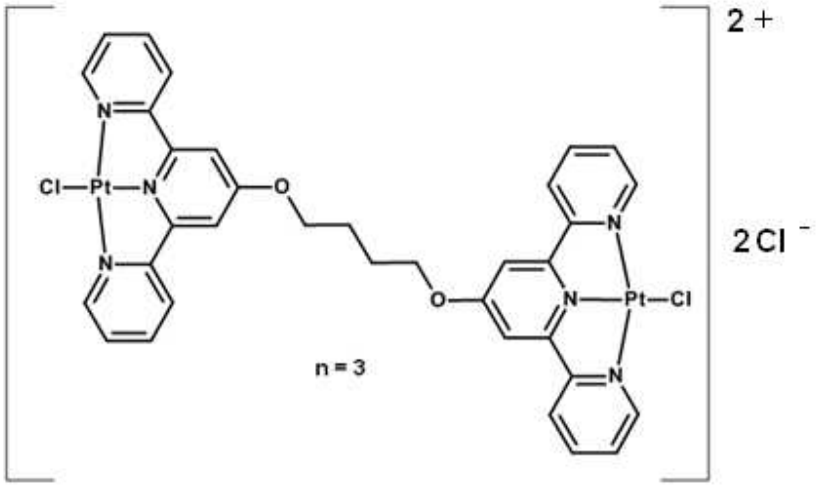

Yield : 24.7 mg, (51 %)

IR cm^{-1} : 746.05(m), 780.52(s), 1028.52(m), 1098.83(w), 1203.62(m), 1220.92(s), 1310.15(w), 1359.65(s), 1402.46(m), 1430.99(m), 1477.81(w), 1561.45(s), 1582.60(w), 1608.05(s), 3006.99(w), 3413.97(bw).

HRMS : **Calcd. For** $C_{34}H_{28}N_6O_2Pt_2Cl_4$: 1013.0936 g/mol
Found: 506.5416 g/mol (M / z)

NMR(^{1}H) : 2.17 ppm (4 H); bs; $C_qOCH_2CH_2$, 4.62 ppm (4 H); bs; $C_qOCH_2CH_2$, 7.92 ppm (4 H); t; J = 6.65 Hz; NCHCH, 8.16 ppm (4 H); s; NC_qCHC_qO, 8.28 ppm (4 H); t; J = 7.87 Hz; NC_qCHCH, 8.41 ppm (4 H); d; J = 7.8 Hz; NC_qCHCH, 8.78 ppm (4 H); d; J = 4.5 Hz; NCH.

NMR (HSQC) : 23.9 (2 C); t; $C_qOCH_2CH_2$, 70.7 (2 C); t; 111.4 (4 C); d; NC_qCHC_qO,126.2 (4 C); d; NC_qCHCH, 130.0 (4 C); d; NCHCH, 142.6 (4 C); d; NC_qCHCH, 152.1 (4 C); d; NCH.

NMR (HMBC) : 157.4 (4 C); s; NC_qCHCH, 158.0 (4 C); s; NC_qCHC_qO, 168.7 (2 C); s; C_qO.

4",4"'-[hexane-1,6-diyl*bis*(oxy)]-2',2":6",2"'-terpyridine-platinum(II)chloride **(L3-Pt)**

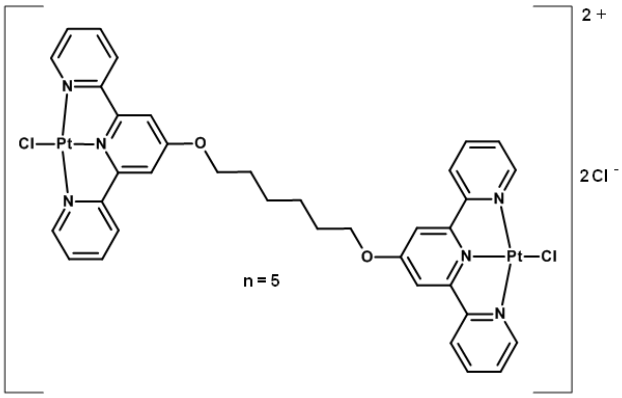

Yield : 28.5 mg, (56 %)

IR cm^{-1} : 713.95(vw), 753.85(w), 773.23(m), 824.84(w), 882.74(w), 1015.07(b), 1112.14(w), 1165.15(W), 1209.95(vs), 1311.94(w), 1351.10(m), 1428.56(s), 1464.60(vw), 1479.60(vw), 1556.83(w), 1605.40(vs), 2972.52(m), 3372.17(b).

HRMS : **Calcd. For $C_{36}H_{32}N_6O_2Pt_2Cl_4$:** 1041.1248 g/mol
Found: 520.5615 g/mol (M / z).

NMR(^{1}H) : 1.66 ppm (4 H); bs; $CqOCH_2CH_2CH_2$, 1.92 ppm (4 H); bs; CqOCH2CH2CH2, 4.42 ppm (4H); t; *J* = 5.7 Hz; $C_qOCH_2CH_2CH_2$, 7.83 ppm (4 H); t; *J* = 6.7 Hz; NCHCH, 8.17 ppm (4 H); s; NC_qCHC_qO, 8.24 ppm (4 H); dt; J = 7.9, 1.5 Hz; NC_qCHCH, 8.42 ppm (4 H); dd; J = 0.73, 8.0 Hz; NC_qCHCH, 8.73 ppm (4 H); d; J = 4.7 Hz; NCH.

NMR (HSQC) : 22.3 (2 C); t; $C_qOCH_2CH_2CH2$, 27.5 (2 C); t; $C_qOCH_2CH_2CH_2$, 69.5 (2 C); t; $C_qOCH_2CH_2CH_2$, 111.1 (4 C); d; NC_qCHC_qO, 125.8 (4 C); d; NC_qCHCH, 129.6 (4 C); d; NCHCH, 142.5 (4 C); d; NC_qCHCH, 151.9 (4 C); d; NCH.

NMR (HMBC) : 158.0 (4 C); s; NC_qCHCH, 169.3 (4 C); s; NC_qCHC_qO, 172.2 (2 C); s; C_qO.

4.5 Preparation of Complex and Nucleophile Solutions for Kinetic Analysis

A known amount of the chloro complex was made up to the required concentration in a volumetric flask using an aqueous solution of NaCl with a constant ionic strength of 0.01 M. The solvent system was chosen to prevent solvolysis of the complexes.

Solutions of the neutral nucleophiles, *viz.* **TU**, **DMTU** and **TMTU**, were prepared by dissolving a known amount of the required nucleophile in 250 ml of a solution possessing a fixed ionic strength (0.01 M NaCl) to afford a final concentration that was *ca.* 150 times greater than that of the experimental complex. Subsequently dilutions with the same solution of fixed ionic strength afforded a series of concentrations, in the order 50, 75, 100, 125 and 150 times the concentration of the metal complex. These concentrations were chosen so as to maintain *pseudo* first-order conditions.

4.6 References

1. W. F. Armarego and D. D. Perrin. *Purification of Laboratory Chemicals* 4th Ed. Butterworth Heinemann, Oxford, **1996** pp.5–7.
2. K. van der Schilden, *PhD Thesis: Design and Development of Polynuclear Ruthenium and Platinum Polypyridyl Complexes in Search of New Anticancer Agents*, Leiden University, Netherlands, **2006**.
3. E. C. Constable, C. E. Housecroft, M. Neuburger, S. Schaffner and C. B. Smith, *Dalton Trans*., **2005**, 2259–2267.
4. K. Suntharalingam, A. J. P. White and R. Vilar., *Inorg, Chem*., **2009**, *48*, 9427–9435.
5. G. M. Sheldrick, SHELXL–97, Program for refinement of crystal structures, University of Göttingen, Germany, **1997**.
6. G. M. Sheldrick, SHELXS–97, Program for refinement of crystal structures, University of Göttingen, Germany, **1997**.
7. J. Farrugia, WinGX v1.70.01, *J. Appl. Cryst.* **1999**, *32*, 837838.
8. R. Blessing, *Acta Cryst.*, **1995**, A51, 3338.
9. *Microcal*™ *Origin*™ *Version 7.5*, Microcal Software, Inc., One Roundhouse Plaza, Northampton, MA, 01060, USA, 19911997.

CHAPTER V

Results and Discussion

5.1 Ligand Synthesis and Characterisation

The ligand synthesis was performed using a modification of the methods described by van der Schilden[1] and Constable *et al.*[2] All reactions were maintained under an inert atmosphere of nitrogen using dried glassware and reagents and employing cannula techniques where necessary. The homoditopic ligands **L1**$^{\alpha}$, **L2**$^{\beta}$ and **L3**$^{\gamma}$ were readily prepared using standard methodology by reacting the appropriate nucleophilic diol with an excess of electrophilic 4′-chloro-2,2′:6′,2″-terpyridine in DMSO in the presence of KOH (***Figure 5.1***). All the ligands were obtained in good yields as off-white powders.

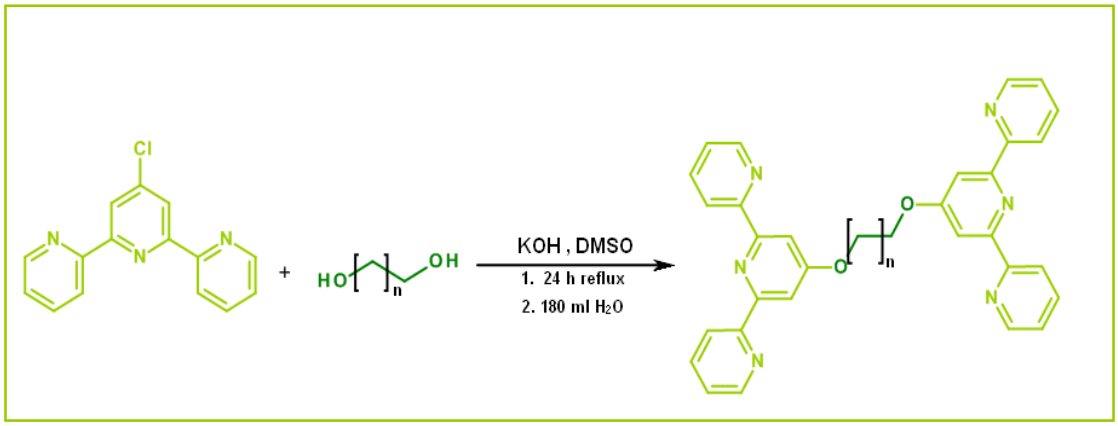

Figure 5.1: Illustration of ligand synthesis.

Due to the novel nature of these *bis*-terpyridine ligands (**L1**, **L2** and **L3**) a complete characterisation was performed using a range of spectroscopic (NMR, IR and UV-Visible) and spectrometric (HRMS, elemental analysis and X-ray) techniques. All ligand structures were verified by a series of NMR experiments including: ^{1}H, ^{13}C, DEPT, COSY, NOESY, HMBC and HSQC where applicable (*see Appendix 1*).

$^{\alpha}$ *bis*[4′-(2,2′:6′,2″-terpyridinyl)]-*1,2-ethanediol*
$^{\beta}$ *bis*[4′-(2,2′:6′,2″-terpyridinyl)]-*1,4-butanediol*
$^{\gamma}$ *bis*[4′-(2,2′:6′,2″-terpyridinyl)]-*1,6-hexanediol*

Upon comparison of the proton spectrum of ligand **L1** (see *Appendix 1*) and the terpyridine starting material (see *Appendix 1*), the presence of both the 2,2′:6′,2″-terpyridine fragment as well as a single extra peak representing the newly bound diol chain was observed. Due to the symmetrical nature of these novel ligands only half of the structure is observed. The HMBC spectrum (***Figure 5.2***) verifies the attachment of the hydrocarbon chain to the terpyridine ring by confirming the existence of a correlation between the proton of the CH_2 of the hydrocarbon at 4.7 ppm and the quaternary carbon of the central pyridine ring at 167 ppm.

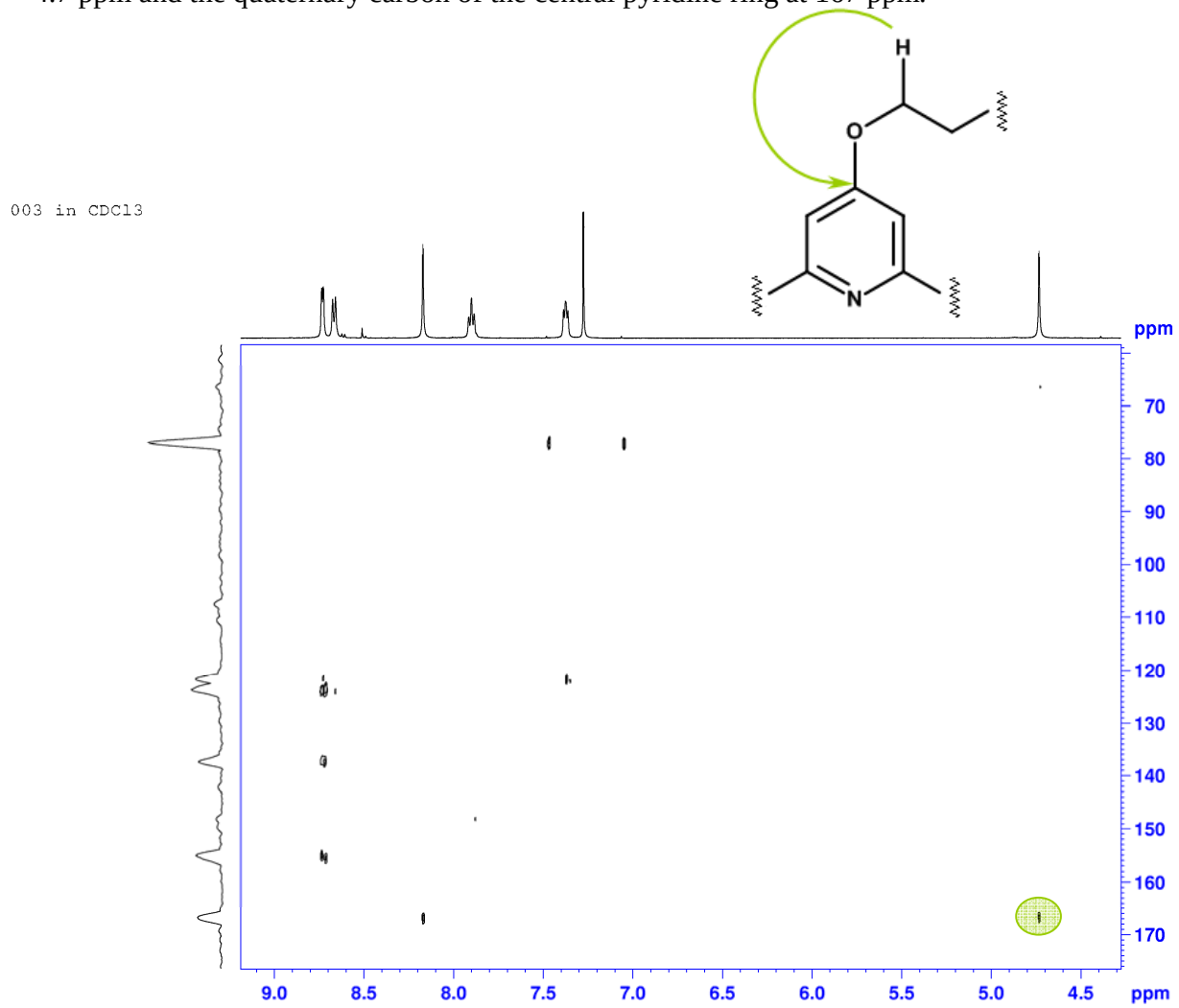

Figure 5.2: HMBC spectrum of **L1** highlighting the cross peak of 4.7 (^{1}H) and 167 (^{13}C) ppm.

In the proton spectrum of **L2** (see *Appendix 1*) the presence of a terpyridine system and a hydrocarbon backbone comprised of not one but now two broad triplet CH_2 peaks were observed. Comparison of the shifts and coupling constants with the chloro-terpyridine and the **L1** indicated a new and different compound. In the NOESY experiment (***Figure 5.3***), selective irradiation of the first proton of the hydrocarbon chain (4.38 ppm) produced a response from the proton on the central pyridine ring (7.98 ppm), verifying the attachment of the chain to the ring.

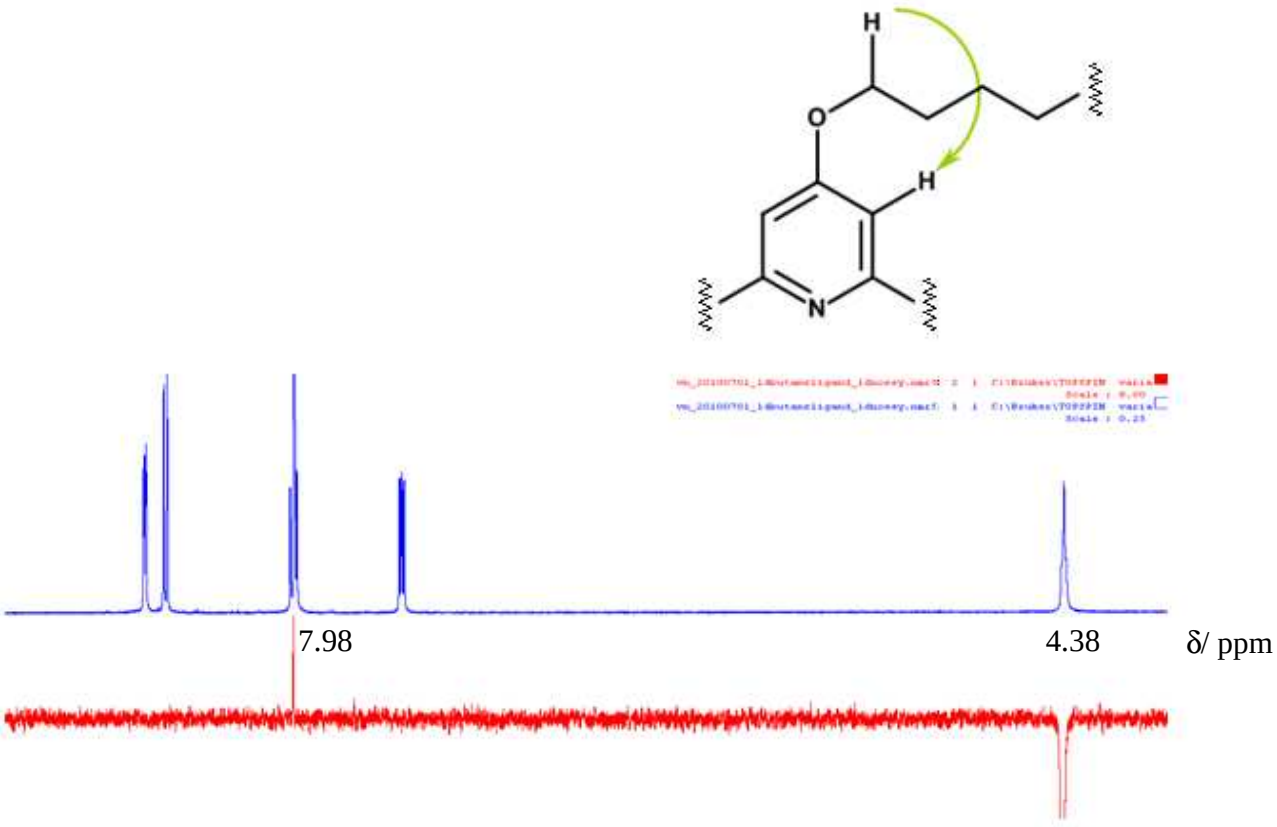

Figure 5.3: NOESY experiment validating attachment of diol chain to terpyridine moiety in **L2** ligand.

The proton spectrum of the **L3** ligand (see *Appendix 1*) once again showed the presence of a terpyridine system and a hydrocarbon backbone now containing three CH_2 signals. Comparison of the shifts and coupling constants with the precursor (chloro-terpyridine) and the other ligands (**L1** and **L2**) indicated a new and different compound.

Clear evidence of the attachment of the hydrocarbon chain to the terpyridine ring was again illustrated through the use of the HMBC experiment (***Figure 5.4***) by showing the correlation between the proton of the CH_2 signal of the hydrocarbon at 4.2 ppm and the quaternary carbon of the central pyridine ring at 167 ppm.

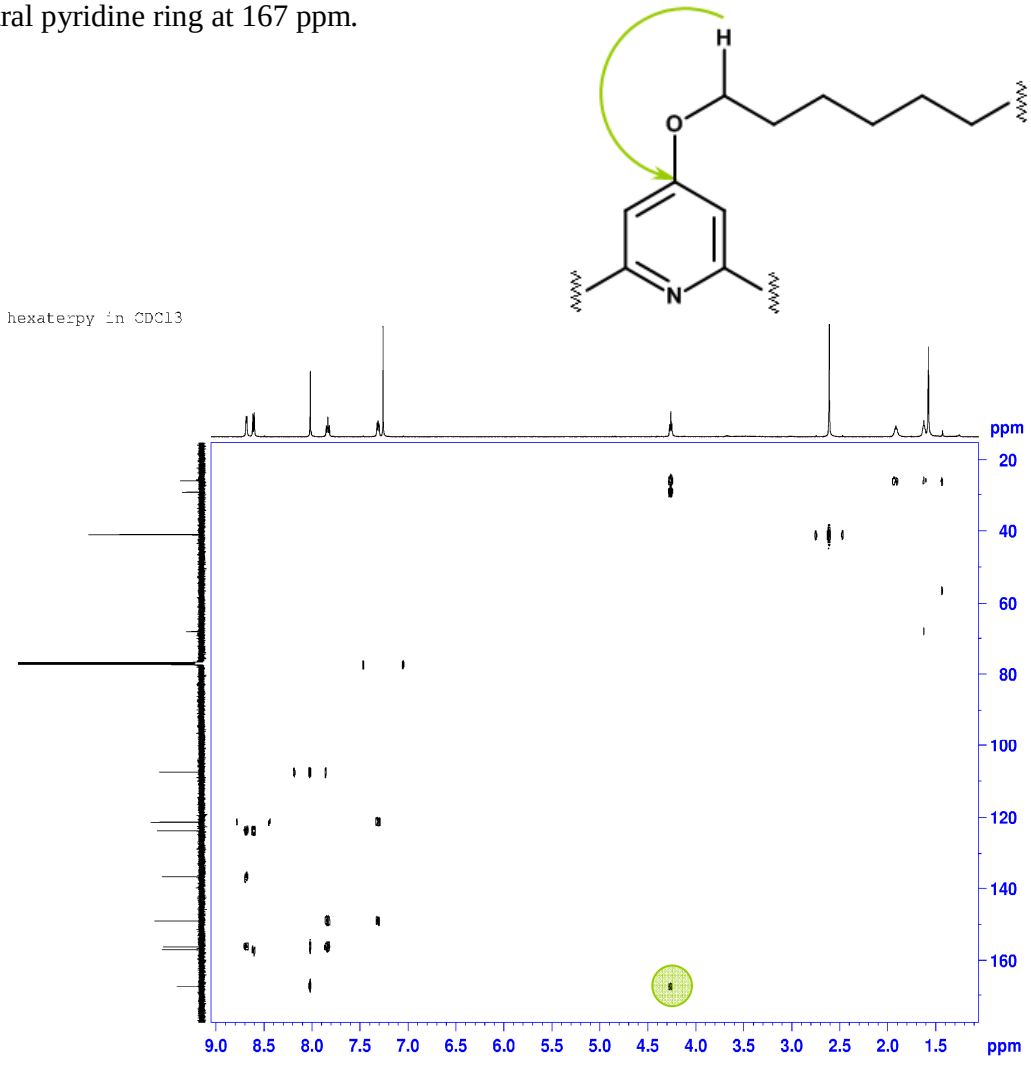

Figure 5.4: HMBC spectrum of **L3** highlighting the cross peak of 4.2 (^{1}H) and 167 (^{13}C) ppm.

The experimental high resolution mass (see *Appendix 3*) and the results of the CHN microanalysis were consistent with the values calculated from the molecular formula (***Table 5.1***).

Table 5.1: CHN microanalysis and HRMS data for the *bis*-terpyridine ligands

		L1 $C_{32}H_{24}N_6O_2$	**L2** $C_{34}H_{28}N_6O_2$	**L3** $C_{36}H_{32}N_6O_2$
Elemental Analysis (CHN)	Calculated %	C, 73.3 H, 4.61 N, 16.0	C, 73.9 H, 5.11 N, 15.2	C, 74.5 H, 5.55 N, 14.5
	Found %	C, 72.9 H, 4.61 N, 16.1	C, 73.5 H, 5.19 N, 15.1	C, 74.1 H, 5.70 N, 14.3
High Resolution Mass Spectrometry (HRMS)	Calculated[α] $[NaL]^+$ g/mol	547.1858	575.2171	603.2484
	Found g/mol	547.1859	575.2171	603.2485

[α] This molecular ion arises from the use of sodium formate during sample preparation.

5.2 X-ray Structure Determination

Slow diffusion of hexane into a chloroform solution of the respective *bis*-terpyridine ligands was used to grow single crystals suitable for X-ray diffraction (***Figure 5.5***).

The crystal structure of **L1** was elucidated from the data collected at 273 K, whilst **L2** and **L3** data were collected at 100 K (***Table 5.2***). **L1** and **L2** crystallised in the triclinic space group *P*-1 with one independent molecule in the asymmetric unit cell of each of the ligands. Due to the crystal system of these ligands there are no restrictions on the axes of reference irrespective of the lengths of [a], [b], or [c] or the values of α, β and γ as shown in ***Table 4.1***.

The **L3** ligand crystallised in the orthorhombic space group *P*bca, with eight independent molecules in the asymmetric unit cell. Due to the crystal system of this ligand there are no restrictions on the relative lengths of [a], [b] and [c] but α = β = γ = 90 º as observed in ***Table 4.1***.

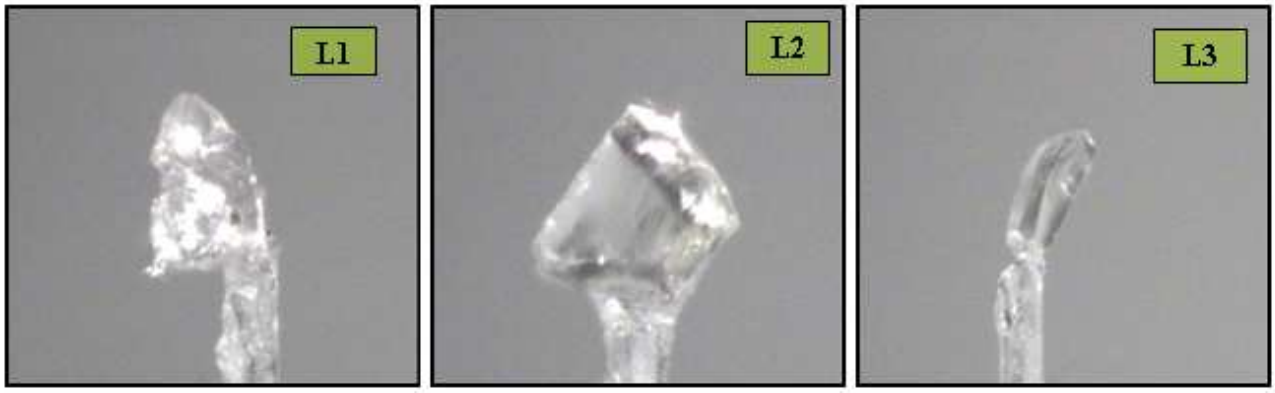

Figure 5.5: Photographs of single crystals of the *bis*-terpyridine ligands

Table 5.2: Molecular structure and the unit cell of the *bis*-terpyridine ligands

	Partially Labelled Thermal Ellipsoid Plot (showing 90 % probability surfaces)	Asymmetric Unit Cell
L1	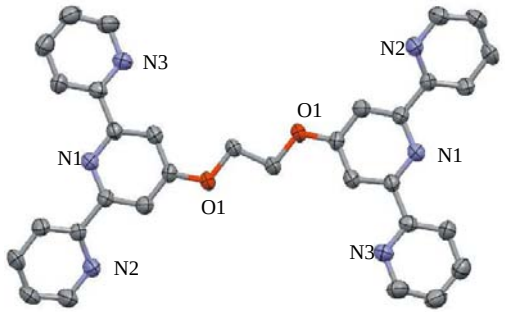 R = 6.31	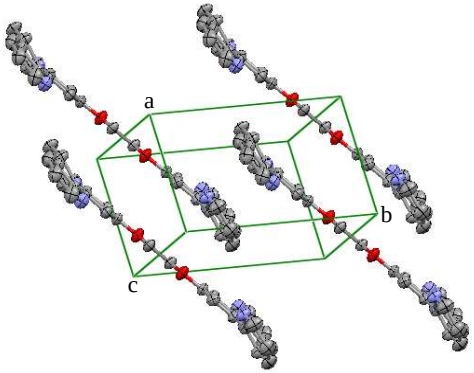
L2	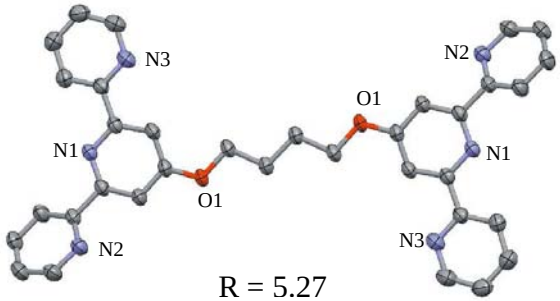 R = 5.27	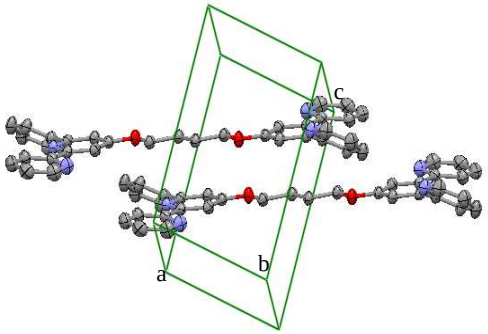
L3	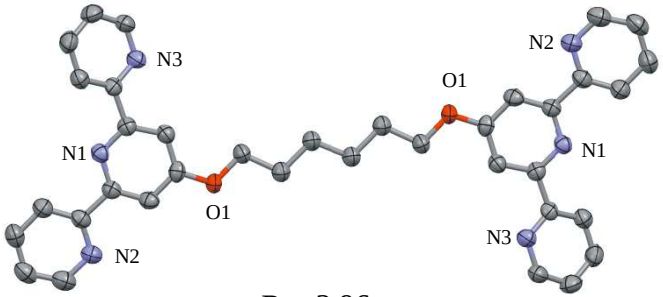 R = 3.96	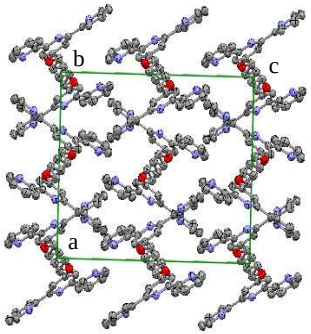

5.3 Complex Synthesis and Characterisation

Various coordination methods described in literature for similar terpyridine systems were attempted but none of these yielded any success as varying complex mixtures were obtained. Ultimately, metallation of the prepared ligands was achieved through modification of the method described by Suntharalingam *et al*.[3] The complexes **L1-Pt**$^{\alpha}$, **L2-Pt**$^{\beta}$ and **L3-Pt**$^{\gamma}$ were prepared by reacting one equivalent of K_2PtCl_4 with the ligand, stirring for three days then adding the second equivalent (***Figure 5.6***). Upon removal of the solvent a very fine orange film was obtained. Since these complexes are novel, a complete characterisation was performed.

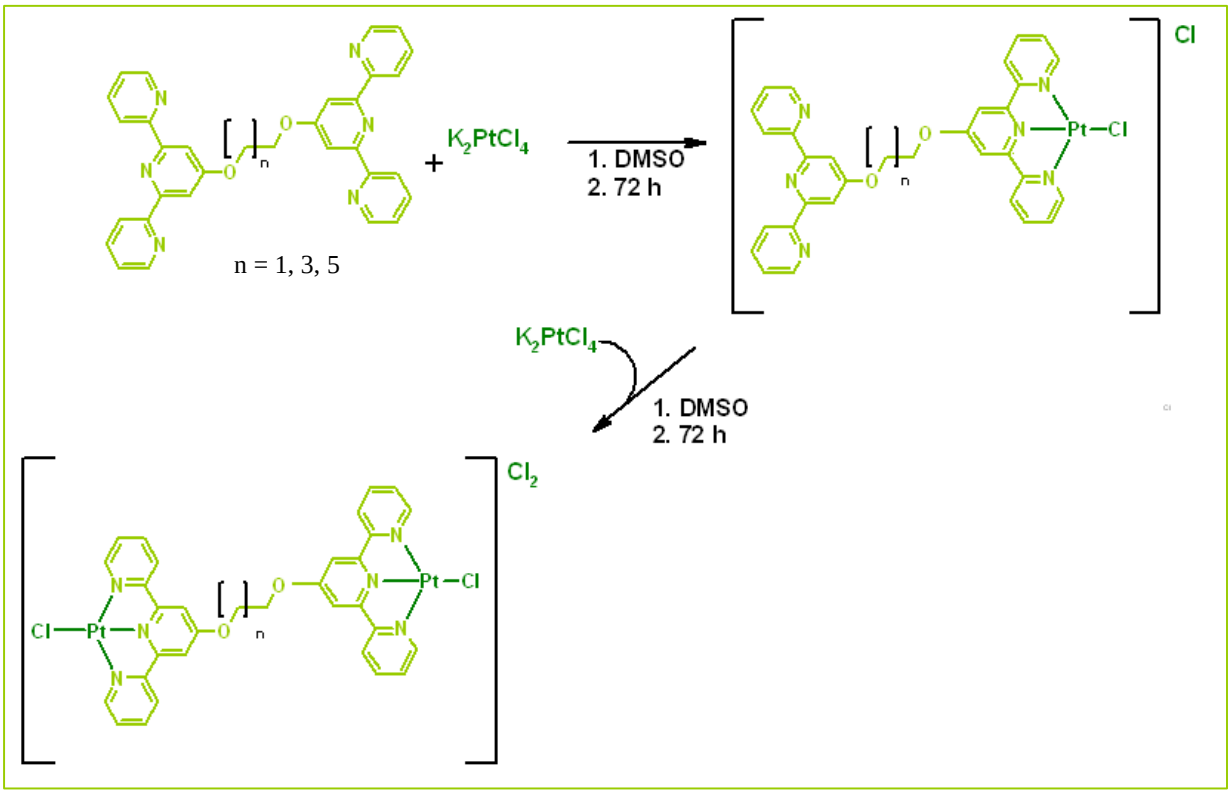

Figure 5.6: Illustration of complex synthesis.

[α] 4",4"'-[ethane-1,2-diyl*bis*(oxy)]-2',2":6",2"'-terpyridine-platinum(II)chloride
[β] 4",4"'-[butane-1,4-diyl*bis*(oxy)]-2',2":6",2"'-terpyridine-platinum(II)chloride
[γ] 4",4"'-[hexane-1,6-diyl*bis*(oxy)]-2',2":6",2"'-terpyridine-platinum(II)chloride

The ^{1}H NMR spectra (see *Appendix 1*) of all three complexes were compared to those of their precursor ligands and were found to contain one symmetrical terpyridine moiety and one CH_2 peak for **L1-Pt**, two for **L2-Pt** and three for **L3-Pt**. An HMBC (***Figure 5.7***) experiment confirmed the ether-hydrocarbon chain was still attached to the terpyridine fragment. Although the signal pattern of the complexes was very similar to that of the ligands, the chemical shifts were different from those of the unmetallated ligands. Unfortunately due to the poor solubility of these complexes no direct ^{13}C experiments could be performed, thus HMBC and HSQC experiments were employed for the indirect detection of ^{13}C chemical shifts.

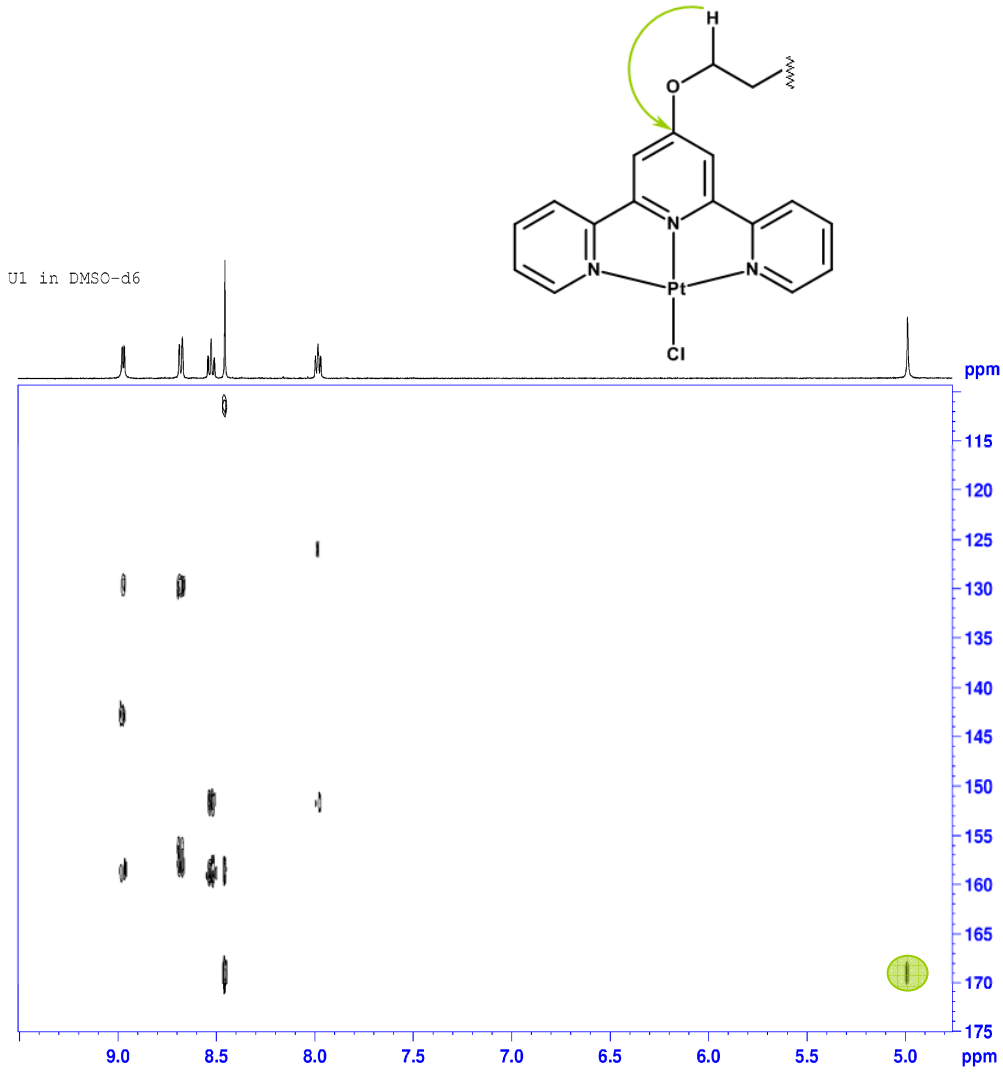

Figure 5.7: HMBC spectrum of **L1-Pt** highlighting chain attachment (For additional spectra see *Appendix 1*).

The experimental high resolution mass data was consistent with the theoretical value accounting for the charge on the molecule (***Table: 5.3***).

Table 5.3: HRMS data for all three *bis*-terpyridine platinum(II) complexes

		L1-Pt $C_{32}H_{24}N_6O_2Pt_2Cl_4$	**L2-Pt** $C_{34}H_{28}N_6O_2\ Pt_2Cl_4$	**L3-Pt** $C_{36}H_{32}N_6O_2\ Pt_2Cl_4$
High Resolution Mass Spectrometry (HRMS)	Calculated g/mol	985.0622	1013.0936	1041.1248
	Found[α] g/mol	492.5307	506.5416	520.5615

a b

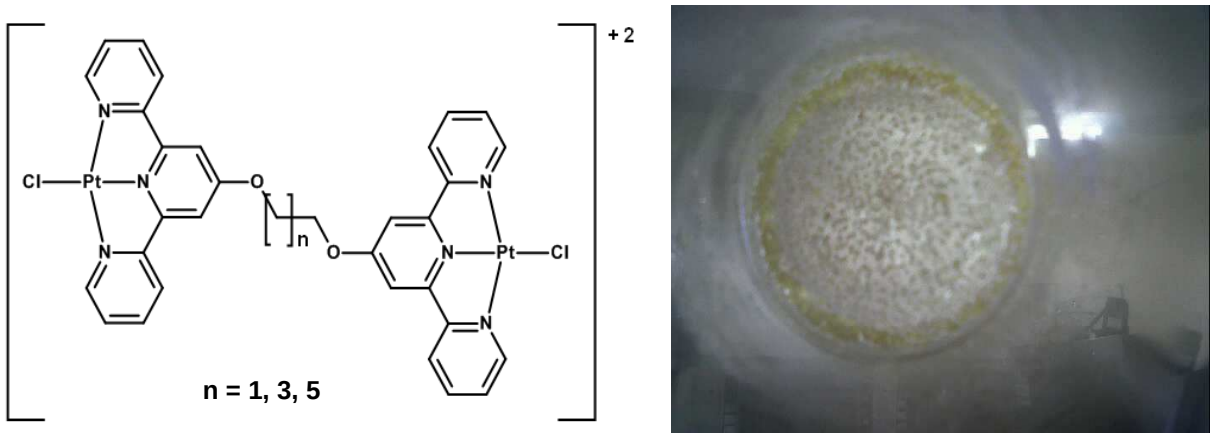

Figure 5.8: (a) $[Pt_2LCl_2]^{2+}$ molecular ions as detected by HRMS. (b) Photograph of a single crystals of **L3-Pt**.

Single crystals of all three complexes where grown several times. Unfortunately, the initial batch grew as clusters and could not be resolved by the software available whilst the second batch (grown utilising a different method) where not large enough to be mounted (***Figure 5.8***, **b**).

[α] As complexes possess a +2 charge the measured m/z ratio has to be doubled to obtain the formula mass.

^{195}Pt NMR experiments (***Figure 5.9***) were performed and a single platinum peak (symmetrical species) was observed in each case. The chemical shifts, measured relative to hexachloroplatinic acid (H_2PtCl_6), are consistent with literature values for the shift of ^{195}Pt in a terpyridine environment.[7a] A comparison of the platinum signals (***Table: 5.4***) for all three complexes indicated a downfield shift with the increase of the chain length.

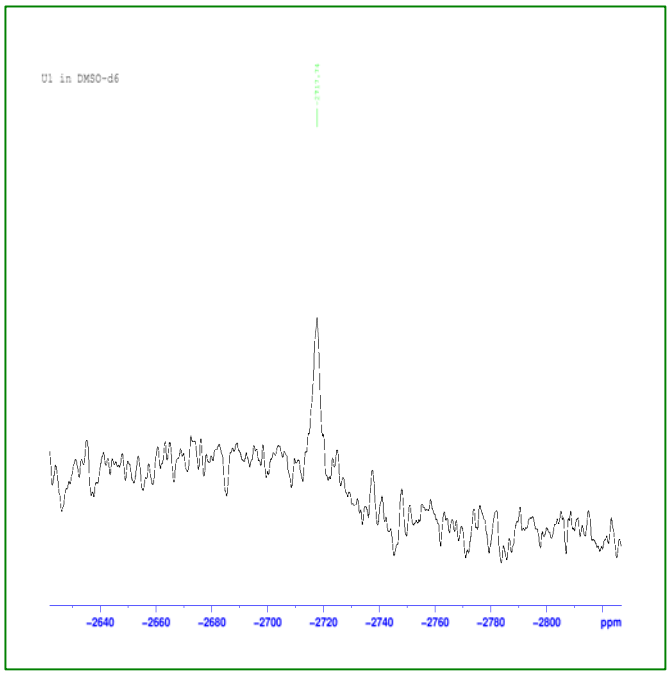

Figure 5.9: ^{195}Pt NMR spectrum of **L1-Pt** (for other spectra see *Appendix 1*).

Table 5.4: Data obtained from ^{195}Pt experiments

	L1-Pt	**L2-Pt**	**L3-Pt**
^{195}Pt Chemical Shift /ppm	-2717	-2710	-2707

A Raman experiment (***Figure 5.10***) was performed to verify the attachment of the chloride ligand to the platinum-terpyridine species, as opposed to a DMSO ligand. The typical Raman Pt—Cl stretch for the terpyridine molecule is approximately 345 cm^{-1}.[5-6] The typical Pt—DMSO stretch is approximately 379 cm^{-1}.[7b] From the data presented in ***Table 5.5*** it is clear that the complex exists as the chloro species.

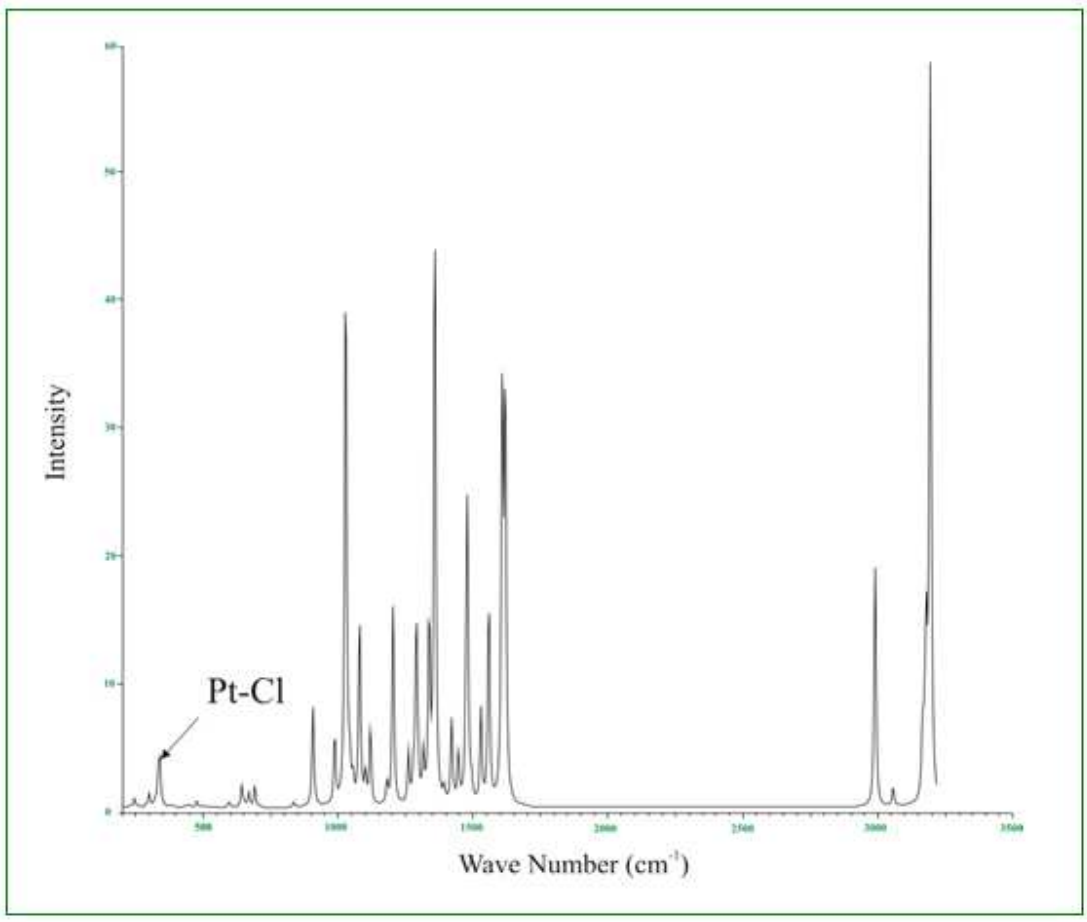

Figure 5.10: Raman spectrum of **L1-Pt** (for additional spectra see *Appendix 4*).

Table 5.5: Data obtained from Raman experiments for all *bis*-terpyridine complexes

	L1-Pt	**L2-Pt**	**L3-Pt**
Raman Pt—Cl Stretch (cm^{-1})	338.5	347.1	347.7

5.4 Kinetic Measurements

Displacement of the coordinated chlorides from the three novel *bis*-terpyridine platinum(II) complexes by three different nucleophiles (Nu), namely: thiourea (**TU**), 1,3-dimethyl-thiourea (**DMTU**) and 1,1,3,3-tetramethyl-thiourea (**TMTU**) was investigated under *pseudo* first-order conditions as a function of concentration and temperature (***Figure 5.11***). The course of chloride substitution was followed initially on a UV-Visible spectrophotometer, which allowed for the determination of the time scale for the substitution process. With the exception of the reaction between **L1-Pt** and **TMTU**, all substitutions were completed in less than sixteen minutes and were thus followed using conventional stopped-flow spectrophometric techniques.

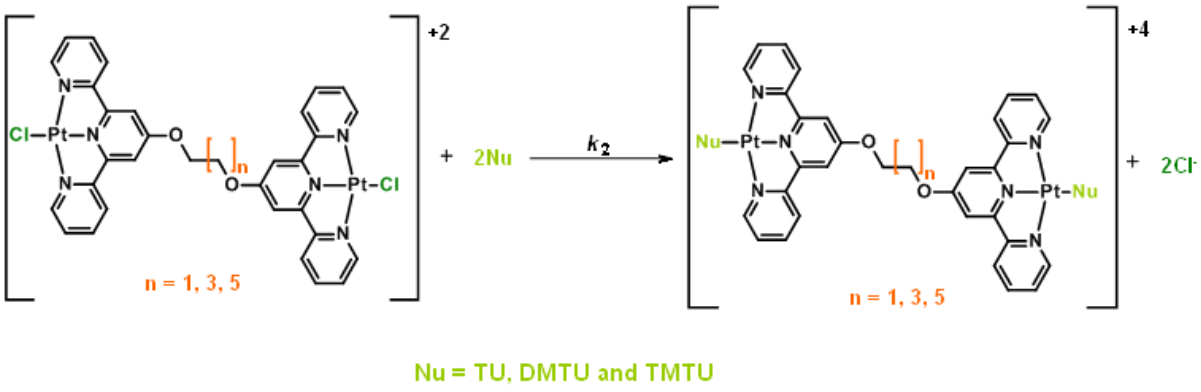

***Figure 5.11*:** Proposed reaction for the substitution of the coordinated chlorides by **TU**, **DMTU** and **TMTU**, followed under *pseudo* first-order conditions.

A typical pre-run was performed by mixing solutions of **L3-Pt** (7.13×10^{-4} M) and **DMTU** (7.13×10^{-4} M) in an ionic strength medium of 0.01 M NaCl[α] in a tandem cuvette and absorbance spectra were recorded over time (***Figure 5.12***). The spectra of the other complexes with nucleophiles were similar in appearance (see *Appendix 5-7*).

[α] NaCl was added to prevent solvolysis

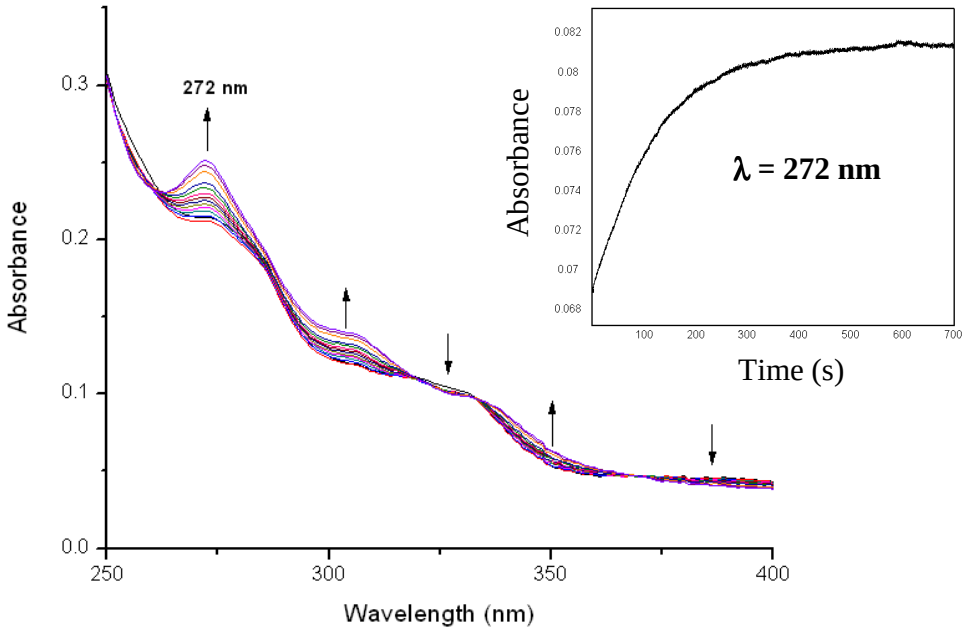

Figure 5.12: Absorbance spectrum of **L3-Pt** (7.13 x10^{-4} M) and **DMTU** (7.13 x 10^{-4} M) in an ionic strength medium of 0.01 M NaCl at 25 °C with the corresponding kinetic trace inset.

The observed *pseudo* first-order rate constants, k_{obs}, were calculated from the kinetic traces using the online non-linear least-squares fit of exponential data to *Equation 5.1*:

$$A_t = A_0 + (A_0 - A_\infty)\exp(-k_{obs}t) \qquad \textbf{…5.1}$$

where A_0, A_t and A_∞ represent the absorbance of the reaction mixture initially, at time *t* and at the end of the reaction, respectively. This plot was recorded at a wavelength of 272 nm and is shown as an inset in ***Figure 5.12***. From this it is clear that there is only one step and the kinetics are first order in nature indicating that chloride substitution in the dinuclear complex occurs simultaneously.

The *pseudo* first-order rate constants were plotted against the concentration of the nucleophiles and were expected to follow *Equation 5.2*.

$$k_{obs} = k_2[\mathrm{Nu}] \qquad \textbf{…5.2}$$

The values of the k_{obs} used represented an average of two replicate scans from the UV-Visible spectrophotometer or ten to twelve independent runs from the stopped-flow spectrophotometer.

Straight lines with zero intercepts were obtained for the substitution reactions of the **L1-Pt**, **L2-Pt** and **L3-Pt** complexes with all nucleophiles. As a result it was unnecessary to study the effect of temperature at every concentration. Only one temperature study was required for each nucleophile. The second-order rate constant, k_2, for the forward reaction of each metal complex with a particular nucleophile was obtained from the slope of the graph.

The temperature dependence of the rate constants was studied in a similar manner over the range of 20 ^{o}C to 35 ^{o}C (or 40 ^{o}C for the **L1-Pt** complex with **DMTU**) in 5 ^{o}C increments for one nucleophile concentration (4.75 x 10^{-4} M). The activation parameters, $\Delta H^{\neq}$ and $\Delta S^{\neq}$ were calculated from the rate constants at the different temperatures using the Eyring equation (*Equation 5.3*). Examples of the plots obtained are shown in ***Figure 5.13*** **(*a*** and ***b*)** with the corresponding data in ***Table 5.6***. Further tables with the reaction rates and activation parameters at 20, 25, 30 and 35 ^{o}C can be found in *Appendices 5-7*.

$$\ln\left(\frac{k_2}{T}\right) = -\frac{\Delta H^{\neq}}{R}.\frac{1}{T} + \left(\ln\frac{k_b}{h} + \frac{\Delta S^{\neq}}{R}\right) \qquad \textbf{…5.3}$$

Where $\ln\frac{k_b}{h} = 23.8$

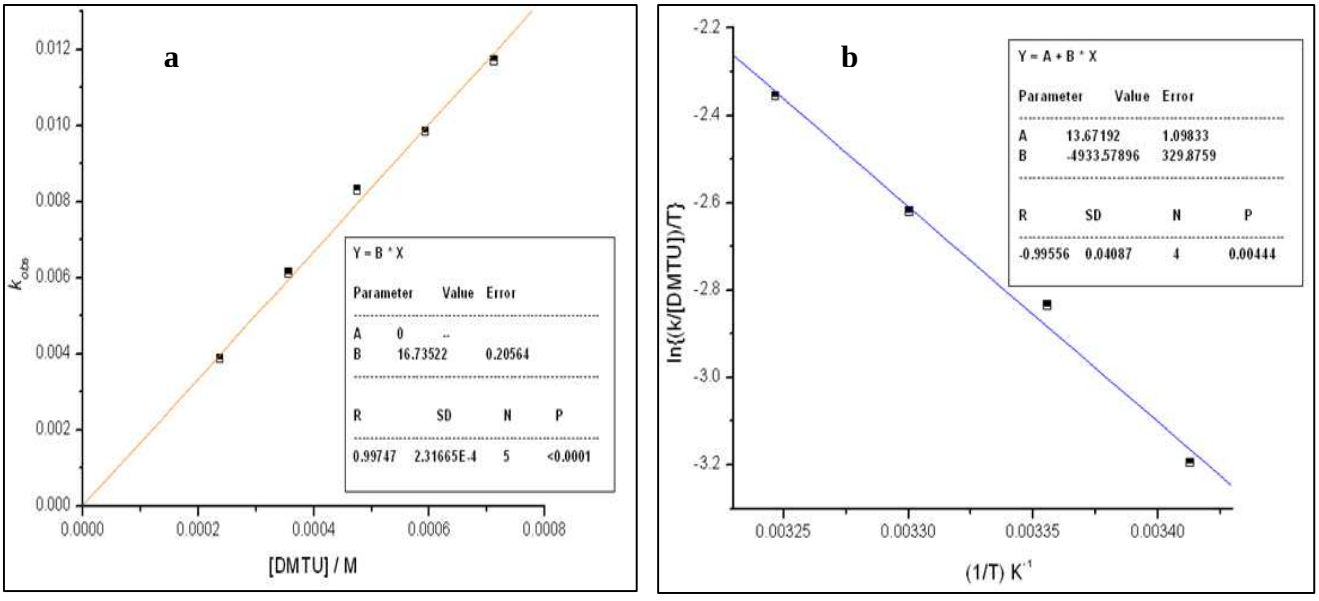

Figure 5.13: (a) Plot to determine rate constant from slope for **L3-Pt** with **DMTU** at 25 °C. (b) Eyring plot for the same reaction.

Table 5.6: Summary of experimentally measured rate constants and activation parameters with error estimates for the substitution reactions of *bis*-terpyridine complexes.

Complexes	Kinetic/ Thermodynamic Parameter	TU 	DMTU 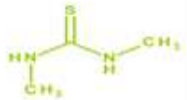	TMTU 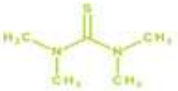
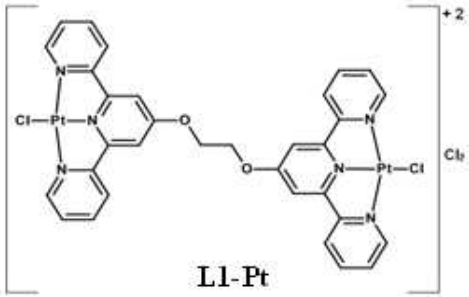 L1-Pt	k_2 ($M^{-1}s^{-1}$)	18.2 ± 0.3	5.62 ± 0.1	3.69 ± 0.2
	$\Delta H^{\neq}$ (kJmol^{-1})	29 ± 4.0	60.7 ± 6.4	78.6 ± 2.0
	$\Delta S^{\neq}$ (J K^{-1} mol^{-1})	−124 ± 2.0	−27.3 ± 2.5	29.2 ± 0.9
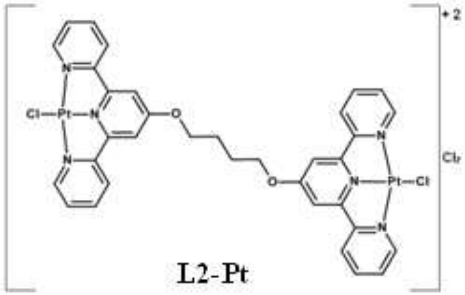 L2-Pt	k_2 ($M^{-1}s^{-1}$)	42.9 ± 0.8	28.9 ± 0.9	27.2 ± 0.5
	$\Delta H^{\neq}$ (kJmol^{-1})	29.1 ± 3.0	33.9 ± 1.4	59 ± 5.0
	$\Delta S^{\neq}$ (J K^{-1} mol^{-1})	−116 ± 1.0	−103.2 ± 0.6	−19.8 ± 2.1
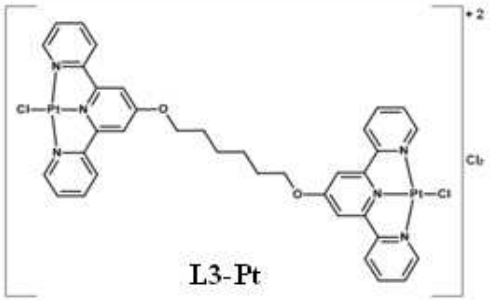 L3-Pt	k_2 ($M^{-1}s^{-1}$)	23.1 ± 0.4	16.7 ± 0.2	16.2 ± 0.3
	$\Delta H^{\neq}$ (kJmol^{-1})	25.6 ± 2.2	41 ± 3.0	53.4 ± 4.4
	$\Delta S^{\neq}$ (J K^{-1} mol^{-1})	−133 ± 1.0	−84.2 ± 1.1	−42.9 ± 1.8

From the kinetic data presented in ***Table 5.6*** it is clear that the reactivity of the complexes with all nucleophiles follows the general trend **L1-Pt** < **L3-Pt** < **L2-Pt**. As expected, a notable enthalpy rise is observed for all three complexes as one moves from a small nucleophile such as **TU** to a sterically hindered nucleophile such as **TMTU**. The dependence of the determined rate constants on the concentration of the incoming nucleophiles, coupled to the values obtained for the activation enthalpies and, with the exception of the substitution of chloride for **L1-Pt** by **DMTU**, the negative activation entropies suggests that the mechanism of substitution is associative, as is typical for most square-planar platinum(II) complexes.

5.5 UV-Visible Measurements

In an attempt to gain further insight into the reactivity of these molecules, a series of absorption UV-Visible spectra were recorded of sequentially diluted solutions of the ligands (in chloroform), ***Figure 5.14 a***, and the complexes (in water), ***Figure 5.15***.

From these spectra, the most prominent spectral band was determined and its intensity at λ_{max} absorption was recorded and plotted *vs* each concentration. Following the Beer-Lambert *Equation 2.54*, a straight line was fitted through the origin and the coefficient of molar absorption was determined (***Figure 5.14 b***).

$$A = \varepsilon \cdot l \cdot c \qquad \textbf{…2.54}$$

Molar absorptivity is a measure of how strongly a chemical species absorbs light at a particular wavelength. Readings at high absorbance values are often unreliable. Since absorbance values tend to infinity as the transmittance tends to zero[8], the experimental conditions where such that the absorbance readings were always below 1.5.

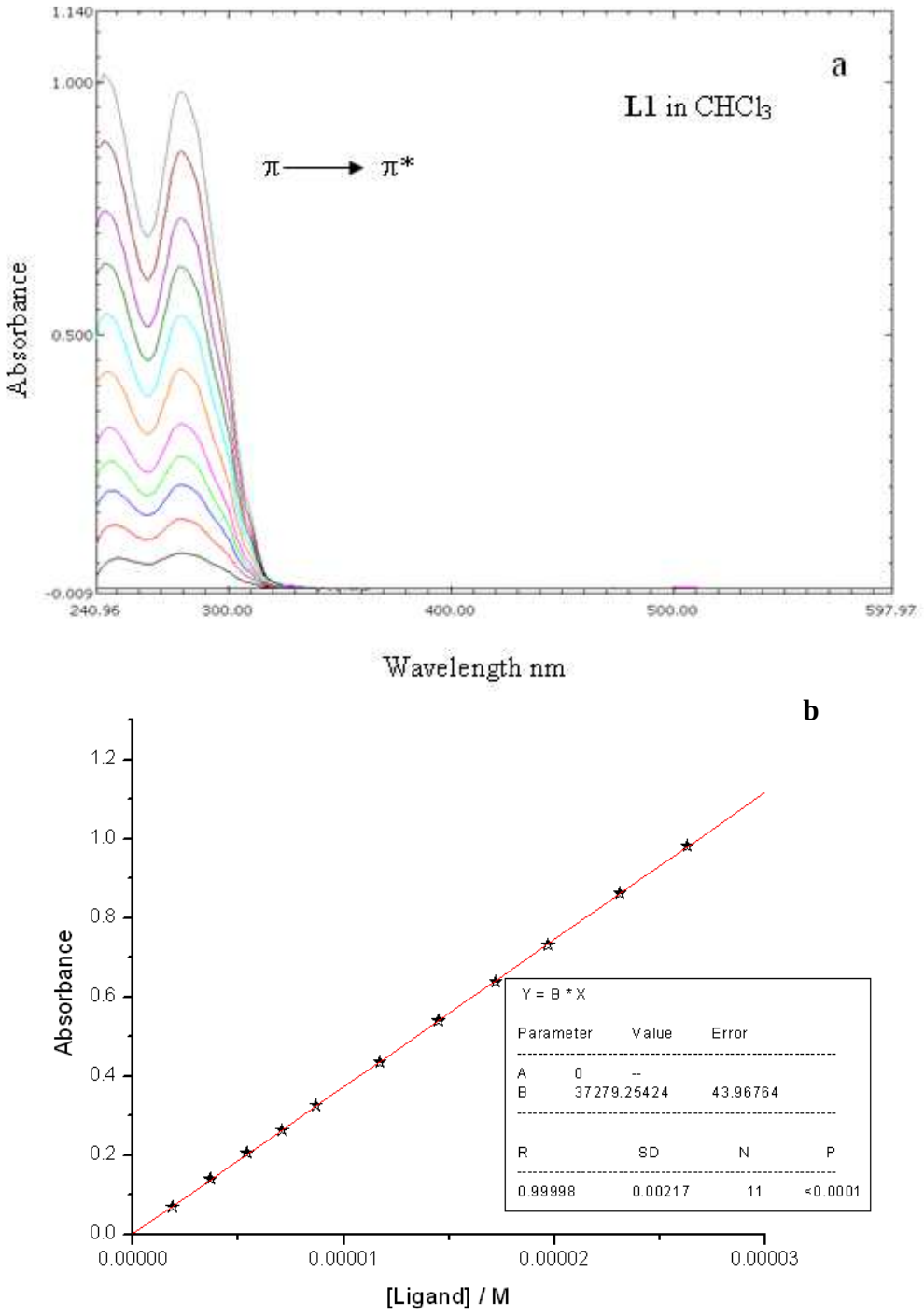

Figure 5.14: (a) UV-Visible spectra obtained upon serial dilution of the **L1** ligand (2.63×10^{-5} M) with chloroform. (b) Beer Lambert plot for **L1** at 25 °C at 279 nm.[α]

[α] Similar spectra were obtained for **L2** and **L3** and can be found in *Appendix 8*

Unfortunately the same solvent could not be used in all experiments as the ligands are only soluble in $CHCl_3$ and DMSO, and although DMSO is more similar to water than chloroform, its spectral window has a higher cut off point.

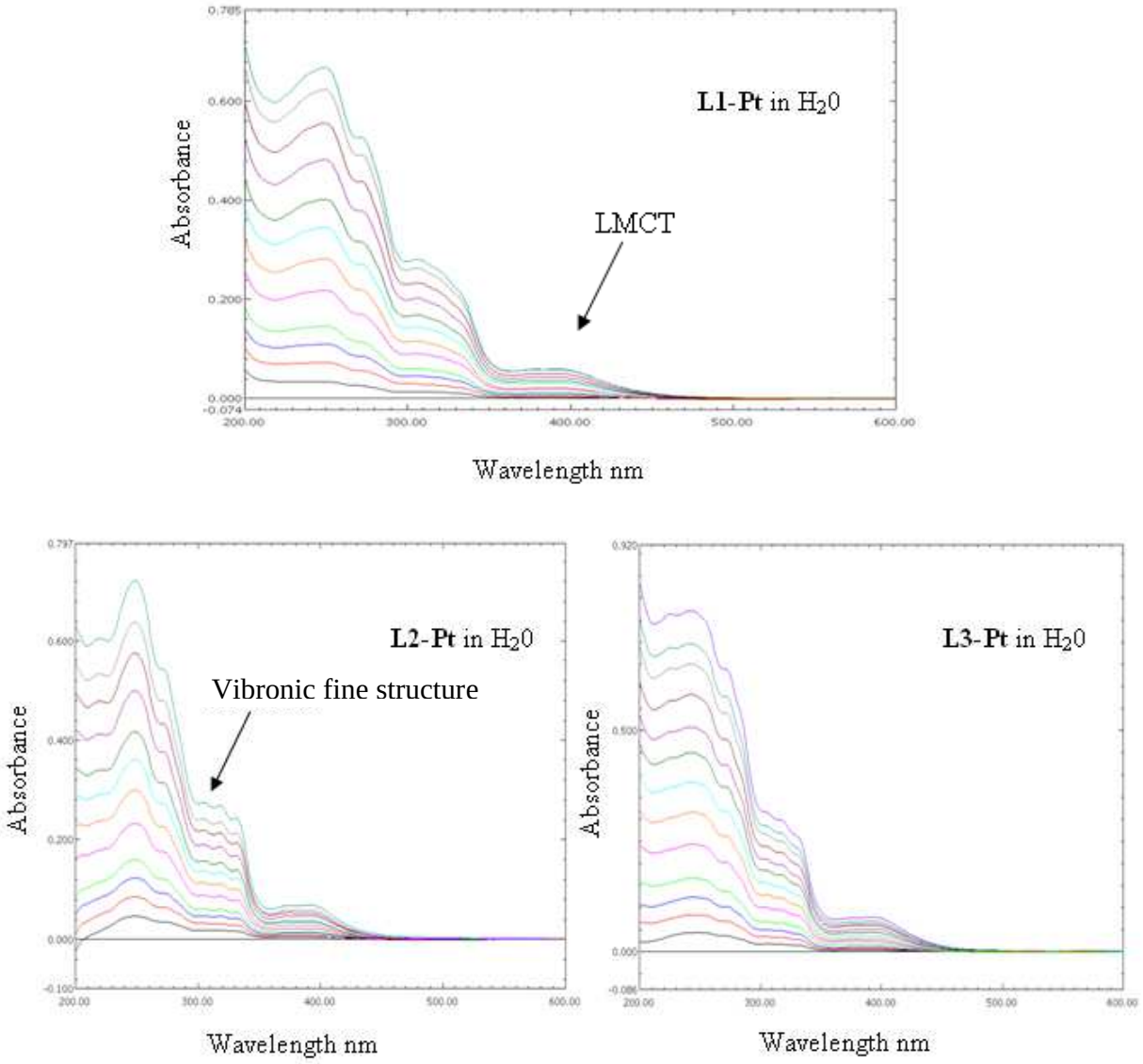

Figure 5.15: UV-Visible spectra obtained upon serial dilution (1.22×10^{-5} to 9.29×10^{-7} M) of the **L1-Pt**, **L2-Pt** and **L3-Pt** complexes with water at 25 ° C.

From the spectra depicted above, several things can be noted. First, the **L2-Pt** complex has the most resolved spectral bands. The complexes' spectral bands are different in number and the wavelength of maximum absorption of those of the ligands, although this may be a result of the use of a different solvent. A series of minor peaks are also observed in the complex spectra and these could be caused by the vibronic contributions. The Beer-Lambert plot for the **L1-Pt** complex is shown in ***Figure 5.16***.

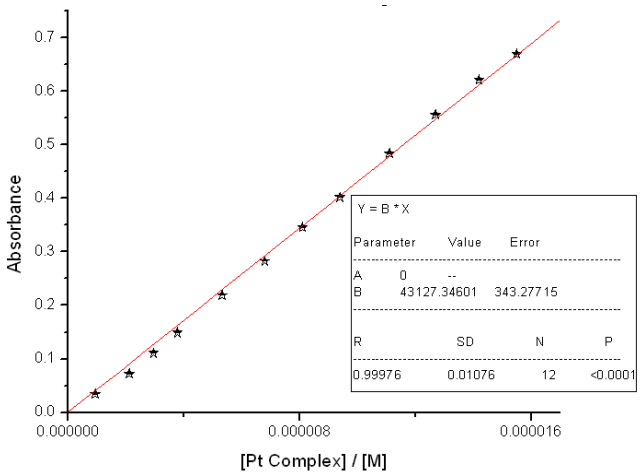

Figure 5.16: Beer-Lambert plot of **L1-Pt** at 25 °C in water at 250 nm.[α]

The molar absorption coefficients obtained from the slope of the Beer-Lambert plots are shown in ***Table 5.7***. The values of ε for the ligands increase in the sequence **L1** < **L2** < **L3**. The magnitude of the ε values is typical of π—π* transitions in the heteroaromatic terpyridine system. When one compares the molar absorption coefficients for the complexes, an interesting anomaly is observed. The values of ε for the complexes increase in the sequence **L1-Pt** < **L3-Pt** < **L2-Pt**. It is difficult to envisage why a difference in the length of the alkyl chain should manifest itself in such an irregular change of the electron density of the heteroaromatic system. The introduction of the metal clearly plays a profound role and from the above data one can begin to consider the possibility of electronic effects associated with the platinum ions being at the root of these complexes reactivity.

[α] Similar spectra were obtained for **L2-Pt** and **L3-Pt** and can be found in *Appendix 8*

Table 5.7: Molar absorption coefficients for the *bis*-terpyridine ligands and their platinum(II) complexes

ε (M^{-1} cm^{-1})			
Ligands		**Complexes**	
L1	37280 ± 40	**L1-Pt**	43130 ± 340
L2	41540 ± 180	**L2-Pt**	71565 ± 860
L3	66000 ± 160	**L3-Pt**	63760 ± 330

5.6 Interpretation of Experimental Findings

As has been established from the kinetic studies, the order of magnitude of the rate constants for the chloride substitution by an incoming nucleophile is as follows: k_2(**L1-Pt**) < k_2(**L3-Pt**) < k_2(**L2-Pt**). Remarkably, a similar trend is observed for the molar absorption coefficients of the platinum complexes at the wavelength of maximum absorbance[α]: ε(**L1-Pt**) < ε(**L3-Pt**) < ε(**L2-Pt**), even though for the free ligands these coefficients are monotonously increasing from **L1** to **L3**. To test whether such similarity is more than a mere coincidence, one has to consider the molecular structures of the platinum complexes and the factors responsible for their reactivity (rate constants) and interaction with the incident light (absorption coefficients).

The rate constants k_2, have been found to be incoming nucleophile dependent. This eliminates the possibility of a dissociative mechanism. In view of the k_2 dependence on the nucleophile concentration and steric bulk, as well as the negative (but in one case) activation entropies, the associative mechanism of substitution appears increasingly likely. Thus, the rate of Cl^- ligand substitution is being controlled by the electrophilicity of the platinum ion centre.

[α] This statement refers to the most intense UV-band, which is likely to represent a $\pi \rightarrow \pi^*$ transition in the aromatic system of terpyridine.

Subsequently, the highest rate constant for the **L2-Pt** complex means the highest positive charge is carried by the platinum centre in this compound. A more detailed discussion of this point follows.

Activation energy is defined as the minimum energy that must be overcome for a chemical reaction to take place (***Figure 5.17***).[9]

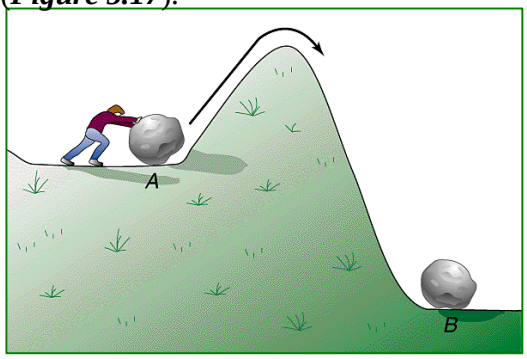

Figure 5.17: Activation energy cartoon.[9]

The Arrhenius equation (*Equation 2.44*) indicates that changes in reactivity might arise from changes in the activation free energy, E_a, and the pre-exponential factor, A.

$$\ln k = \ln A - \frac{E_a}{R} \cdot \left(\frac{1}{T}\right) \qquad \textbf{…2.44}$$

In the course of a reaction between two species, the molecular system commonly passes through a maximum of free energy. The height of this maximum is instrumental in all theories of reaction rates. A molecular system at the top of the potential barrier is called the *activated complex* (***Figure 5.18***) and its state is called the *transition state*.[10]

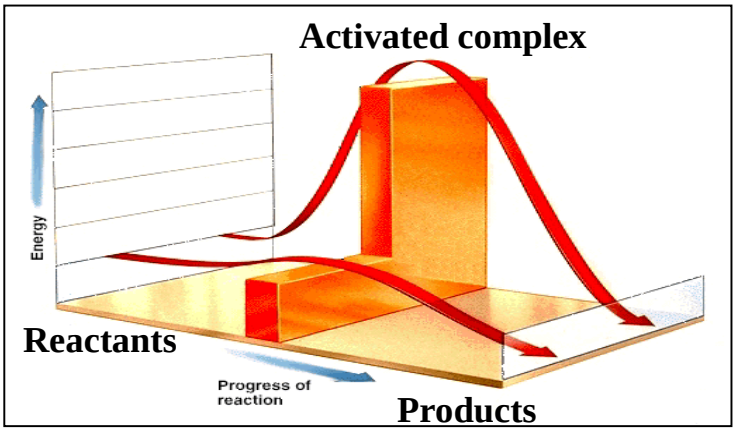

***Figure 5.18*:** Diagram illustrating relative energies of two activated complexes.[11]

For a fast reaction to occur, the transition state for an associative mechanism (in this case a penta-coordinated reaction intermediate) must be stabilised in some way.

According to Einstein's theory of electronic transitions in atoms,[12] the intensity of the spectral lines, conveniently represented by the molar absorption coefficient, ε, is proportional to the *transition dipole moment*:

$$\vec{\mu}_{fi} = \langle f | \vec{\mu} | i \rangle \equiv \int \Psi_f^* \, \vec{\mu} \, \Psi_i d\tau \qquad \textbf{…2.45}$$

The most intense bands in the UV-Visible spectra of the ligands (and their platinum(II) complexes) can be attributed to the $\pi \rightarrow \pi^*$ transitions of the aromatic system of the terpyridine moiety. Subsequently, special extent of the ground state orbitals (as well as excited orbitals), which might be affected by, for example, π-back donation of the 5*d*-electron density of platinum into the π-system of the terpyridine, will contribute to the increased intensity of the spectral bands.

Preliminary quantum-mechanical calculations[α] of the platinum complex geometry at the DFT level, for the **L1-Pt** and **L2-Pt**[β] complexes, both in the gas phase and in a simulated aqueous medium, revealed that the molecules are linear, with almost coplanar terpyridine moieties, ***Figure 5.19***.

[α] Originally, quantum mechanical calculations were not envisaged to be a part of this project. Subsequently, no detailed discussion of the computational particulars will be given here. The calculations were performed at author's request in a friendly research group of the School, and serve a purely illustrative purpose. It should be noted that the systems in question, with two to four heavy platinum atoms, and a large number of light atoms, are computationally very demanding (typical number of basis functions is between 1500 and 3500), even when calculations are performed on a powerful modern workstation.

[β] The structure of **L3-Pt** complex is not yet optimised in view of high computational demands for this very large system, but it is expected to be similar to those for **L1-Pt** and **L2-Pt**.

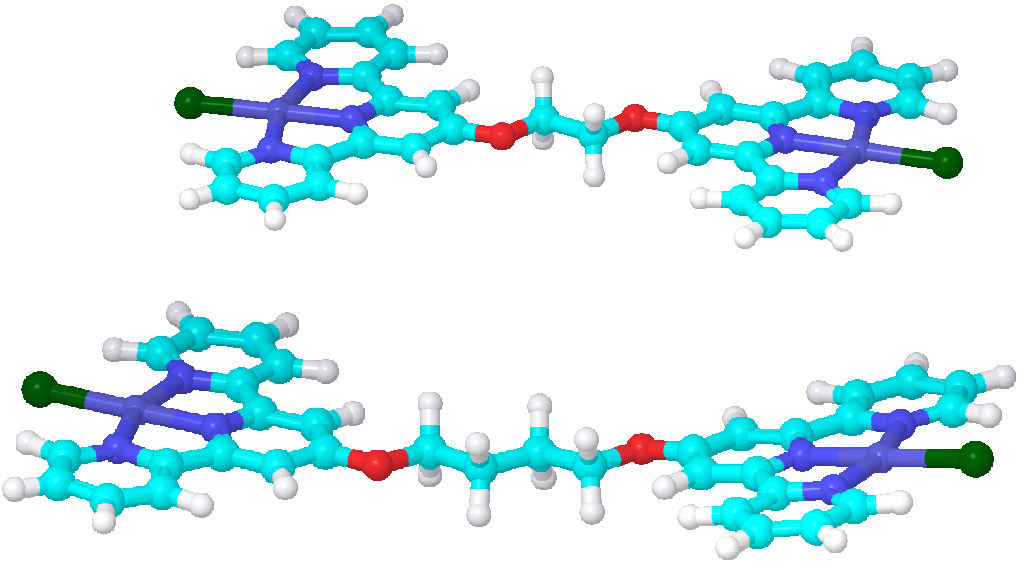

***Figure 5.19*:** Computed structures of the **L1-Pt** and **L2-Pt** complexes in a simulated aqueous medium.

If these geometries adequately represent molecular shapes of the platinum complexes in solution, it is hard to envisage how the platinum centre could become progressively more electrophilic with increasing length of the polymethylene chain, let alone account for the maximum of reactivity and intensity of absorption bands for the **L2-Pt** complex.

A plausible assumption that can explain both the kinetic and spectroscopic facts is that of possible self-association of the platinum complexes in solution. The heteroaromatic moiety of the terpyridine is well known to form π-stacked oligomers, whilst square-planar platinum(II) complexes with aromatic ligands are also known to aggregate due to the formation of direct Pt—Pt bonds. Self-association in solution of the platinum terpyridine units may occur within the same molecule in a clam-shell manner, due to the folding-over of the complex, if the bridge between two terpyridine units is long enough and flexible enough to afford favourable orbital overlap, ***Figure 5.20***, without steric strain, or between two molecules with the formation of a doubly bonded dimer, ***Figures 5.21-5.22***. Formation of higher order associates is less likely in view of the low overall concentration of complexes in solutions used in the kinetic and spectroscopic experiments (10^{-5} – 10^{-7} M). In both cases the self-association could be driven by π-stacking, direct Pt—Pt bonding, or both of the above effects.

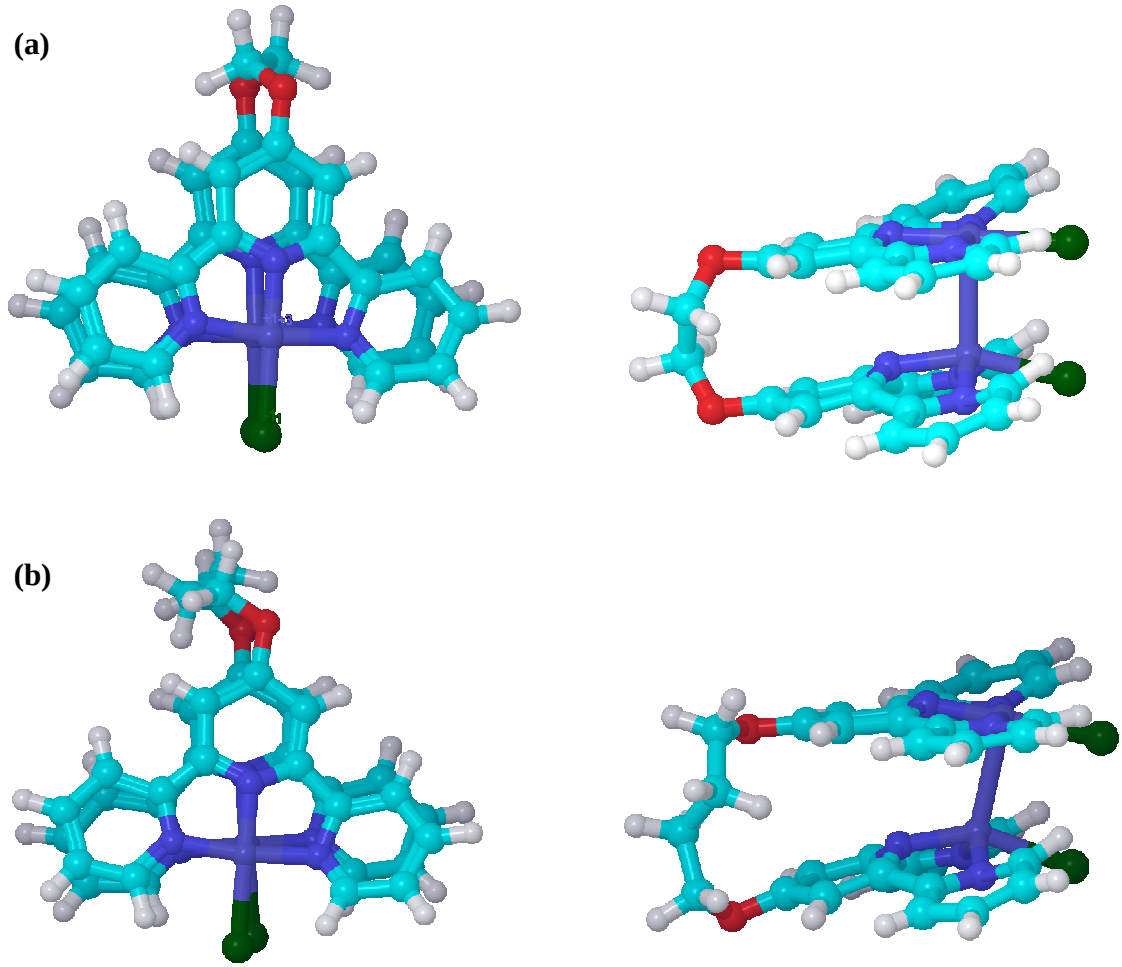

***Figure 5.20*:** Two projections of the clam-shell structures for: (a) **L1-Pt** complex, and (b) **L2-Pt** complex in a simulated aqueous environment.

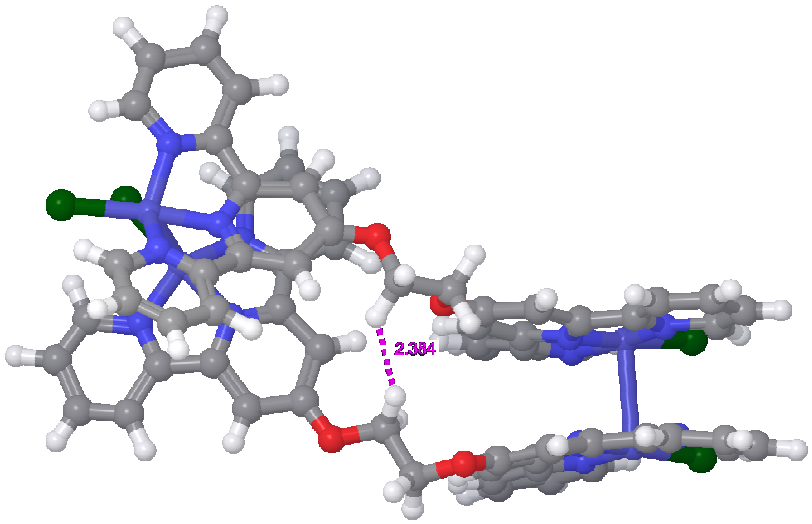

***Figure 5.21*:** Simulated dimer structure for the **L1-Pt** complex. The distance of the closest approach of two methylene hydrogens is in Å.

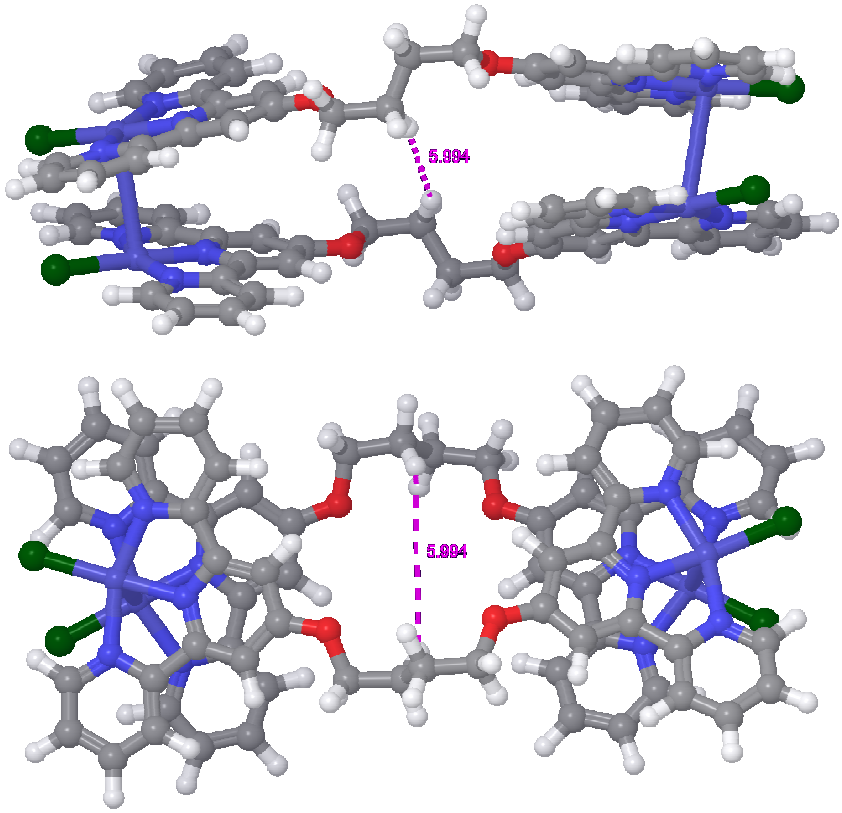

***Figure 5.22*:** Two projections of the simulated dimer structure for the **L2-Pt** complex. The distance of the closest approach of two methylene hydrogens is in Å.

To probe the hypothesis of self-association in these platinum complexes, and, hopefully, to distinguish between the *intra*- and *inter*-molecular self-association, an additional NMR study was conducted with focus placed on the temperature and concentration dependence of the chemical shifts.

5.7 Additional NMR Measurements

The phenomenon of aggregation in solution, driven by either Pt—Pt or π—π interactions or both, has been observed in other dinuclear platinum terpyridinyl complexes in which the terpyridinyl units are bridged by a flexible spacer.[13] Unfortunately, no studies of the substitution kinetics for these systems have been reported. Similar aggregation has been found to occur for dinuclear complexes with rigid spacers[14] and for mononuclear platinum terpyridinyl complexes.[15] The study was conducted on samples prepared by dissolving pure solid complexes in DMSO-d_6 to yield initial concentrations of about 2×10^{-3} M. The overlay of the ^{1}H NMR spectra for the **L1-Pt**, **L2-Pt**, and **L3-Pt** complexes in DMSO-d_6 at 30 °C is shown in ***Figure 5.23***. Data tabulated in the proceeding tables shown in red indicates an upfield shift, whilst that in blue indicates a downfield shift.

Several general observations can be made. Firstly, the spectral resolution decreases with increasing chain length, particularly that of the α-proton closest to the platinum atom. Secondly, all signals are shifted upfield with increasing chain length (shift changes in Hz shown in ***Table 5.8***). Interestingly, the largest change in chemical shift is that of the CH_2 signal. Thirdly, the changes between complexes **L1-Pt** and **L2-Pt**, but for the β-proton, are greater than the changes between complexes **L2-Pt** and **L3-Pt**.

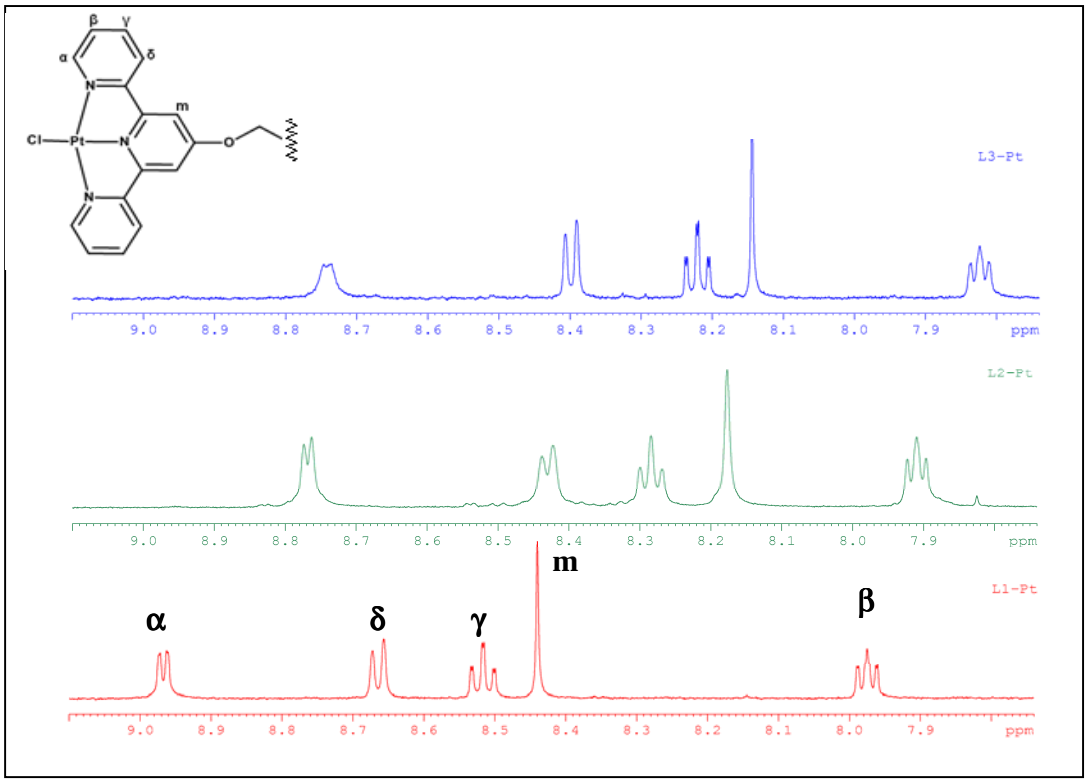

Figure 5.23: Generic structure of the **L1-Pt**, **L2-Pt**, and **L3-Pt** complexes and comparison of their ^{1}H NMR spectra, showing the aromatic region only.

Table 5.8: Changes in ^{1}H chemical shifts with an increase in chain length (Hz)

Resonance	(L1-Pt) – (L2-Pt)/Hz	(L2-Pt) – (L3-Pt)/Hz
α	**100**	**25**
β	**33**	**49**
γ	**117**	**35**
δ	**117**	**17**
m	**132**	**17**
CH_2	**178**	**104**

The decrease in signal resolution and upfield change in the chemical shifts with increasing chain length of the spacer is consistent with observations of a molecular interaction between two platinum-terpyridinyl units in solution.[13] Moreover, the change in chemical shift of the α-proton in this work (125 Hz, 0.25 ppm) is of the same order of magnitude as that described by Yam and co-workers (145 Hz, 0.29 ppm).[13] The upfield shift is attributed to shielding associated with Pt—Pt and/or π—π stacking arising from the molecular interaction (whether *inter*molecular or *intra*molecular). The CH_2 signal experiences the largest chemical shift change, and future work will entail performing DFT calculations, in an attempt to clarify why this is so (*Chapter 6*).

5.7.1 L1 – Pt complex

A variable temperature and concentration ^{1}H NMR study of the **L1-Pt** complex was performed. The spectra recorded at different temperatures are shown in ***Figure 5.24***.

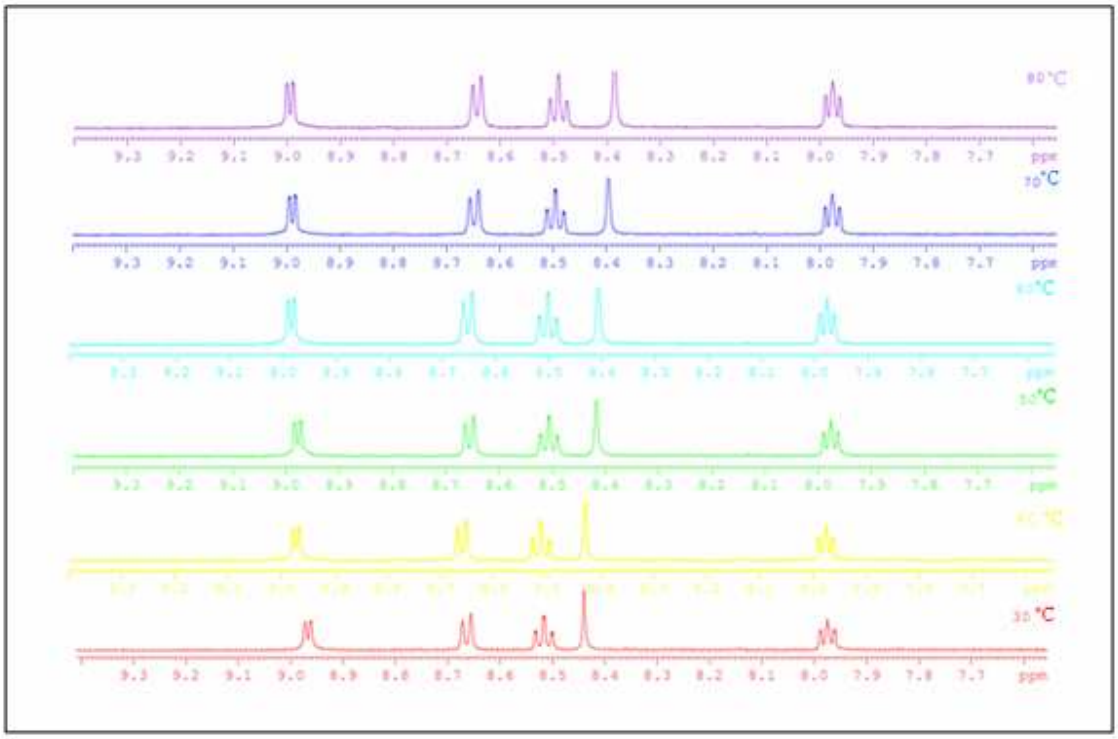

Figure 5.24: ^{1}H NMR spectra (aromatic region only) of **L1-Pt** complex in DMSO-d_6 at various temperatures (in the range 30 °C to 80 °C).

Table 5.9 contains numerical values of the chemical shift changes for the spectra shown above.

Table 5.9: ^{1}H chemical shift changes with temperature for the solution of **L1-Pt** complex

Δδ / Hz						
#	**Temperature change / °C**					
	30 – 40	**40 – 50**	**50 – 60**	**60 – 70**	**70 – 80**	**30 – 80**
α	3	3	3	3	3	15
β	0. 2	0. 2	0. 1	0	0	0. 5
γ	3	3	3	3	3	15
δ	2	2	2	2	2	12
m	6	6	5	5	5	31
CH_2	4	3	3	3	3	16

As can be seen from the data presented, the chemical shift for the α-hydrogen atom moves downfield with an increase in the sample temperature, while all other resonances move upfield. The largest downfield shift is that of the CH_2-hydrogens (16 Hz), closely followed by the α-hydrogen (15 Hz). The largest upfield shift is observed for the *m*-hydrogen (31 Hz). The β-hydrogen resonance remains unchanged. Practically no change in resolution of the multiplets is observed in the range 30 °C to 80 °C.

A concentration dependence study (successive two-fold dilutions) of the **L1-Pt** complex in DMSO-d_6 was conducted at a constant temperature of 30 °C, and the results are presented in ***Figure 5.25*** and ***Table 5.10***.

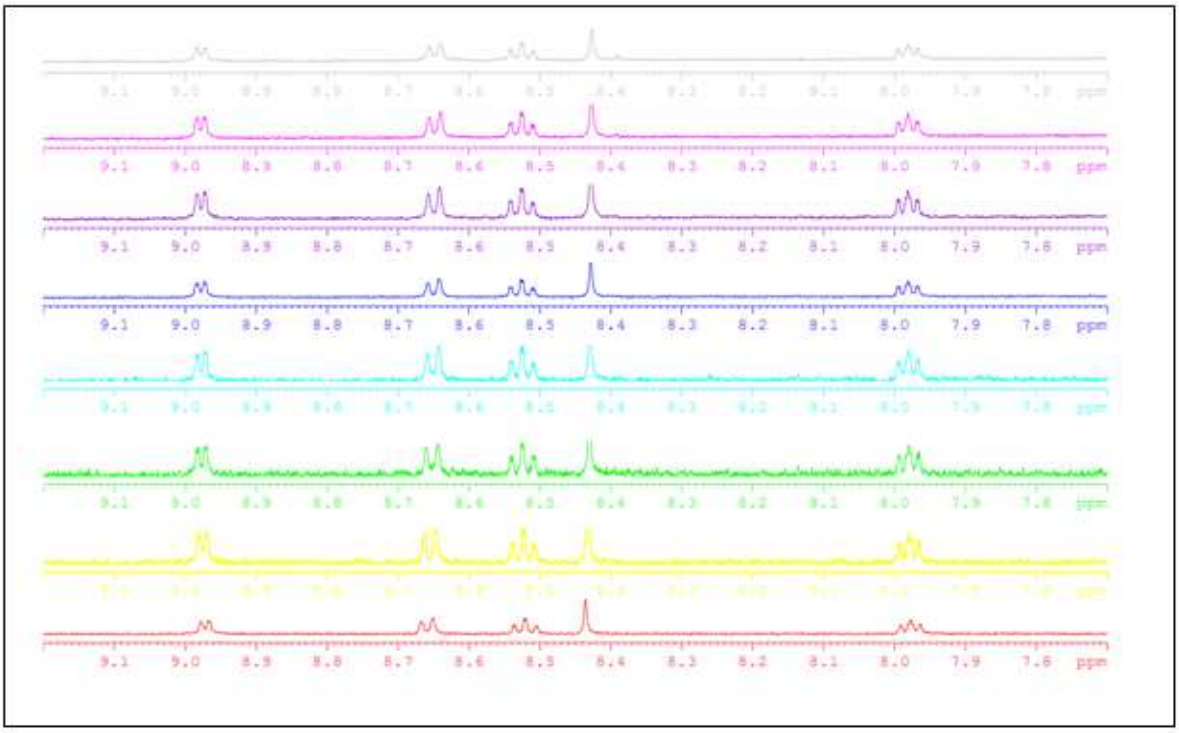

Figure 5.25: ^{1}H NMR spectra (aromatic region only) of **L1-Pt** complex in DMSO-d_6 at different degrees of dilution. The most concentrated sample is at the bottom; every next sample is half-dilute in comparison to the previous one.

Table 5.10: ^{1}H chemical shift changes with concentration for the solutions of **L1-Pt** complex

Δδ / Hz								
#	**C – C/2**	**C/2 – C/4**	**C/4 – C/8**	**C/8 – C/16**	**C/16 – C/32**	**C/32 – C/64**	**C/64 – C/128**	**C – C/128**
α	1. 5	1	0	0	0	0	0	3
β	0. 5	0. 5	0	0	0	0	0	1
γ	1	1	0	0	0	0	0	2
δ	1. 5	1. 5	0	1	0	0	0	4
m	1. 5	1	0. 5	0	0	0. 5	0	3. 5
CH_2	1	1	0	0. 5	0	0. 5	0	3

There are essentially no changes in the position of the chemical shifts or the resolution of the multiplets with dilution in this system. As will be shown further, such behaviour is dramatically different from that observed in the **L2-Pt** or **L3-Pt** systems.

5.7.2 L2 – Pt complex

Similar studies were performed on the **L2-Pt** complex solutions. The variable temperature spectra are shown in ***Figure 5.26***.

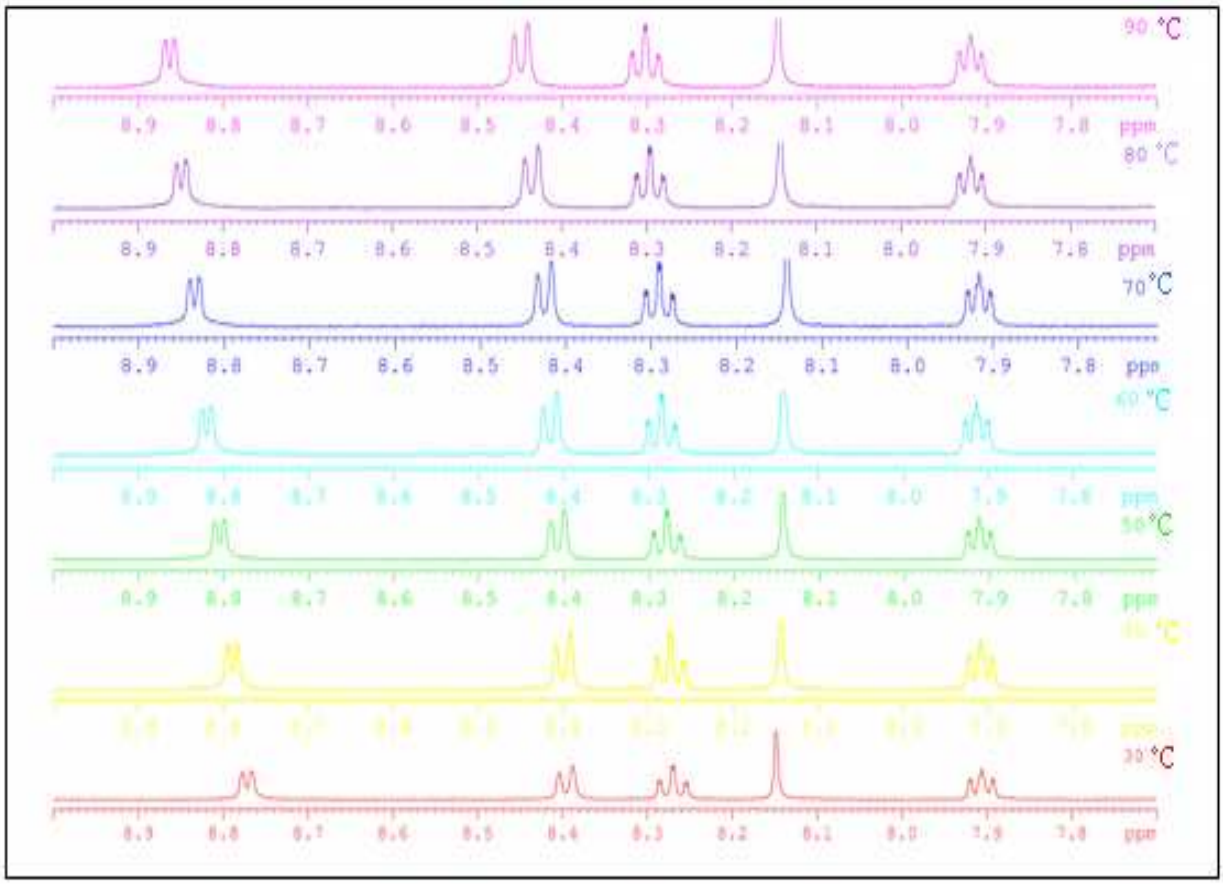

***Figure 5.26*:** ^{1}H NMR spectra (aromatic region only) of **L2-Pt** complex in DMSO-d_6 at various temperatures (in the range 30 °C to 90 °C).

Numerical values of the chemical shift changes are collected in ***Table 5.11***.

Table 5.11: ^{1}H chemical shift changes with temperature for the solution of **L2-Pt** complex

Δδ / Hz							
#	Temperature change / °C						
	30 – 40	40 – 50	50 – 60	60 – 70	70 – 80	80 – 90	30 – 90
α	9	7. 5	7. 5	7	7	6. 5	44. 5
β	1. 5	1	1	1	1	0. 5	6
γ	2	2. 5	3	3	3	3	16. 5
δ	2	4	4	4. 5	5. 5	6	26
m	2	1	1	0	1	2	1
CH_2	2	2. 5	2. 5	2	2. 5	2	13. 5

All of the chemical shifts in the ^{1}H spectrum of this complex move downfield with increasing temperature (but for the *m*-hydrogen resonance, which remains virtually unchanged). The largest downfield shift is that of α-hydrogen (44.5 Hz), whilst the smallest is of the β-hydrogen (6 Hz). The chemical shift of the *m*-hydrogen remains essentially constant. The resolution of the multiplets improves with increasing temperature, particularly for the α-hydrogen doublet.

The results of the concentration dependence study (successive two-fold dilutions) in DMSO-d_6 at a constant temperature of 30 °C for the **L2-Pt** complex can be seen in ***Figure 5.27***.

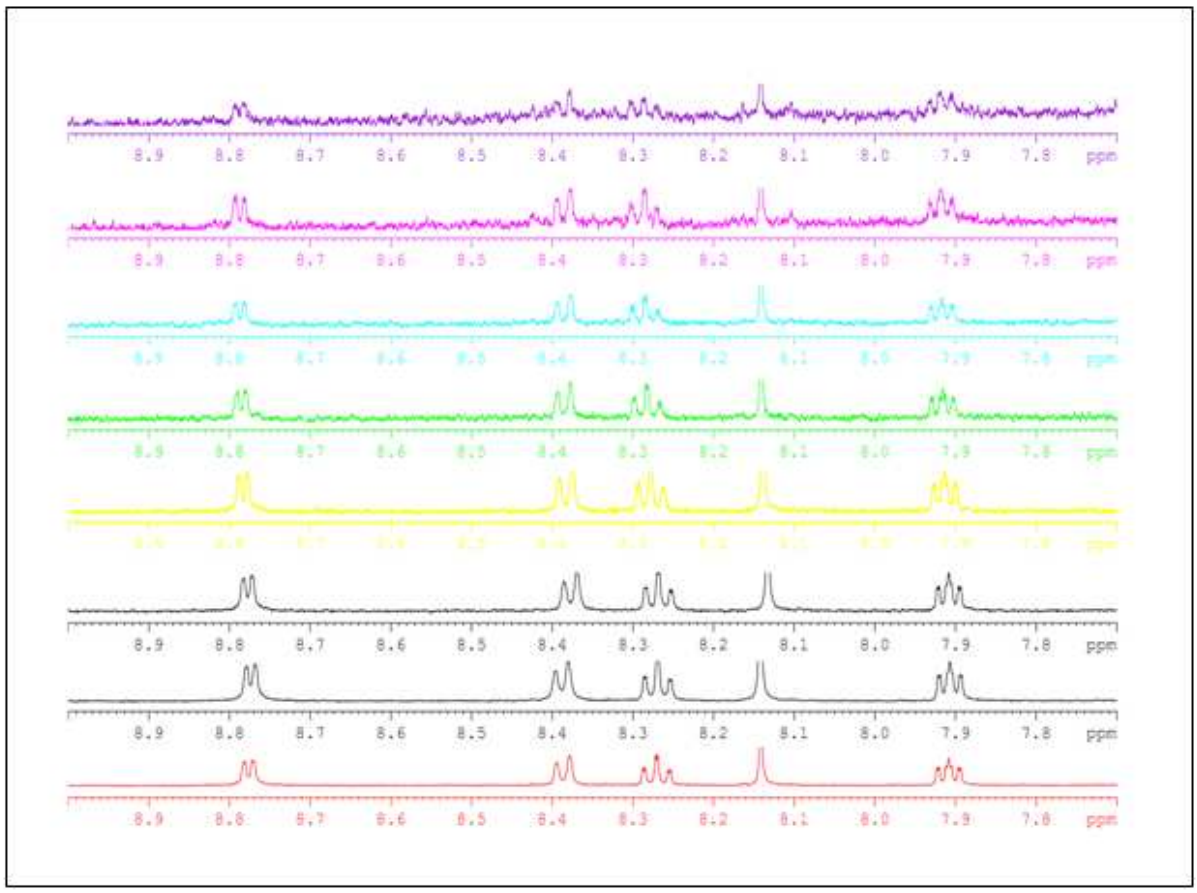

Figure 5.27: ^{1}H NMR spectra (aromatic region only) of **L2-Pt** complex in DMSO-d_6 at different degrees of dilution. The most concentrated sample is at the bottom; every next sample is half-dilute in comparison to the previous one. Two black spectra represent anomalies.

The numerical values of the chemical shift changes are shown in ***Table 5.12***. From the overlapped spectra depicted above, an anomaly is observed with regard to the **C/2** and **C/4** samples (black spectra). In each of these dilutions, the resonances shift both upfield and downfield with no discernible pattern. Since the chemical shift changes for **C/2** and **C/4** samples were minor, they were disregarded as anomalies (*cf* **L1-Pt** and **L3-Pt**). For the other dilutions, the α-, β-, and γ-proton signals moved slightly downfield with declining concentration, whilst the δ-, *m*-, and the CH_2-proton signals remained essentially unchanged.

The largest downfield shift is that of the γ-hydrogen (8 Hz), closely followed by the shifts of the α- and β-hydrogens (5.5 Hz and 5 Hz, respectively). Dilution has no effect on the resolution of the multiplets in this system.

Table 5.12: ^{1}H chemical shift changes with concentration for the solutions of **L2-Pt** complex

Δδ / Hz								
#	C – C/2	C/2 – C/4	C/4 – C/8	C/8 – C/16	C/16 – C/32	C/32 – C/64	C/64 – C/128	C – C/128
α	1. 5	2	3	1. 5	0. 5	0	0	5. 5
β	1	1	2. 5	1. 5	0. 5	0. 5	0	5
γ	0. 5	0. 5	5	2. 5	1	0	0. 5	8
δ	0. 5	5	3	1	0	0	0	0. 5
m	0. 5	4. 5	3	1	0	0	0	0
CH_2	0	0	0	0	0	0	0	0

5.7.3 L3 – Pt Complex

Variable temperature and concentration ^{1}H NMR studies of the **L3-Pt** complex were also performed. The spectra recorded at different temperatures are shown in ***Figure 5.28***, while numerical values of the chemical shift changes are collected in ***Table 5.13***.

A significant move downfield with increasing temperature is observed for all chemical shifts in this system (but for the *m*-hydrogen which remains practically unchanged). The largest downfield shift is that of the α-proton (85 Hz), the smallest is that of the *meta*-proton (3 Hz). Downfield shifts of the β-, γ-, and δ-hydrogens are close at about 40 Hz. Oddly, the downfield change for CH_2-signal (23 Hz) is significantly greater than that of the *m*-proton. Also a substantial improvement in signal resolution, most noticeable in the α-hydrogen doublet, is observed.

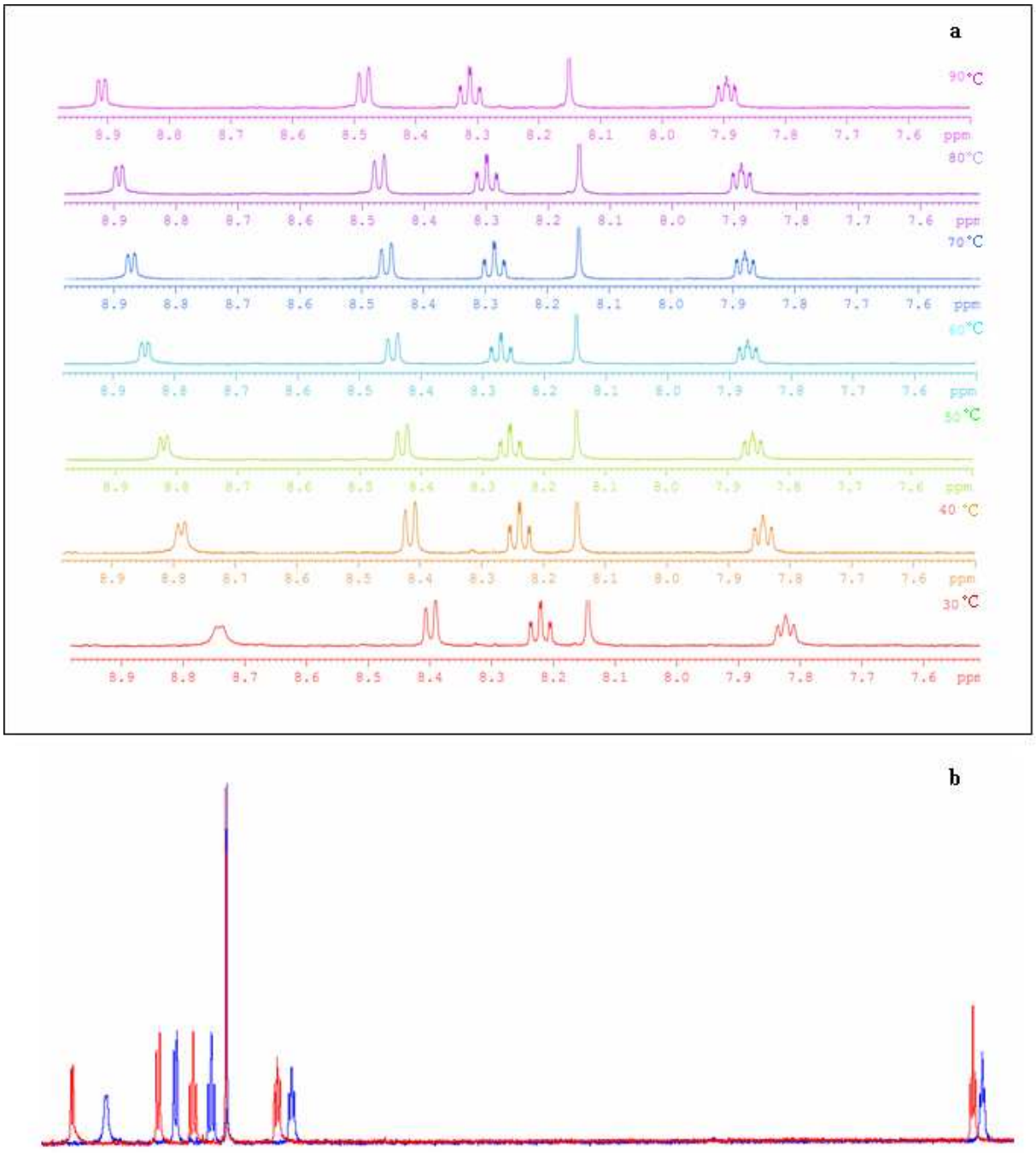

Figure 5.28: (a) ^{1}H NMR spectra of **L3-Pt** complex in DMSO-d_6 at various temperatures (in the range 30 °C to 90 °C). (b) Overlaid ^{1}H NMR spectra of **L3-Pt** complex in DMSO-d_6 at 30 °C (blue) and at 90 °C (red).

Table 5.13: ^{1}H chemical shift changes with temperature for the solution of **L3-Pt** complex

Δδ / ppm							
#	**Temperature change / °C**						
	30 – 40	**40 – 50**	**50 – 60**	**60 – 70**	**70 – 80**	**80 – 90**	**30 – 90**
α	22	18	13	12	11	9	85
β	10	8	6	5	4	3	36
γ	9	8	7	7	7	6	44
δ	8	8	7	7	6	6	42
m	0.7	0. 6	0. 6	0. 4	0. 4	0. 3	3
CH_2	2	3	4	4	5	5	23

The spectra of the concentration dependence study (successive two-fold dilutions) in DMSO-d_6 at a constant temperature of 30 °C for the **L3-Pt** complex are shown in ***Figure 5.29.*** The numerical shift data follow in ***Table 5.14***.

A noticeable shift downfield with dilution is observed for all the resonances with the exception of the CH_2-proton, which is moving upfield (12 Hz), and a negligible change in the chemical shift of the *m*-proton (3 Hz). The largest downfield shift is that of the α-hydrogen (57 Hz, 50 Hz of which occurs between the samples of concentration **C** and **C/16**), followed by progressively diminishing shifts of the β-hydrogen (29 Hz), γ-hydrogen (15 Hz), and δ-hydrogen (10.5 Hz). There is a significant improvement in resolution of the α-hydrogen doublet with dilution. This is a characteristic feature of this system.

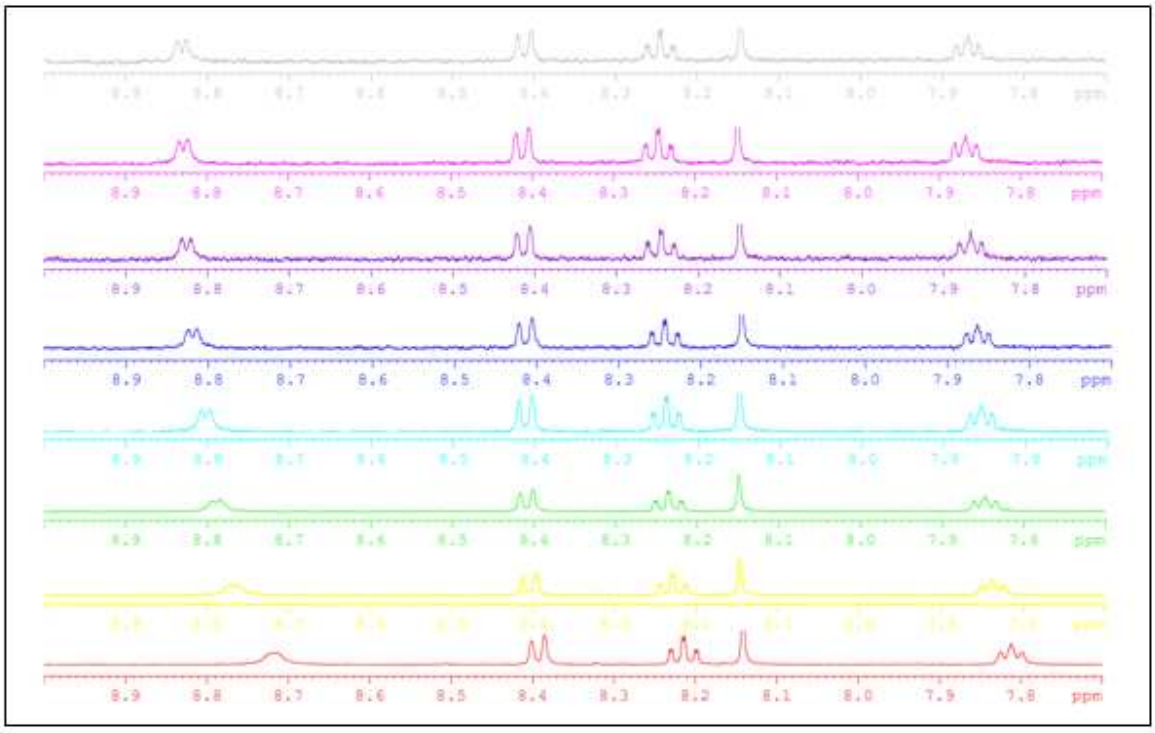

Figure 5.29: ^{1}H NMR spectra (aromatic region only) of **L3-Pt** complex in DMSO-d_6 at various dilutions. The most concentrated sample is at the bottom; every next sample is half-dilute in comparison to the previous one.

Table 5.14: ^{1}H chemical shift changes with concentration for the solutions of **L3-Pt** complex

Δδ / Hz								
#	**C – C/2**	**C/2 – C/4**	**C/4 – C/8**	**C/8 – C/16**	**C/16 – C/32**	**C/32 – C/64**	**C/64 – C/128**	**C – C/128**
α	25	7	10	8	4	2	1	57
β	13	5	4	4	2	0. 5	0. 5	29
γ	7	3	2	2	1	0	0	15
δ	6	3	1	1	0	0	0. 5	10. 5
m	3	1	0. 5	0	0. 5	0. 5	0. 5	3
CH_2	5	2	1	2	1	0. 5	0. 5	12

5.8 Interpretation of the Additional NMR Data

According to the NMR spectra of the platinum complexes at different temperatures and concentrations presented in the previous section, there is a fundamental difference in the behaviour between the **L1-Pt** complex on one hand, and the **L2-Pt** and **L3-Pt** complexes on the other. In the DMSO solution of **L1-Pt**, the chemical shift of the α-hydrogen drifts downfield with increasing temperature (15 Hz), while all other resonances move upfield (but for the β-hydrogen resonance, which remains unchanged). Practically no change in resolution of the multiplets is observed for this complex in the range 30 °C to 80 °C. In contrast, all of the chemical shifts in the ^{1}H spectrum of complexes **L2-Pt** and **L3-Pt** move downfield with increasing temperature (but for the *m*-hydrogen resonance, which remains virtually unchanged). The largest downfield shift in both systems is that of the α-proton (44.5 Hz for **L2-Pt** and 85 Hz for **L3-Pt**). The resolution of the multiplets improves in the same direction, particularly so for the α-hydrogen doublet between 30 °C and 40 °C. Both effects are considerably more pronounced for the **L3-Pt** complex.

Practically no change in the position of the chemical shifts or the resolution of the multiplets with dilution is observed in the **L1-Pt** system. Yet again, in contrast, there is a downfield change with dilution for the α-, β-, and γ-proton signals (slight for **L2-Pt** complex at 5.5 Hz (α), whilst substantial for the **L3-Pt** complex at 57 Hz (α)). The δ-, *m*-, and CH_2-proton signals remained essentially unchanged for the **L2-Pt** complex and dilution had no effect on the resolution of the multiplets in this system. For the **L3-Pt** complex the α-, β-, γ-, and δ-hydrogen resonances returned progressively diminishing shifts (57 Hz, 29 Hz, 15 Hz, and 10.5 Hz, respectively) with dilution, whilst the *m*-proton remained small (3 Hz), and the CH_2-protons, were moving upfield (12 Hz). Significant improvement in the resolution of the α-hydrogen doublet with dilution is a characteristic feature of this system. These facts can be interpreted as an indication that while the **L1-Pt** complex remains in its' monomeric form, the **L2-Pt** and **L3-Pt** complexes self-associate into dimers, with a higher extent of association expected for the latter complex.

For the **L1-Pt** complex the changes in the ^{1}H NMR spectra with temperature are small in comparison to those of the **L2-Pt** and **L3-Pt** complexes, and the resonances of the different hydrogen atoms move both upfield and downfield. Signal resolution remains unaffected by the sample temperature. It can thus be assumed that the **L1-Pt** complex does not form molecular associates. The lack of impact of changes in the complex concentration on the chemical shifts or signal resolution for the **L1-Pt** complex is also in accordance with the assumption that this complex is monomeric and exists in a linear conformation (see ***Figure 5.25***). The increased resolution of the α-hydrogen resonance with increasing temperature for the **L2-Pt** and **L3-Pt** complexes, and with dilution for the **L3-Pt** complex is clear evidence of the breakage of the self-associated species at a higher temperature or in a more dilute solution. The concordant shifts of all the resonances in the same direction (downfield) with increasing temperature for the **L2-Pt** and **L3-Pt** complexes also supports the idea of aggregation.

Molecular self-association could be either *inter*molecular, between different dinuclear platinum complex molecules, or *intra*molecular, between two platinum terpyridine units of the same molecule with the molecule folding over onto itself as described by Yam and co-workers.[13] From the concentration dependence study it can be concluded that the association in solution is *inter*molecular, because an *intra*molecular association would be concentration independent as observed previously. The temperature changes of the chemical shifts for the **L2-Pt** and **L3-Pt** systems can be attributed to the disruption of the *inter*molecular interactions (a consistent movement downfield of the protons closest to the platinum(II) centre and the large magnitude of the changes in comparison to the **L1-Pt** complex). The downfield changes of the chemical shifts with increasing temperature are consistent with the disruption of shielding molecular interactions (*e.g.*, π-stacking), as has been reported for some mononuclear platinum terpyridine complexes.[14]

Formation of higher order associates is less likely in view of the relatively low overall complex concentration in solution (2×10^{-3} M for the most concentrated sample used in the NMR study). In fact, the most significant changes in the ^{1}H spectrum of the **L3-Pt** complex with dilutions occur within the concentration range of 2×10^{-3} M to 1.6×10^{-5} M.

*Intra*molecular self-association, clam-shell type folding of the complex and the formation of π-stacked, and possibly Pt—Pt bound platinum terpyridine associates (see ***Figure 5.20***), may be ruled out at the higher complex concentrations encountered in the NMR study on the grounds of strong concentration dependence of the chemical shifts and multiplet resolution. However, the conformational structures derived from clam-shell type folding remain more favourable for **L2-Pt** and **L3-Pt** at the much lower concentrations employed in the kinetic studies (9×10^{-6} M) and UV-Visible studies (10^{-5}-10^{-7} M).

5.9 Electronic Interactions in the Self-Associated Complexes

Vast literature is devoted to the subject of π-π stacking of aromatic and hetero-aromatic organic molecules, as well as π-π stacking in metal complexes with aromatic ligands.[16-27] This matter will not be discussed here but rather focus will be directed on the theory underlying the stabilisation of molecular "sandwiches" due to direct Pt—Pt bonding.

For a platinum(II) ion in a square-planar coordination environment, the valence bond theory (***Figure 5.30,a***) places eight *5d* electrons in four *d*-orbitals in pairs, whilst the fifth *d*-orbital combines with a 6*s* and two 6*p* orbitals to form four dsp^2-hybridised orbitals whose extremities are directed towards the corners of a square about the central atoms.[28] These are used to accommodate lone pairs of electrons supplied by the four ligands, whilst the third p-orbital remains empty (***Figure 5.30,b***).[28] If the $5d_{z^2}$ and $6p_z$ orbitals (they share common symmetry and have major lobes placed along the z-direction) are allowed to mix, further equivalent hybrid orbitals are formed (***Figure 5.30,c***). The lower orbital is populated with two remaining 5*d* platinum electrons, whilst the upper one remains empty. In a mono-nuclear complex no advantage is derived from such hybridisation.

However, the situation changes when two or more platinum centres in similar coordination environments approach one another along the *z*-direction. As both sets of orbitals are of the same symmetry, considerable mixing of the lower and higher states occurs. Subsequently, the lower set of orbitals is stabilised, whilst the higher one is destabilised. Since only the lower set is populated with electrons, a net energy lowering is achieved.

This model accounts for direct Pt—Pt bonding and the formation of molecular dimers.[27] Similar ideas can be extended to three or more platinum centres, which become capable of forming a linear chain with adjacent atoms having the same valence structure.[12] Each of the neighbours contributes one electron per bond in the chain. Unfortunately ***Figure 5.30*** does not reveal the relationship between light absorption and the Pt—Pt distance. A molecular orbital (MO) treatment as suggested by Rundle[29], Miller[30] and Gray[18], is better suited for this purpose (***Figure 5.31***). The interaction of two adjacent nuclei is considered first. The two $5d_{z^2}$ atomic orbitals (AO) combine to give bonding and anti-bonding molecular orbitals. The bonding orbital has a_{1g}[α] symmetry whilst the anti-bonding orbital has symmetry of a_{2u}.[28] In a similar manner, two $6p_z$ atomic orbitals which have a_{1g} symmetry, combine to give a pair of molecular orbitals. The four available electrons fill the two lowest levels (one bonding, one weakly anti-bonding). Normally this should give no bonding advantage but since non-degenerate molecular orbitals of the same symmetry repel one another (configuration interaction), the lower a_{1g} orbital is displaced to lower energies and the upper to higher energies.[28] The same is true for the a_{2u} molecular orbitals. As a result the total energy of the system decreases and bonding occurs. The configuration interaction causes a change in the character of the orbitals. Molecular orbitals from $5d_{z^2}$ orbitals adopt *p* character whilst those from the $6p_z$ acquire *d* character.[28]

[α] When two mononuclear sqaure-planar platinum complexes are in eclipsed formation. For a staggered conformation, the symmetry will be a_1 and b_2, respectively.

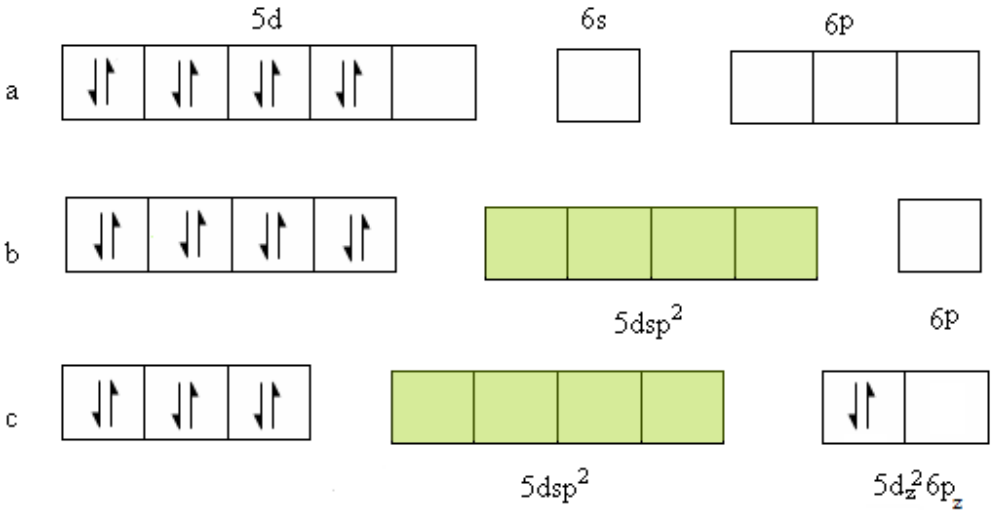

Figure 5.30: (a) Electron configuration of Pt^{2+} ion in unperturbed state, (b) the dsp^2-hybridised state, and (c) the state with the addition of $5d_{z^2}$ $6p_z$-hybridisation.[28] Shaded boxes represent orbitals that in a complex are filled with the ligand lone pair electrons.

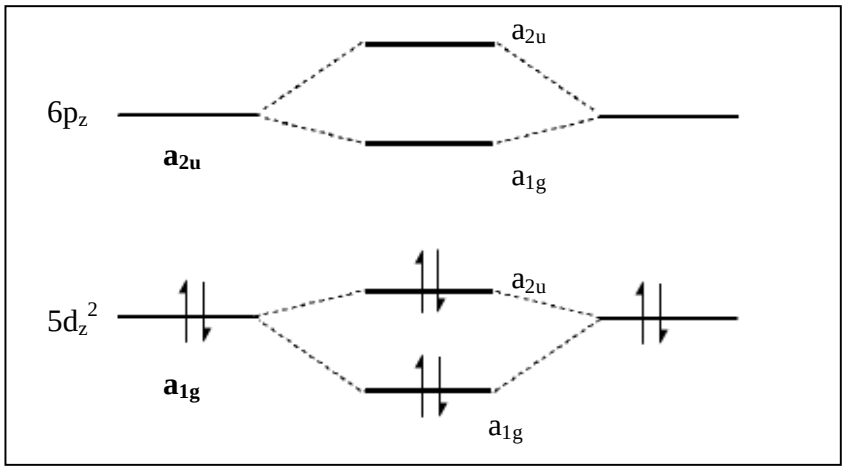

Figure 5.31: Molecular orbital scheme for a platinum-platinum interacttion.[31]

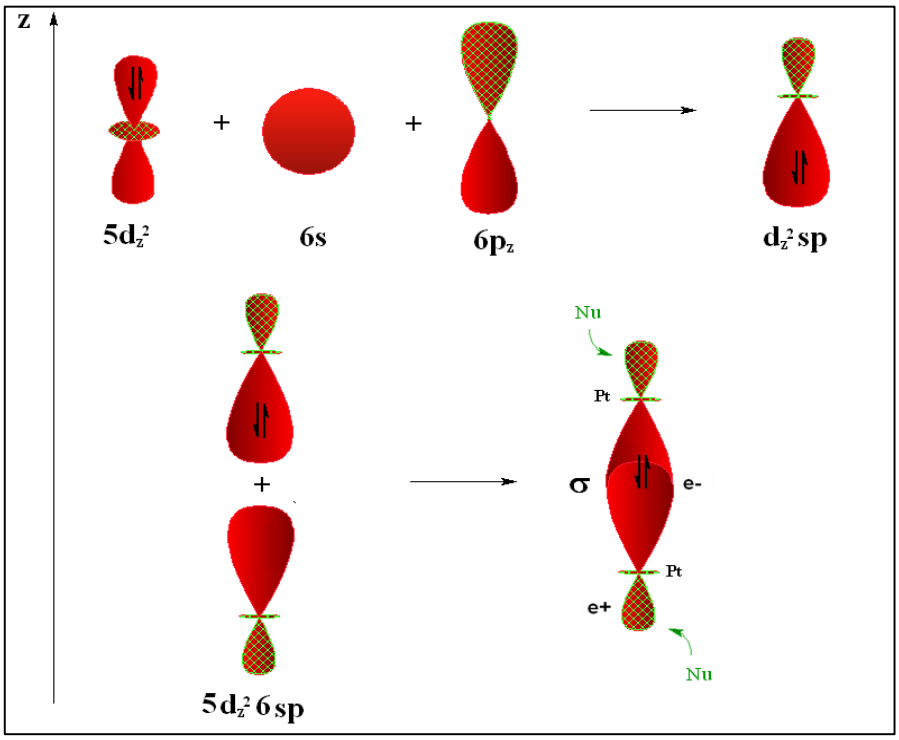

Figure 5.32: Diagram illustrating the stabilisation effect on the activated complex due to the direct Pt—Pt bond formation.[31]

To summarise, ***Figure 5.32*** shows that electron density is localised predominantely between two platinum nuclei rather than being equally distributed on each side of the platinum ion along the *z*-direction, thus increasing the susceptibility of the platinum centre to the attack by an incoming nucleophile above the plane of the platinum terpyridine complex (reduced Coulomb and Pauli repulsion). In other words, the six-coordinate transition state becomes stabilised, and as a result, the rate of substitution increases.

The overlaid absorption spectra of the three *bis*-terpyridine complexes studied in this work specifically, the 360-425 nm region is shown in ***Figure 5.33***. The concentration chosen for these measurements is approximately 10^{-5} M which closely resembles the concentration used for the kinetic studies. As the Beer-Lambert plots (see *Appendix 8*) at this concentration show, there is no aggregation in solution, *i.e.* we are dealing with monomeric species in solution. Of interest are the positions of the peak maxima for the bands at approximately 380 nm.

These absorptions can be assigned unequivocally to a dz^2(platinum)-π^* (terpyridine) or MLCT transition.[17-27] A close comparison of the three overlaid bands shows in the first instance that the **L2-Pt** complex absorbs at 389 nm, while the **L3-Pt** complex absorbs at a maximum of 393 nm. Although this red shift of 4 nm is small, it is clearly discernable from the overlaid spectra. Less certain is the position of the band maximum for the **L1-Pt** complex, since the band is very broad; in fact, MLCT bands of this type measured for platinum terpyridine complexes are in general rather broad.[17-27]

It should be noted that in order to explain the red shift in the absorption maximum for the **L2-Pt** and **L3-Pt** complexes, there must be a change in energy of the dz^2 orbital and or π^* orbitals for these two complexes. A significant red shift of this type cannot be attributed to the different number of methylene groups that link the two platinum terpyridine units for these two complexes together. There has to be an alternative explanation for the difference in electronic structure for these two complexes. It is concluded that the change in energy of the MLCT transition between the two complexes is due to different extents of π-π and or dz^2-dz^2 interactions caused by folding of the complexes in such a way as to allow these kinds of interactions to take place. It has already been shown that a variation of chain length enables folding of this type without introducing bond angle strain or steric crowding. Moreover, changes in the rate of substitution between these two complexes fit with the idea that there are different extents of dz^2-dz^2 interactions in the folded species. Noteworthy is that the longest wavelength absorption is clearly measured for the complex with the longest linking chain of six methylene groups, this shows that the intramolecular interactions that affect the energy of the MLCT transition are strongest for the longest linking chain species. It will be shown later that this is entirely consistent with the second fastest rate of substitution for the platinum **L3** complex. It is a pity that the absorption band measured for the **L1** complex is too broad to allow for further comparison of this trend; however it certainly does not contradict the conclusions that have been drawn based on the better defined absorption maxima measured for the other two complexes. Measurement of these spectra at higher concentrations could help sharpen the MLCT absorption bands but this would serve no purpose as at higher concentrations aggregation has been shown to occur and we would not be dealing with monomers as in the kinetic experiments.

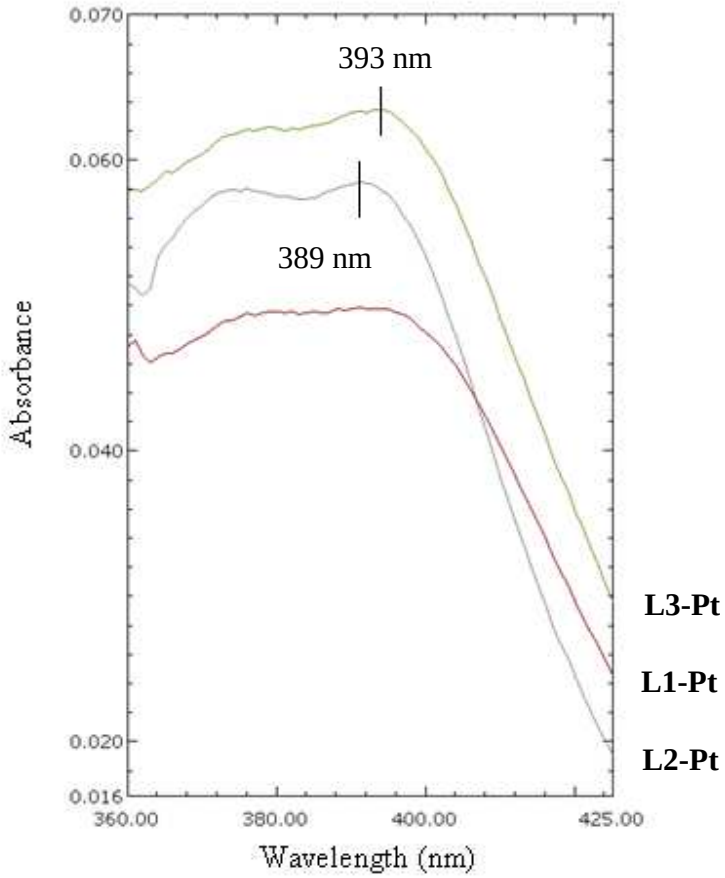

***Figure 5.33*:** MLCT range for the *bis*-terpyridine complexes showing a red shift.

5.10 Interpretation of Kinetic and Electronic Spectroscopy Results

The primary objective is to explain the kinetic trends in relation to the complex geometry and electronic structure. As mentioned previously, k_{obs} is nucleophile dependent, and hence the reactions follow an associative mechanism. For all the nucleophiles the general trend of the rate of the reaction is: **L2-Pt** > **L3-Pt** > **L1-Pt**. Initially, such findings were perplexing. Although this particular set of complexes is new, previous kinetic studies with **TU**, **DMTU** and **TMTU** nucleophiles, performed on monuclear platinum(II) complexes, exhibited monotonous changes in reactivity.[32]

From the UV-Visible spectrophotometric studies of these *bis*-terpyridine platinum(II) complexes, the trend of molar absorption coefficients is the same as for the rate constants: **L2-Pt** > **L3-Pt** > **L1-Pt**. Such similarity is more than a mere coincidence. The common denominator between the two phenomena, reactivity and light absorption, is the electron distribution within the platinum complex molecule. The highest rate constant for the **L2-Pt** complex implies that the platinum atom in this compound is likely to carry either the highest positive charge, or have the lowest electron density in the axial direction away of the square-planar complex. The highest molar absorptivity of the **L2-Pt** complex implies the highest transition dipole moment for the $\pi \rightarrow \pi^*$ bands, which in turn is traceable to the spatial extent of the bonding and anti-bonding π-orbitals in the heteroaromatic system of the terpyridine. The electronic state of the platinum ion and coordinating terpyridine moiety in the complex are clearly interrelated. Donation of electron density by ligands into the $5dsp^2$ orbitals of the platinum affects the energy, population, and the symmetry of both the $5d_{z^2}$ and $6p_z$-orbitals, whereas π-back bonding, in turn, supplies electron density from the platinum into the π-system of the terpyridine.

Fundamentally, one can envisage two mechanistic possibilities: a) the substitution on a monomeric square-planar platinum centre, and b) the substitution on a dinuclear Pt—Pt "sandwich", where two square-planar moieties, originating from the same molecule or from two different molecules, are bound on one side. The forces behind such aggregation are likely to be a combination of π-stacking interactions between the terpyridine units and direct Pt—Pt bonding, although, one cannot rule out entirely that one of these factors could be dominating. ***Figure 5.34*** illustrates the first of these possibilities. Substitution on a mononuclear centre follows an associative reaction pathway, with the formation of a five-coordinate transition state of trigonal bypiramidal geometry.[33-39]

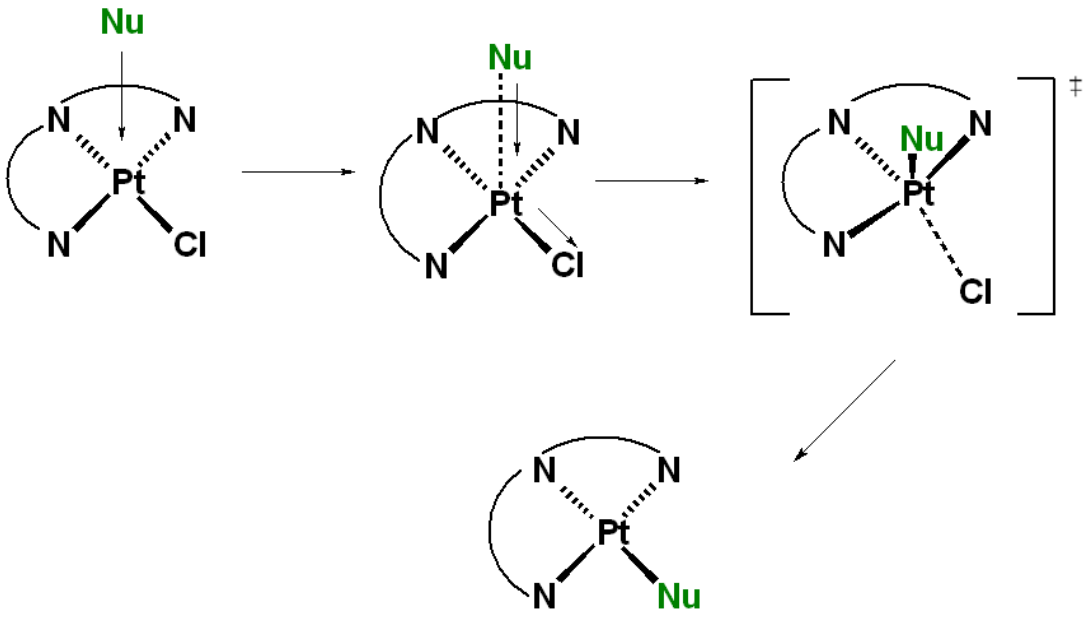

Figure 5.34: Ligand substitution on a mononuclear square-planar platinum(II) centre by way of a trigonal bipyramidal intermediate.[33-39]

In all probability the **L1-Pt** complex follows this mechanism. However, the problem with the interpretation of the kinetic results within such a model is that it is unable to explain non-regular changes in reactivity for the complexes with variable length of the spacer between two terpyridine units. Preliminary computational results of the complexes in their linear form revealed very little difference in the geometric parameters of the platinum terpyridine centre for all three complexes, as well as very close values of partial Mulliken charges on the platinum ion and spatial extent of the $5d_{z^2}$ orbitals. Certainly, no "peaking" of the electronic properties for **L2-Pt** complex is revealed.

Figure 5.35 illustrates the second possibility. Substitution on a dinuclear platinum centre can proceed *via* a similar associative reaction pathway, but this time each platinum ion will probably end in a quasi-octahedral transition state. Subsequently, the chloride ligand is unlikely to depart in the direction *trans* to the incoming nucleophile because of the steric constraint imposed by the second platinum terpyridine unit.

It is a speculation at this time that it might be departing at an angle close to 90° with respect to the direction of the incoming nucleophile. Another set of important geometric parameters in such a case includes the Pt—Pt distance, Pt—Cl distance and the Cl—Cl distance. The close proximity of two chloride anions will destabilise the system, weakening the Pt—Cl bond (which is expected to elongate), and subsequently increasing the rate of the transition state passing over into the valley of the products. In other words, it is expected to see a correlation between the values of $r_{Pt—Pt}$, $r_{Pt—Cl}$, $r_{Cl—Cl}$ in dinuclear platinum complexes and their reactivity in the substitution reactions.

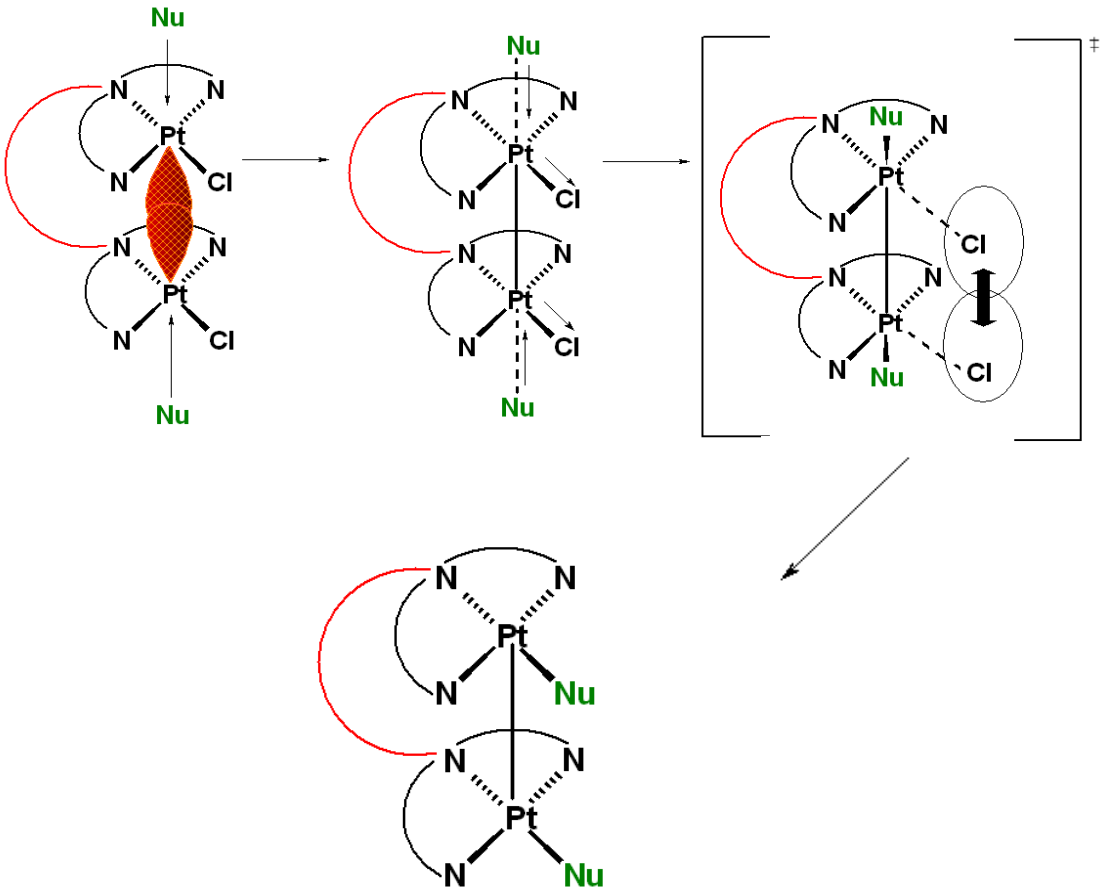

Figure 5.35: Ligand substitution on a dinuclear Pt—Pt cluster with the square-planar ligand arrangement is in eclipsed conformation.

The question still remains: what is the nature of the platinum dinuclear "sandwich"? Is it an *inter*molecular dimer or an *intra*molecular monomer?

As discussed in ***section 5.6***, there is no evidence of molecular self-associations in solution for the **L1-Pt** complex. Its temperature and concentration dependence NMR spectra (***section 5.8***) show little to no drift of chemical shifts in the terpyridine protons. Where these shifts do exhibit movement, it is both upfield and downfield and does not match the trend of the other two complexes. This indicates an absence of dimerisation. Consequently, the five coordinate transition state is not stabilised by the effects of Pt—Pt bonding and π—π interaction, and the reaction rate remains slow.

From the additional NMR experiments it is evident that molecular self-association of **L2-Pt** and **L3-Pt** complexes occurs to some extent when compared to **L1-Pt**. The data collected have shown that the extent of self-association of these two complexes is concentration dependent; hence, we may conclude that the association is *inter*molecular in nature. Experimental data for **L2-Pt** and **L3-Pt** complexes suggest that these two complexes dimerise in DMSO solutions in the concentration range ($2 \times 10^{-3} - 1.6 \times 10^{-5}$ M). As discussed previously, such self-association arises from either Pt—Pt or π—π interactions, or it could be a combination of the two. Both these interactions affect the electronic make-up of the complex and are expected to manifest themselves in changes in the UV-Visible spectra. Since aggregation stabilises the transition state, thus accelerating the reaction rate, one would expect the degree of self-association to be greater for the **L2-Pt** complex than for the **L3-Pt** complex. However, the NMR spectra clearly indicate stronger association in the case of **L3-Pt** complex. This discrepancy between the fastest kinetics of **L2-Pt** complex and highest self-association of the **L3-Pt** complex can be attributed to the concentration factor. While additional NMR studies were conducted on samples of millimolar concentration[α], the kinetic and UV-Visible studies were performed at the concentration levels of 10^{-6} M and (10^{-5} - 10^{-7}) M, respectively. In such dilute solutions the statistical probability of dimerisation is low and the molecules of the complexes remain monomeric. However, the driving forces of self-association remain, and for the molecules with sufficiently long (and flexible) spacers between two platinum terpyridine units, the clam-shell folding self-association may occur.

[α] Sensititvity of the NMR method invokes a limit on the lowest sample concentration, at which meaningful spectrum still may be collected.

However, at high concentrations of platinum(II) complexes, *inter*molecular associations (dimers) dominate (as supported by NMR data when solution concentration and temperature are varied). This still needs to be tested computationally, but it can be hypothesised that such folding might be optimal for the **L2-Pt** complex. Short alkyl chains put *severe* steric strain on the folded-over or dimeric complex, as can be seen from the ***Figure 5.36*** for **L1-Pt**. Initial-guess geometry for this complex places two methylene hydrogen atoms on opposing chains at a distance of 2.38 Å, which is shorter than the sum of the van der Waals radii (2.4 Å). Quantum mechanical optimisation of this structure was terminated after 42 refinement steps, as it became evident that the dimer moves towards dissociation. As one can see from the figure below, the distance between the sterically crowded methylene hydrogens of opposing chains has increased, relieving the stress, but at the expense of both π-stacking and Pt—Pt bonding interactions in the left hand side unit (dihedral angle between the planes of two platinum terpyridine units has increased significantly and the Pt—Pt distance has nearly doubled from initial value of 2.82 Å – 5.09 Å).

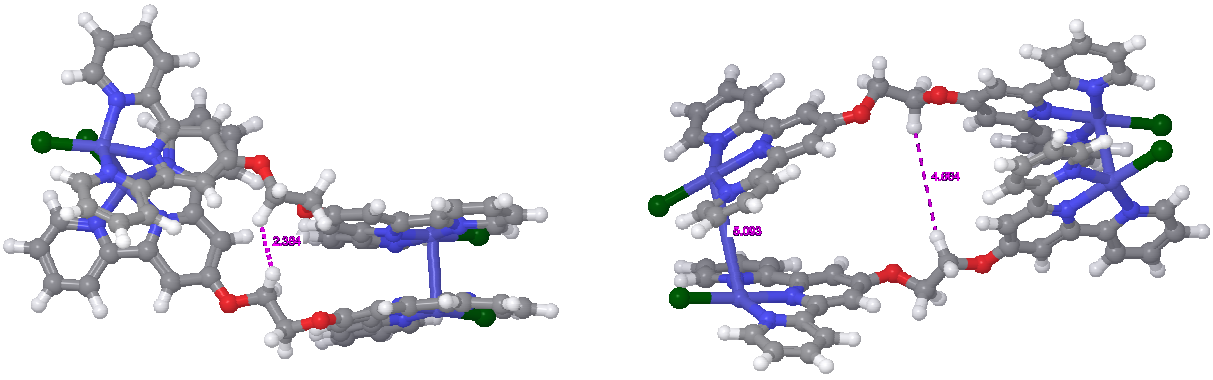

Figure 5.36: Computationally generated structure of the dimeric **L1-Pt** complex (on the left: initial guess, on the right: the structure after 43 refinement steps).

In the modelled stacking arrangements of the **L2-Pt** complex (***Figure 5.37***) the atoms of the two alkyl chains are separated by more than double the distance in **L1-Pt**. In fact, a cavity exists between the two chains removing the steric obstacle to dimer formation.

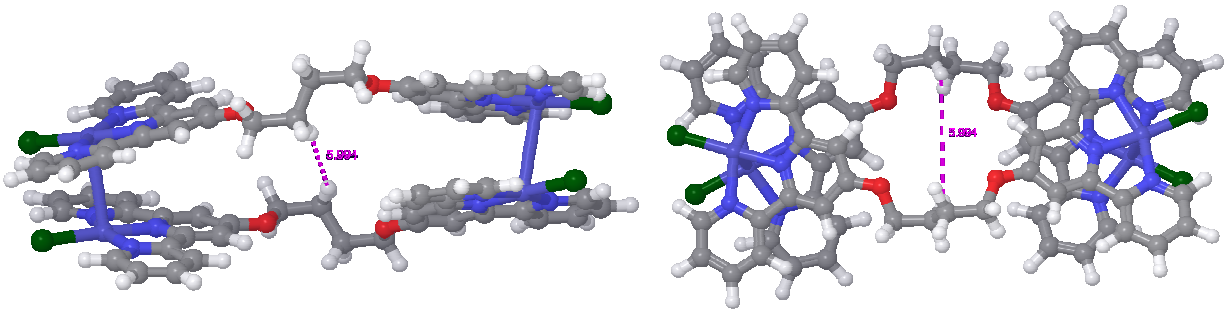

Figure 5.37: Two projections of the computationally generated structure for the **L2-Pt** dimer (this is initial-guess structure). Note the relief of the steric strain in comparison to the **L1-Pt** dimer.

The structures of the **L3-Pt** complexes have not been computed yet in view of the high demand of the task (see *Chapter 6*) but they are expected to be similar to those of **L2-Pt**. Further increased length of the spacer affords more flexibility and allows for better release of the steric strain in the dimeric complex, which is the most associated according to the NMR data.

Similar arguments can be applied to the folded monomeric self-associates, whose structures remain to be computed. However, the spacer length is probably too long for the **L3-Pt** complex to form the most stable associate and it becomes disadvantaged over the **L2-Pt** complex by an unfavourable entropy contribution. Consequently, optimal spacer length for the clam-shell self-associate structure of the **L2-Pt** complex affords the best stabilisation of the transition state and the fastest kinetics of substitution of a pendant monodentate ligand.

5.11 References

1. K. van der Schilden, *PhD Thesis: Design and Development of Polynuclear Ruthenium and Platinum Polypyridyl Complexes in Search of New Anticancer Agents*, Leiden University, Netherlands, **2006**.
2. E. C. Constable, C. E. Housecroft, M. Neuburger, S. Schaffner and C. B. Smith, *Dalton Trans.*, **2005**, 2259–2267.
3. K. Suntharalingam, A. J. P. White and R. Vilar., *Inorg, Chem.*, **2009**, *48*, 9427.
4. W. F. Armarego and D. D. Perrin. *Purification of Laboratory Chemicals* 4th Ed. Butterworth Heinemann, Oxford, **1996** pp. 5–7.
5. S. D. Cummings., *Coord. Chem Rev.*, **2009**, *253*, 449–478.
6. W. Huang, C. Li, J. Wang and L. Zhu., *Spectroscopy Lett*ers, **1998**, *31*, 1793–1809.
7. a. C. Grimmer, *personal communication*. b. L. V. Konovalov and V. G. Pogareva., *Zhurnal Strukturnoi Khimii*, **1980**, *22*, 159–162.
8. P. W. Atkins and R. S. Friedman. Molecular Quantum Mechanics 3rd Ed. Oxford University Press, United States, **1970**, 195–205.
9. a) http://itl.chem.ufl.edu/2045/lectures/lec_m.html Retrieved 2011–11–17. b) P. Atkins and J. de Paula. Atkins' Physical Chemistry 7th Rd. Oxford University Press, United States, **2002**, 879–881.
10. K. J. Laidler, J. H. Meiser and B. C. Sanctuary., *Physical Chemistry 4th Ed*. Houghton Mifflin, New York, **2003**, pp. 383–385
11. http://njms2.umdnj.edu/biochweb/education/bioweb/PreK2010/EnzymeProperties.html Retrieved 2011–11–21.
12. P. W. Atkins and R. S. Friedman, *Molecular Quantum Mechanics* 3rd Ed, Oxford University Press, Oxford, **1997**, pp. 195-198.
13. V. W–W. Yam, K. H–Y. Chan, K. M–C. Wong, B. W–K. Chu, *Angew. Chem.*, **2006**, *118*, 6315 – 6319; V. W–W. Yam, K. H–Y. Chan, K. M–C. Wong, B. W–K. Chu, *Angew. Chem. Int. Ed*, **2006**, *45*, 6169 – 6173.
14. G. Arena, G. Calogero, S. Campagna, L. M. Scolaro, V. Ricevuto, R. Romeo, *Inorg. Chem.*, **1998**, *37*, 2763 – 2769.

15. S. C. F. Kui, Y–C. Law, G. S. M. Tong, W. Lu, M–Y. Yuen, C–M. Che, *Chem. Science*, **2011**, *2*, 221 – 228.
16. C. Janiak, *J. Chem. Soc., Dalton Trans*., **2000**, 3885-3896.
17. H-K. Yip, L-K. Cheng, K-K. Cheung and C-M. Che, *J. Chem. Soc., Dalton Trans.*, **1993**, 2933-2938.
18. J. A. Bailey, M. G. Hill, R. E. Marsh, V. M. Miskowski, W. P. Schaefer and H. B. Gray, *Inorg. Chem.*, **1995**, *34*, 4591-4599.
19. D. R. McMillin and J. J. Moore, *Coord. Chem. Rev*., **2002**, *229*, 113-121.
20. J. S. Field, R. J. Haines, D. R. McMillin and G. C. Summerton, *J. Chem. Soc. Dalton Trans.*, **2002**, 1369-1376.
21. J. F. Michaelec, S. A. Bejune and D. R. McMillin, *Inorg. Chem.*, **2000**, *39*, 2708-2709.
22. T. K. Aldridge, E. M. Stacey and D. R. McMillin, *Inorg. Chem.*, **1994**, *33*, 722-727.
23. D. K. C. Tears and D. R. McMillin, *Coord. Chem. Rev*., **2001**, 211, 195-205.
24. V. W-W. Yam, K. M-C. Wong and N. Zhu, *J. Am. Chem. Soc*., **2002**, *124*, 6506-6507.
25. Q-Z. Yang, L-Z Wu, Z-X. Wu, L-P. Zang and C-H. Tung, *Inorg. Chem*., **2002**, *41*, 5653-5655.
26. V. W-W. Yam, K. M-C. Wong and N. Zhu, *Angew. Chem. Int. Ed*., **2003**, *42*, 1400-1403.
27. M. H. Wilson, L. P. Ledwaba, J. S. Field and D. R. McMillin, *Dalton Trans.*, **2005**, 2754-2759.
28. K. Krogmann, *Angew. Chem. Int. Ed*, **1969**, *8*, 35–43.
29. R. E. Rundle., *J. Phys. Chem*., **1957**, *61*, 45–47.
30. J. R. Miller., *J. Chem. Soc. Dalton Trans*., **1965**, 713–715.
31. W. B. Connick, R. E. Marsh, W. P. Schaefer and H. B. Gray., *Inorg. Chem*., **1997**, *36*, 913–922.
32. a) A. Hofmann, L. Dahlenburg and R. van Eldik, *Inorg. Chem*., **2003**, *42*, 6528–6538. b) D. Jaganyi, D. Reddy, J. A. Gertenbach, A. Hofmann and R. van Eldik, *Dalton Trans*., **2004**, 299–304.
33. M. L. Tobe and J. Burgess, *Inorganic Reaction Mechanisms*, Addison Wesley Longman, Ltd., Essex, **1999**, pp. 73–81.

34. D. Reddy, K. Akerman, M. Akerman and D. Jaganyi, *Transition. Met. Chem*., **2011**, *36*, 593–602.
35. B. Pitteri and M. Bortoluzzi., *Polyhedron*, **2006**, *25*, 2698–2704.
36. B. Pitteri, G. Marangoni, F. V. Viseutim, L. Cattalini and T. Babbo., *Polyhedron*, **1998**, *17*, 475–482.
37. A. Hofmann, L. Dahlenburg and R. Van Eldik., *Inorg*. *Chem*., **2003**, *42*, 6528–6538.
38. Z. D. Bugarcic, G. Liehr and R. Van Eldik., *J. Chem. Soc., Dalton Trans*., **2002**, 2825–2830.
39. A. Jelling, K. Orrell, A. Osborune and V. Sik., *Dalton*. *Trans*., **1998**, 937–945.

CHAPTER VI

Conclusions

1. A series of *bis*-(4'-terpyridyl)-α,ω-alkyldiol ligands and their respective chloro-platinum(II) complexes were synthesised and fully characterised by microanalysis, FTIR, NMR, UV-Visible spectroscopy, and MS-ToF. All structures were verified by a series of NMR experiments including: ^{1}H, ^{13}C, DEPT, COSY, NOESY, ROESY, HMBC, HSQC and ^{195}Pt, where applicable.

2. Single crystals of all three ligands were obtained and their molecular and crystal structures were determined by X-ray diffraction.

3. A study of the chloride substitution by **TU**, **DMTU** and **TMTU** was conducted and second order rate coefficients were determined. In all cases the reaction rates were dependent on the concentration and nature of incoming nucleophile. An associative reaction mechanism is suggested for the pendant ligand substitution. The activation parameters, enthalpy and entropy, determined from the temperature dependence of rate coefficients, were in accord with an associative mechanism. The measured rate coefficients followed the trend **L1-Pt** < **L3-Pt** < **L2-Pt**, which is attributed to variable complex structures and associated electronic effects.

4. UV-Visible absorption spectra were recorded on sequentially diluted solutions of the ligands (in chloroform), and the platinum complexes (in water). These spectra obeyed the Beer-Lambert law. The values of the molar absorption coefficients, at the wavelengths of maximum absorption, corresponding to the $\pi \rightarrow \pi^*$ transitions of the terpyridine heteroaromatic system, determined for the ligands followed the trend **L1** < **L2** < **L3**, whilst for the complexes the trend was **L1-Pt** < **L3-Pt** < **L2-Pt**. It has been concluded that at low concentrations the **L2-Pt** and **L3-Pt** complexes undergo *intra*molecular folding in solution.

5. Additional NMR spectroscopy studies, following the temperature and concentration variation of the chemical shifts, were performed on all three terpyridine complexes. It was established that at higher complex concentrations (10^{-3} - 10^{-5} M) *inter*molecular self-association in solution takes place for the **L2-Pt** and **L3-Pt** complexes but not for the **L1-Pt** complex.

6. From the work done on these novel *bis*-terpyridine complexes it has been found that their reactivity is predominately determined by their structural conformation in solution. It is suggested that at low concentrations (10^{-5} - 10^{-7} M), the **L1-Pt** complex remains in its linear conformational state, whilst the **L2-Pt** and **L3-Pt** complexes undergo *intra*molecular folding with the formation of a Pt—Pt bonded and π—π stacked dinuclear platinum terpyridine centre. It is further suggested that the stability of such complexes is highest for the **L2-Pt**, in correlation with its highest reactivity towards nucleophilic substitution and the highest molar absorptivity among the complexes studied.

7. Preliminary computational structures of the **L2-Pt** and **L3-Pt** complexes were generated the reasons for the folding and self-association in the systems are related to the steric crowding and stress in the spacer region of the folded or self-associated complexes.

CHAPTER VII

As a result of the current investigation, significant progress has been made and insight gained into the nature of novel *bis*-terpyridinyl ligands and their platinum complexes. However, to fully understand how these molecules function in both the liquid and solid state one would like to extend the complex sequence to include longer length chains (*e.g.*, with eight or ten carbon atoms), run kinetic measurements, and establish the optimal chain length for maximum reactivity, absorptivity, and self-association. Further investigation of the chloride ion substitution with an extended range of nucleophiles, including ionic (SCN^-, I^- and Br^-), azole (bio-mimics such as pyrazole, imidazole and substituted derivatives) and biological (L-Histidine, DL-Penicillamine, L-Cysteine, 5'-GMP and L-Methionine) entities should be performed.

Full scale DFT calculations should be performed on the core complexes (**L1-Pt**, **L2-Pt**, and **L3-Pt**) with a wide range of objectives in mind: to establish the geometry, orbital symmetry, and partial electric charge on the platinum atoms, assign the IR-vibrational bands and simulate UV-Visible spectra. Then, such calculations would be extended to the folded monomeric and self-associated dimeric platinum complexes. Hopefully, this will provide a more detailed explanation of the reaction rates, UV-Visible and NMR spectral data. In particular, an explanation as to why the CH_2 closest to the terpyridine fragment experiences such prominent changes in both variable temperature and variable concentration NMR spectroscopy studies has to be offered. It would also be useful to conduct variable temperature and variable concentration NMR spectroscopy studies on the nucleophile-bound complexes, in an attempt to determine whether aggregation persists and to establish whether the direct Pt—Pt bonding and or π—π stacking remains in place.

One should convert these complexes to their aqua forms and perform a pK_a study, a speciation study, and a study of the substitution kinetics. Such data would be essential if these complexes were to be considered as potential anticancer leads. An attempt to attain crystal structures of some, if not all, of these nucleophile bound complexes would be made. It would be advantageous to determine the missing thermodynamic parameters (diffusion coefficients and activation volumes) of both the chloro- and the aqua- species.

The biological component of this strongly physical chemistry work would involve studying how these complexes bind to DNA by performing experiments with calf thymus DNA. Another facet of this multi-dimensional work would involve the substitution kinetics (of both the aqua and chloro species) of the dimeric complexes. Once complete, a comparison could be drawn between the reactivity of the folded monomer in relation to the reactivity of the related dimer. A final extension of this work would be to synthesise and fully characterise similar ligands and complexes in which the two ether functional groups are replaced with thioether and amino derivatives. Having completed a full substitution kinetics study on the platinum complexes of these ligands, one could better ascertain the effect of the ligand structure on the platinum(II) centre, and the applications of such complexes including a potential anticancer cure.